MONTHLY NOTICES

OF THE

ROYAL ASTRONOMICAL SOCIETY

Volume 119 No. 2 1959

Published and Sold by the

ROYAL ASTRONOMICAL SOCIETY
BURLINGTON HOUSE
LONDON, W.1

Price £1 0*s.* 0*d.*; *in U.S.A.* $3

Annual Subscription for volume of six numbers: £5 5*s.* 0*d.* ; *in U.S.A.* $16

MONTHLY NOTICES

OF THE

ROYAL ASTRONOMICAL SOCIETY

Volume 119 No. 2 1959

NOTICE

The Council regrets that, as a consequence of the stoppage of work following the recent printing dispute, publication of the present issue of *Monthly Notices* has been so long delayed.

It is inevitable that the appearance of the large number of papers now awaiting publication will continue to be retarded, but it is hoped in forthcoming issues progressively to reduce the delay and to restore the normal rate of publication by the end of the current volume.

September 1959

Published and Sold by the

ROYAL ASTRONOMICAL SOCIETY
BURLINGTON HOUSE
LONDON, W.1

Price £1 0*s.* 0*d.*; *in U.S.A.* $3

Annual Subscription for volume of six numbers: £5 5*s.* 0*d.* ; *in U.S.A.* $16

The Geophysical Journal

OF THE

ROYAL ASTRONOMICAL SOCIETY

Editors

A. H. Cook
M.A., Ph.D., F.R.A.S., F.G.S.
National Physical Laboratory
Teddington

T. F. Gaskell
M.A., Ph.D., F.R.A.S.
British Petroleum Company
London

Price £1 per number; in U.S.A. $3. *Annual Subscription £3; in U.S.A.* $9

Volume 2 No. 2 June 1959

CONTENTS

H. Takeuchi, Torsional oscillations of the Earth and some related problems.

M. Landisman, Y. Sato and M. Ewing, The distortion of pulse-like earthquake signals by seismographs.

L. R. Cooper and C. Jones, The determination of virgin strata temperatures from observations in deep survey boreholes.

J. Ross Macdonald, Rayleigh-wave dissipation functions in low-loss media.

Research Note

J. C. Bhattacharji, An Earth Model and the reduction of gravity observations for use in Stokes's integral.

Letter to the Editors

E. Irving, Magnetic "cleaning".

Note on Progress in Geophysics

Bruce C. Heezen, Dynamic processes of abyssal sedimentation: erosion, transportation, and redeposition on the deep-sea floor.

Reports of Discussions

The characteristics of the Antarctic Ice Sheet (R.A.S. Discussion of 1959 February 27).
The geological and geophysical results of the cruises of R.R.S. *Discovery II*, 1958 May–July (Cambridge Discussion of 1959 March 4).

Orders should be addressed to:
The Assistant Secretary
Royal Astronomical Society, Burlington House, London, W.1.

MONTHLY NOTICES

OF THE

ROYAL ASTRONOMICAL SOCIETY

Vol. 119 No. 2

NUTATION: COMPARISON OF THEORY AND OBSERVATIONS

Harold Jeffreys

(Received 1958 December 11)

Summary

Theoretical values are given for the principal, semiannual, and fortnightly nutations, based on the central particle and Roche Earth models. These are compared with Federov's observed values. Agreement is better than in any previous comparison. The fortnightly terms are almost the same for both models and agree with observation. Both components of the semiannual motion agree best with the central particle model. The observed 19-yearly motion in obliquity agrees best with the central particle model, that in longitude best with the Roche model, and some discrepancy would remain for any model.

1. The rate of precession and the amplitude of the 19-yearly nutation, on the hypothesis that the Earth is a rigid body, are given theoretically by a pair of equations containing the Earth's dynamical ellipticity $(C-A)/C$ and the Moon's mass. Their observed values are the basis of the estimates of the two latter quantities given in the older lists of astronomical constants. The position was changed by Hinks's determination of the lunar inequality from the Eros observations of 1901. This inequality is a monthly motion of the Earth about the centre of mass of the Earth and Moon together. It was found to give the mass of the Moon with much smaller uncertainty than the previous method, and more recent procedure has been to use the lunar inequality to estimate the mass of the Moon and then the rate of precession to estimate the dynamical ellipticity. However Jackson (1930) pointed out that the results of the two methods were actually inconsistent. His conclusion was emphasized by Spencer Jones (1941) who estimated from the lunar inequality and the precession that the amplitude of the nutation in obliquity should be $9''{\cdot}2272 \pm 0''{\cdot}0008$, while the observed values according to several reductions lay between $9''{\cdot}207$ and $9''{\cdot}213$. The standard value of Newcomb is $9''{\cdot}210$.

According to the work of several writers, especially Poincaré (1910), allowance for elasticity of the Earth has no appreciable effect on the theoretical value. But Bondi and Lyttleton called my attention to a passage in Lamb's *Hydrodynamics*, based on work of Poincaré, concerning the effects of a liquid core. No data on the actual core had of course been available to Poincaré and to previous writers on the subject, including Kelvin, Greenhill and Hough, but the qualitative results were that a liquid core would shorten the free (Eulerian) period and reduce the amplitude of the 19-yearly nutation. The latter effect depends considerably on the ellipticity of the core boundary. Assuming that this is given by the hydrostatic theory of the Earth's interior, which is likely to be accurate at such depths, I found (Jeffreys 1948) that with a rigid shell and a homogeneous core the free period would be reduced from 305 days, as for a

The Geophysical Journal

OF THE

ROYAL ASTRONOMICAL SOCIETY

Editors

A. H. Cook
M.A., Ph.D., F.R.A.S., F.G.S.
National Physical Laboratory
Teddington

T. F. Gaskell
M.A., Ph.D., F.R.A.S.
British Petroleum Company
London

Price £1 per number; in U.S.A. $3. Annual Subscription £3; in U.S.A. $9

Volume 2 No. 2 June 1959

CONTENTS

H. Takeuchi, Torsional oscillations of the Earth and some related problems.

M. Landisman, Y. Sato and M. Ewing, The distortion of pulse-like earthquake signals by seismographs.

L. R. Cooper and C. Jones, The determination of virgin strata temperatures from observations in deep survey boreholes.

J. Ross Macdonald, Rayleigh-wave dissipation functions in low-loss media.

Research Note

J. C. Bhattacharji, An Earth Model and the reduction of gravity observations for use in Stokes's integral.

Letter to the Editors

E. Irving, Magnetic "cleaning".

Note on Progress in Geophysics

Bruce C. Heezen, Dynamic processes of abyssal sedimentation: erosion, transportation, and redeposition on the deep-sea floor.

Reports of Discussions

The characteristics of the Antarctic Ice Sheet (R.A.S. Discussion of 1959 February 27).
The geological and geophysical results of the cruises of R.R.S. *Discovery II*, 1958 May–July (Cambridge Discussion of 1959 March 4).

Orders should be addressed to:
The Assistant Secretary
Royal Astronomical Society, Burlington House, London, W.1.

MONTHLY NOTICES

OF THE

ROYAL ASTRONOMICAL SOCIETY

Vol. 119 No. 2

NUTATION: COMPARISON OF THEORY AND OBSERVATIONS

Harold Jeffreys

(Received 1958 December 11)

Summary

Theoretical values are given for the principal, semiannual, and fortnightly nutations, based on the central particle and Roche Earth models. These are compared with Federov's observed values. Agreement is better than in any previous comparison. The fortnightly terms are almost the same for both models and agree with observation. Both components of the semiannual motion agree best with the central particle model. The observed 19-yearly motion in obliquity agrees best with the central particle model, that in longitude best with the Roche model, and some discrepancy would remain for any model.

1. The rate of precession and the amplitude of the 19-yearly nutation, on the hypothesis that the Earth is a rigid body, are given theoretically by a pair of equations containing the Earth's dynamical ellipticity $(C-A)/C$ and the Moon's mass. Their observed values are the basis of the estimates of the two latter quantities given in the older lists of astronomical constants. The position was changed by Hinks's determination of the lunar inequality from the Eros observations of 1901. This inequality is a monthly motion of the Earth about th centre of mass of the Earth and Moon together. It was found to give the mass of the Moon with much smaller uncertainty than the previous method, and more recent procedure has been to use the lunar inequality to estimate the mass of the Moon and then the rate of precession to estimate the dynamical ellipticity. However Jackson (1930) pointed out that the results of the two methods were actually inconsistent. His conclusion was emphasized by Spencer Jones (1941) who estimated from the lunar inequality and the precession that the amplitude of the nutation in obliquity should be $9''{\cdot}2272 \pm 0''{\cdot}0008$, while the observed values according to several reductions lay between $9''{\cdot}207$ and $9''{\cdot}213$. The standard value of Newcomb is $9''{\cdot}210$.

According to the work of several writers, especially Poincaré (1910), allowance for elasticity of the Earth has no appreciable effect on the theoretical value. But Bondi and Lyttleton called my attention to a passage in Lamb's *Hydrodynamics*, based on work of Poincaré, concerning the effects of a liquid core. No data on the actual core had of course been available to Poincaré and to previous writers on the subject, including Kelvin, Greenhill and Hough, but the qualitative results were that a liquid core would shorten the free (Eulerian) period and reduce the amplitude of the 19-yearly nutation. The latter effect depends considerably on the ellipticity of the core boundary. Assuming that this is given by the hydrostatic theory of the Earth's interior, which is likely to be accurate at such depths, I found (Jeffreys 1948) that with a rigid shell and a homogeneous core the free period would be reduced from 305 days, as for a

rigid Earth, to 270 days, and the nutation amplitude by about 1 part in 160, about three times too much to account for the observed discrepancy, but in the right direction.

Later work showed that allowance for elasticity of the Earth's shell would again lengthen the free period and make the reduction of the nutation amplitude smaller, but a detailed quantitative comparison, based on an Earth model in accordance with modern geophysical information, was rendered possible by work of Takeuchi (1950) on the elastic yielding of the Earth under tidal forces.

There is a complication due to the fact that the core is not uniform. The radius is about 0·55 of that of the Earth. Within it, however, there is an inner core, with radius about 0·36 of that of the main core, which may be solid. Its density is doubtful; the mean density of the core is about 10, but there may be a discontinuous increase of density at the inner core boundary by as much as 10. The effect of this is small for most observable phenomena since the volume concerned is small.

Theoretical values of the corrections to the coefficients in the 19-yearly, semiannual and fortnightly nutations have been calculated by Jeffreys and Vicente (1958 a, b). These are based on Takeuchi's solution for the shell, itself based on one of Bullen's distributions of density, and on two models for the core. In one of these the core is replaced by a homogeneous incompressible fluid with an extra particle at the centre. In the other, which we call the Roche model, it is taken as having a quadratic density distribution, the variation of density being taken as wholly due to compression. In both the constants are adjusted to make the mass and moment of inertia of the core agree with a compromise between Bullen's extremes. In fact about half the departure of the core from uniformity of density (judged by the departure of the ratio I/Ma^2 from 0·4) is due to compression and half to the probable rise of density in the inner core, and interpolation between the two extremes should be at least a useful guide.

In all discussions of observations until recently the ratio of the amplitudes of the nutations in obliquity and longitude has been assumed to be the same as for a rigid Earth. This is not true for an Earth with a liquid core. The data have however recently been rediscussed by Federov (1958 a, b) who has used 135 000 observations for the 19-yearly term and 230 000 for the fortnightly term; he quotes also a solution by Popov for the semiannual term based on observations at Poltava. The coefficients in obliquity and longitude are estimated separately. Thus there is now a basis for a detailed comparison between theory and observation.

2. Before proceeding to such a comparison I offer some remarks on the theory for a rigid Earth. The published theory is rendered more difficult by the facts that (1) the Euler angle ψ (longitude of the pole) is sometimes measured in the direct and sometimes in the retrograde sense, (2) some theories refer only to the axis of figure, while others use an intermediary, namely the instantaneous axis (Oppolzer and Woolard (1953)), or the axis of angular momentum (Federov), and give displacements of the intermediary axis as the "nutation", while the difference between the axis of figure and the intermediary axis is called the "diurnal nutation". I think that this separation makes for confusion. Either intermediary axis involves derivatives of the angular coordinates, and it is impossible to measure a time-derivative, since the error does not tend to 0 when the

interval between observations does. It is said that the instantaneous axis is determinable by observing through a sidereal day, but some of the nutations vary within a day by quantities larger than the error tolerated in the calculations. What is observed is the displacement of the vertical at a place relative to the stars, and for a rigid Earth the whole effect is determined by the displacement in space of the axis of figure, and there is no need for any intermediary.

If θ, ψ, ϕ are Euler's angles, so that θ is the celestial colatitude of the pole of figure and ψ its longitude, measured from west to east, we have as usual

$$\dot{\phi} + \dot{\psi}\cos\theta = \omega = \text{constant} \tag{1}$$

and the equations of motion, to the first order, for a periodic disturbance, are

$$A\ddot{\theta} + C\omega\sin\theta\,\dot{\psi} = \alpha\cos\sigma t \tag{2}$$

$$C\omega\dot{\theta} - A\sin\theta\,\ddot{\psi} = \beta\sin\sigma t. \tag{3}$$

For the fortnightly and semiannual nutations α is nearly $-\beta\cos\epsilon$, where ϵ is the mean obliquity. Put

$$\theta = \epsilon + \theta', \quad \theta' = \lambda\cos\sigma t, \quad \psi = \psi_0 + pt + \psi', \quad \psi' = \mu\sin\sigma t. \tag{4}$$

Then

$$\lambda = -\frac{C\omega\beta - A\sigma\alpha}{C^2\omega^2\sigma - A^2\sigma^3}, \quad \mu = \frac{C\omega\alpha - A\sigma\beta}{C^2\omega^2\sigma - A^2\sigma^3}. \tag{5}$$

In the elementary treatment (for instance in Tisserand's book) $\ddot{\theta}$ and $\ddot{\psi}$ in (2) (3) are neglected, giving the approximations

$$(\lambda, \mu) \doteqdot (-\beta/C\omega\sigma, \quad \alpha/C\omega\sigma). \tag{6}$$

But for the fortnightly term this introduces errors of about 1 part in 14.

The displacements of the instantaneous axis relative to the axis of figure are

$$(-\sin\theta\dot{\psi}/\omega, \quad \dot{\theta}/\omega) = \left(-\frac{\mu\sigma}{\omega}\cos\sigma t, \quad -\frac{\lambda\sigma}{\omega}\sin\sigma t\right). \tag{7}$$

Thus if λ', μ' refer to the instantaneous axis

$$(C^2\omega^2\sigma - A^2\sigma^3)\lambda' = -C\omega\beta - (C-A)\sigma\alpha + A\beta\sigma^2/\omega \tag{8}$$

$$(C^2\omega^2\sigma - A^2\sigma^3)\mu' = C\omega\alpha - (C-A)\sigma\beta - A\alpha\sigma^2/\omega. \tag{9}$$

On account of the smallness of $C-A$ the terms in σ on the right are small, and even the terms in σ^2 approximately cancel the term in σ^2 in the first factor on the left. Thus the neglect of second derivatives in the equations of motion gives the motion of the instantaneous axis with much greater accuracy than that of the axis of figure. This is pointed out by Woolard.

The displacements of the axis of angular momentum relative to that of figure are $\frac{A\mu\sigma}{C\omega}\cos\sigma t$, $-\frac{A\lambda\sigma}{C}\sin\sigma t$, and we find

$$(C^2\omega^2\sigma - A^2\sigma^3)\left(\lambda - \frac{A\mu\sigma}{C\omega}\right) = -C\omega\beta + \frac{A^2\sigma^2\beta}{C\omega} \tag{10}$$

so that the elementary theory actually gives the motion of the axis of angular momentum exactly, so far as σ is concerned. This result is given by Federov.

Woolard's method of calculating $\lambda - \lambda'$ and $\mu - \mu'$ is to rewrite by transferring second derivatives to the right side, substitute the first approximations to $\ddot{\theta}$ and $\ddot{\psi}$ on the right, and integrate. This has the effect, in comparison with (5), of removing the term $A^2\sigma^3$ in the denominator. The resulting errors of order σ^2/ω^2 of the motion are usually negligible, but not quite so for the fortnightly

motion when the calculations are done to 0″·0001, but the difference will be neglected here.

If σ is positive, λ, μ are always greater than the first approximations and have the same sign, so that the motion is direct. If negative, these statements are reversed. As Federov points out, the axis of angular momentum has one definite advantage over the instantaneous axis, since it is totally unaffected by the 14-monthly and annual variations of latitude.

Since the dynamical theory as developed by Vicente and me takes a circular motion of the pole as standard ($\alpha = -\beta$) and actually α is not quite equal to $-\beta$, it is necessary to resolve each nutation into a pair of circular movements in opposite directions.

3. Woolard's values for the axis of figure, with his two parts stated separately, are as follows.

	Obliquity (cosines)	Longitude (sines)
Principal (Ω)	9″·2100 − 0″·0010	17″·2327 − 0″·0034
Fortnightly ($2\mathbb{D}$)	0″·0884 + 0″·0059	0″·2037 + 0″·0162
Semiannual ($2\odot$)	0″·5522 + 0″·0028	1″·2729 + 0″·0075

These need an adjustment since the latest work on the solar parallax and the mass of the Moon indicates that 9″·210 should be increased to 9″·2272 or 9″·2242 according as Spencer Jones's or Rabe's parallax is adopted (Jeffreys and Vicente 1957 b, p. 172). I take the former; it requires lunar terms to be multiplied by 1·00187 and solar ones by 0·99598. I also multiply the coefficients in longitude by $\sin\epsilon = 0{\cdot}39738$ to give displacements. Then altogether the relevant terms for a rigid body are:

$$\text{Obliquity} \quad l_0 = 9''{\cdot}2262\cos\Omega + 0''{\cdot}0945\cos 2\mathbb{D} + 0''{\cdot}5528\cos 2\odot.$$
$$\text{Longitude} \quad m_0 = 6''{\cdot}8594\sin\Omega + 0''{\cdot}0875\sin 2\mathbb{D} + 0''{\cdot}5068\sin 2\odot.$$

We have to resolve these into pairs of circular motions; we have

$$\begin{aligned} l_0 + im_0 &= \theta' + i\sin\epsilon\psi' \\ &= 8''{\cdot}0428\,e^{i\Omega} + 1''{\cdot}1834\,e^{-i\Omega} \\ &\quad + 0''{\cdot}0910\,e^{2i\mathbb{D}} + 0''{\cdot}0035\,e^{-2i\mathbb{D}} \\ &\quad + 0''{\cdot}5298\,e^{2i\odot} + 0''{\cdot}0230\,e^{-2i\odot}. \end{aligned}$$

This corresponds to ζ_0 of previous papers (Jeffreys and Vicente 1957 a, b).

To derive ζ, the value with allowance for elasticity of the shell and fluidity of the core, we must multiply by the factors ζ/ζ_0 given previously, the symbol n of the previous papers being σ of the present. Then for the central particle model (factors in Jeffreys and Vicente, p. 160)

$$\begin{aligned} l + im &= 8''{\cdot}0138\,e^{i\Omega} + 1''{\cdot}1877\,e^{-i\Omega} \\ &\quad + 0''{\cdot}0934\,e^{2i\mathbb{D}} + 0''{\cdot}0038\,e^{-2i\mathbb{D}} \\ &\quad + 0''{\cdot}5483\,e^{2i\odot} + 0''{\cdot}0251\,e^{-2i\odot} \\ &= 9''{\cdot}2015\cos\Omega + 0''{\cdot}0972\cos 2\mathbb{D} + 0''{\cdot}5734\cos 2\odot \\ &\quad + i(6''{\cdot}826\sin\Omega + 0''{\cdot}0896\sin 2\mathbb{D} + 0''{\cdot}5232\sin 2\odot). \end{aligned}$$

For the Roche model (factors in Jeffreys and Vicente, p. 169)

$$\begin{aligned} l + im &= 8''{\cdot}0339\,e^{i\Omega} + 1''{\cdot}1848\,e^{-i\Omega} \\ &\quad + 0''{\cdot}0934\,e^{2i\mathbb{D}} + 0''{\cdot}0037\,e^{-2i\mathbb{D}} \\ &\quad + 0''{\cdot}5143\,e^{2i\odot} + 0''{\cdot}0260\,e^{-2i\odot} \\ &= 9''{\cdot}2187\cos\Omega + 0''{\cdot}0971\cos 2\mathbb{D} + 0''{\cdot}5403\cos 2\odot \\ &\quad + i(6''{\cdot}8491\sin\Omega + 0''{\cdot}0897\sin 2\mathbb{D} + 0''{\cdot}4883\sin 2\odot). \end{aligned}$$

We have suggested (p. 169) that for the actual core the ☊ and 2☽ terms might be interpolated, with weight 0·4 for the central particle model and 0·6 for the Roche model. Such interpolation would not be justified for the 2☉ terms because there are resonances in the neighbourhoods, but it may as well be done as an experiment. Then the interpolated values would be

$$l+im = 9''\cdot2118\cos\Omega + 0''\cdot0971\cos 2☽ + 0''\cdot5535\cos 2☉ + i(6''\cdot8399\sin\Omega + 0''\cdot0897\sin 2☽ + 0''\cdot5023\sin 2☉).$$

Federov's values (1958 b) are*

$$\theta' = (9''\cdot198 \pm 0''\cdot002)\cos\Omega + (0''\cdot0949 \pm \cdot0010)\cos 2☽ + (0''\cdot578 \pm 0''\cdot004)\cos 2☉$$

$$\sin\epsilon\psi' = (6''\cdot853 \pm 0''\cdot002)\sin\Omega + (0''\cdot0918 \pm 0''\cdot0010)\sin 2☽ + (0''\cdot0533 \pm 0''\cdot0004)\sin 2☉.$$

There is some check on the uncertainties because Federov also estimates terms giving phase shifts,

$$\theta' = (-0''\cdot001 \pm 0''\cdot002)\sin\Omega + (0''\cdot0019 \pm 0''\cdot0010)\sin 2☽$$

$$\sin\theta\psi' = (-0''\cdot008 \pm 0''\cdot002)\cos\Omega + (0''\cdot0019 \pm 0''\cdot0010)\cos 2☽.$$

For reasons already given (Jeffreys 1950, p. 466; Jeffreys and Vicente 1957 b, p. 171), it is extremely unlikely that there are any measurable phase shifts. The equilibrium amplitudes of the larger diurnal tides K and O are of the order of 10 cm, and even if the phase shift was $\frac{1}{2}\pi$ they could only produce couples of the order of 10^{-5} of the nutational couples; and the evidence of tidal friction shows that the phase shift cannot be more than a fraction of a degree. Then it is reasonable to use the estimates of the damping terms to give an additional estimate of uncertainty. With weight 1 for the ☊ terms and 2 for the 2☽ terms, on account of the different numbers of observations, the standard error would be 0″·0037 for the ☊ terms and 0″·0027 for the 2☽ terms. These are on only four degrees of freedom but at any rate suggest that Federov's uncertainties may be a little too low on account of correlation of errors.

The cos ☊ term in the obliquity is in agreement with the central particle model, but not with the Roche model or the interpolated model. On the other hand the sin ☊ term in the longitude agrees better with the Roche model.

With the increased estimate of uncertainty the sin 2☽ terms agree with either model.

The observations are affected by the tidal deflexion of the vertical. The value for a rigid Earth is multiplied by the factor $1+k-l$ (where l will not be confused with the direction cosine). Its theoretical values corresponding to components considered here are as follows:

	C.P. model	Roche model
−2☽	1·162	1·188
−2☉	1·134	1·226
☊	1·119	1·161
−☊	1·121	1·163
2☉	1·149	1·180
2☽	1·160	1·183

* A mistake in copying has affected the 2☽ terms. I give here revised values communicated to me by Federov in a letter.

Federov has applied a correction using the factor 1·1, which is a little too small, but as the whole effect is only in the third decimal (1958 a, p. 86) the difference is unlikely to be important.

In any case the agreement between theory and observation has been much improved, though it is still not quite satisfactory. It should be noticed that the different behaviour of the obliquity and longitude terms is quite fundamental. It depends on the fact that the steady state solution is exact for speed 0, for any model; and for speeds $\pm\sigma$, with σ very small, the correcting factors must be of the form $1 \pm p$. No change of model could account for the fact that each component of the Ω terms agrees with one model and not with the other. It is in any case curious that three comparisons agree better with the central particle model, and one better with the Roche model, since the former makes no allowance for the compressibility of the Earth's core, which is very well known, whereas the density of the inner core is still in much doubt. Compressibility alone would produce an increase of density towards the centre comparable with that assumed in the Roche model, and its effects cannot be negligible.

Most correlations between errors would be likely to affect both the components, and also both phases for each component. It seems likely therefore that the use of the anomalies of phase to estimate an uncertainty is valid. In addition there is an unexplained systematic variation during the night, which was discussed at the Moscow I.A.U. meeting (I was afterwards reminded of it by Dr Atkinson). This might conceivably contribute to the semiannual terms but hardly to the 19 yearly ones.

It may be recalled that both models, with a correction for the effect of the ocean, give almost the same value for the free period, and this agrees with observation. The main object of the work has been to test whether Earth models consistent with the geophysical data are also consistent with the astronomical ones. Agreement would give a comprehensive check on the Earth models. The actual agreement is not quite satisfactory, but much better than in any previous comparison; and the discrepancies that remain are of a sort that could not, apparently, be removed by any change of the Earth model at all.

160 *Huntingdon Road,*
Cambridge:
1958 *December* 10.

References

E. P. Federov, 1958 a. Nutacheye e venuzhdennie dvezhenye polusov zemle, Acad. Sci. Ukraine, C.C.P.
—— 1958 b. Nutation as derived from latitude observations, I.A.U. Moscow (mimeographed).
J. Jackson, 1930. *M.N.*, **90**, 733–742.
H. Jeffreys, 1948. *M.N.*, **108**, 206–209.
—— 1950. *M.N.*, **110**, 460–466.
—— and R. O. Vicente, 1957 a, *M.N.*, **117**, 142–161; 1957 b, *M.N.*, **117**, 162–173.
H. Spencer Jones, 1941. *M.N.*, **101**, 365.
H. Poincaré, 1910. *Bull. Astr.*, **27**, 321–356.
H. Takeuchi, 1950. *Trans. Amer. Geophys. Un.*, **31**, 651–689.
E. W. Woolard, 1953. *Astr. Pap. Amer. Eph.*, **15**, Part I, 1–165.

RADIATIVE RECOMBINATION OF HYDROGENIC IONS

M. J. Seaton

(Received 1959 February 3)

Summary

Using the first three terms in the asymptotic expansion of the Kramers-Gaunt factor, calculations are made for the rate of recombination and for the mean kinetic energy of the recombining electrons.

For the study of the recombination spectra of gaseous nebulae one requires the rate coefficients for radiative recombination to individual quantum states of hydrogenic ions and for the study of the ionization equilibria one requires the radiative recombination rates summed over all quantum states (**1**). Further, for the study of the thermal balance in nebulae, it is necessary to calculate the rate of loss of electron kinetic energy due to recombination processes (**2, 3**). For hydrogenic ions all these quantities may be calculated exactly but the calculations become increasingly difficult with increasing n, where n is the principal quantum number. If errors as great as 20 per cent are of no importance one may put the Kramers–Gaunt g-factor equal to unity and hence obtain relatively simple expressions. A considerable improvement is obtained on using the asymptotic expansion of the g-factor, as derived by Menzel and Pekeris (**4**) and corrected by Burgess (**5**). From the expansion of g we obtain asymptotic expansions which enable the rate coefficients to be calculated with errors which will not exceed 2 per cent for temperatures of order 10^4 °K or less but which may be greater for temperatures of order 10^6 °K. We present a systematic tabulation of the various functions which occur in these asymptotic expansions.

1. *Coefficients for recombination to level n.*—Let $\alpha_n(Z, T)$ be the rate coefficient for radiative recombination to level n of a hydrogenic ion, Z being the nuclear charge and T the kinetic temperature; the number of recombinations on n per unit volume per unit time is then $\alpha_n N_e N_+$. The recombination coefficient is given by

$$\alpha_n(Z,T)=\frac{1}{c^2}\left(\frac{2}{\pi}\right)^{1/2}(mkT)^{-3/2}\,2n^2e^{I_n/kT}\int_{I_n}^{\infty}(h\nu)^2e^{-h\nu/kT}a_n(Z,h\nu)d(h\nu). \quad (1)$$

where

$$I_n=\frac{hRcZ^2}{n^2} \quad (2)$$

is the threshold ionization energy for level n and R is the Rydberg wave number. The cross-section for photo-ionization from level n is

$$a_n(Z,h\nu)=\frac{2^6\alpha\pi a_0^{\,2}}{3\sqrt{3}}\frac{n}{Z^2}(1+n^2\epsilon)^{-3}g_{II}(n,\epsilon) \quad (3)$$

where α is the fine-structure constant, a_0 the Bohr radius and

$$h\nu=hRcZ^2\left(\frac{1}{n^2}+\epsilon\right). \quad (4)$$

Note that the energy of the ejected electron is $Z^2\epsilon$ in Rydberg units (13·60 eV). The Kramers–Gaunt factor g_{II} in (3) is of order unity.

From equations (1) to (4) we obtain

$$\alpha_n(Z,T)=\mathscr{D}Z\frac{\lambda^{1/2}}{n}x_nS_n(\lambda) \tag{5}$$

where

$$\mathscr{D}=\frac{2^6}{3}\left(\frac{\pi}{3}\right)^{1/2}\alpha^4ca_0^2$$

$$=5{\cdot}197\times10^{-14}\ \text{cm}^3\ \text{sec}^{-1}, \tag{6}$$

$$\lambda=\frac{hRcZ^2}{kT}$$

$$=157890\frac{Z^2}{T}\qquad(T\text{ in }^\circ\text{K}), \tag{7}$$

$$x_n=\lambda/n^2 \tag{8}$$

and

$$S_n(\lambda)=\int_0^\infty\frac{g_{II}(n,\epsilon)e^{-x_nu}}{(1+u)}\,du \tag{9}$$

with $u=n^2\epsilon$.

The asymptotic expansion for g_{II} is (**4, 5**)

$$g_{II}(n,\epsilon)=1+0{\cdot}1728n^{-2/3}(u+1)^{-2/3}(u-1)$$
$$-0{\cdot}0496n^{-4/3}(u+1)^{-4/3}(u^2+\tfrac{4}{3}u+1)+\ldots. \tag{10}$$

Substitution of (10) in (9) gives

$$S_n(\lambda)=S^{(0)}(x_n)+\lambda^{-1/3}S^{(1)}(x_n)+\lambda^{-2/3}S^{(2)}(x_n)+\ldots \tag{11}$$

where

$$S^{(0)}(x)=e^x\mathscr{E}i(x), \tag{12}$$

$$S^{(1)}(x)=0{\cdot}1728x^{1/3}X_1(x), \tag{13}$$

$$S^{(2)}(x)=-0{\cdot}0496x^{2/3}X_2(x), \tag{14}$$

and

$$\mathscr{E}i(x)=\int_x^\infty\frac{e^{-v}}{v}\,dv, \tag{15}$$

$$X_1(x)=\int_0^\infty(u+1)^{-5/3}(u-1)e^{-xu}\,du, \tag{16}$$

$$X_2(x)=\int_0^\infty(u+1)^{-7/3}(u^2+\tfrac{4}{3}u+1)e^{-xu}\,du. \tag{17}$$

Extensive tables of the exponential integral, $\mathscr{E}i(x)$, are available (**6**). For all finite x

$$S^{(0)}(x)=e^x\left\{-\ln x-\gamma+\frac{x}{1\cdot1!}-\frac{x^2}{2\cdot2!}+\frac{x^3}{3\cdot3!}-\ldots\right\} \tag{18}$$

where $\gamma=0{\cdot}5772\ldots$ is the Euler–Mascheroni constant. In the limit of large x, $S^{(0)}$ has asymptotic form

$$S^{(0)}(x)\underset{x\to\infty}{\sim}\frac{1}{x}\left\{1-\frac{1!}{x}+\frac{2!}{x^2}-\frac{3!}{x^3}+\ldots\right\}. \tag{19}$$

TABLE I

x	$xS^{(0)}$	$xS^{(1)}$	$xS^{(2)}$	x	$xS^{(0)}$	$xS^{(1)}$	$xS^{(2)}$	x	$xS^{(0)}$	$xS^{(1)}$	$xS^{(2)}$
0·020	·06845	·00417	−·00120	0·20	·2987	·0074	−·0095	2·0	·7226	−·0882	−·0625
·022	·07335	·00444	−·00131	·22	·3140	·0068	−·0103	2·2	·7384	−·0972	−·0674
·024	·07808	·00469	−·00142	·24	·3284	·0060	−·0110	2·4	·7524	−·1058	−·0722
·026	·08268	·00493	−·00153	·26	·3419	·0053	−·0118	2·6	·7649	−·1141	−·0768
·028	·08714	·00516	−·00164	·28	·3547	·0044	−·0126	2·8	·7761	−·1220	−·0814
·030	·09148	·00538	−·00175	·30	·3668	·0035	−·0133	3·0	·7862	−·1295	−·0859
·032	·09570	·00558	−·00186	·32	·3783	·0025	−·0141	3·2	·7955	−·1368	−·0904
·034	·09982	·00578	−·00197	·34	·3892	·0016	−·0148	3·4	·8039	−·1438	−·0947
·036	·10385	·00597	−·00207	·36	·3996	+·0005	−·0155	3·6	·8117	−·1506	−·0989
·038	·10778	·00614	−·00218	·38	·4096	−·0005	−·0162	3·8	·8188	−·1571	−·1031
·040	·11163	·00631	−·00228	·40	·4191	−·0016	−·0170	4·0	·8254	−·1634	−·1072
·045	·1209	·0067	−·0025	·45	·4413	−·0044	−·0187	4·5	·8399	−·1784	−·1174
·050	·1297	·0070	−·0028	·50	·4615	−·0072	−·0204	5·0	·8521	−·1923	−·1272
·055	·1382	·0073	−·0030	·55	·4799	−·0101	−·0221	5·5	·8626	−·2053	−·1367
·060	·1462	·0076	−·0033	·60	·4968	−·0130	−·0237	6·0	·8716	−·2174	−·1460
·065	·1540	·0078	−·0035	·65	·5124	−·0160	−·0253	6·5	·8795	−·2289	−·1550
·070	·1615	·0080	−·0038	·70	·5269	−·0190	−·0269	7·0	·8865	−·2397	−·1638
·075	·1687	·0082	−·0040	·75	·5404	−·0220	−·0284	7·5	·8927	−·2499	−·1723
·080	·1757	·0083	−·0043	·80	·5530	−·0250	−·0299	8·0	·8982	−·2596	−·1807
·085	·1824	·0085	−·0045	·85	·5648	−·0279	−·0314	8·5	·9032	−·2689	−·1890
·090	·1889	·0086	−·0047	·90	·5759	−·0308	−·0329	9·0	·9077	−·2777	−·1970
·095	·1953	·0087	−·0050	·95	·5864	−·0337	−·0344	9·5	·9118	−·2862	−·2049
·100	·2015	·0087	−·0052	1·00	·5963	−·0366	−·0359	10·0	·9156	−·2944	−·2127
·11	·2133	·0088	−·0056	1·1	·6146	−·0422	−·0388	11	·9223	−·3099	−·228
·12	·2245	·0088	−·0061	1·2	·6311	−·0478	−·0416	12	·9279	−·3242	−·243
·13	·2352	·0088	−·0065	1·3	·6461	−·0532	−·0444	13	·9328	−·3376	−·257
·14	·2454	·0087	−·0070	1·4	·6598	−·0586	−·0471	14	·9370	−·3502	−·272
·15	·2552	·0086	−·0074	1·5	·6724	−·0638	−·0497	15	·9408	−·3622	−·285
·16	·2646	·0084	−·0078	1·6	·6840	−·0689	−·0523	16	·9441	−·3736	−·299
·17	·2736	·0082	−·0082	1·7	·6947	−·0739	−·0549	17	·9471	−·3844	−·312
·18	·2823	·0080	−·0086	1·8	·7047	−·0788	−·0575	18	·9498	−·3948	−·325
·19	·2906	·0077	−·0091	1·9	·7140	−·0835	−·0600	19	·9522	−·4047	−·337
·20	·2987	·0074	−·0095	2·0	·7226	−·0882	−·0625	20	·9544	−·4147	−·350

The integrals X_1 and X_2 may be expressed in terms of confluent hypergeometric functions (7). We obtain

$$X_1(x) = -3 + (1+3x)\Psi(1, \tfrac{4}{3}; x) \tag{20}$$

and

$$X_2(x) = -\tfrac{3}{2}(1+x) + (1+2x+\tfrac{3}{2}x^2)\Psi(1, \tfrac{5}{3}; x) \tag{21}$$

where

$$(c-1)\Psi(1, c; x) = \Gamma(c)x^{1-c}e^x - \Phi(1, c; x) \tag{22}$$

and where the series

$$\Phi(1, c; x) = 1 + \frac{x}{c} + \frac{x^2}{c(c+1)} + \ldots \tag{23}$$

converges for all finite x. In the limit of large x,

$$\Psi(1, c; x) \underset{x\to\infty}{\sim} \left\{1 - \frac{(2-c)}{x} + \frac{(2-c)(3-c)}{x^2} - \ldots\right\}. \tag{24}$$

The functions X_1 and X_2 have been evaluated using (23) for $x \leqslant 2$, numerical integration for $2 \leqslant x \leqslant 10$ and the asymptotic expansion (24) for $x \geqslant 10$. Table I gives $xS^{(0)}$, $xS^{(1)}$ and $xS^{(2)}$ for $0{\cdot}02 \leqslant x \leqslant 20$. The intervals in x are such that linear interpolation will introduce errors no greater than 2 in the last significant figure. To the accuracy of Table I, for small x,

$$\left.\begin{aligned} xS^{(0)} &= x\,e^x\{-\ln x - 0{\cdot}5772 + x\} \\ xS^{(1)} &= 0{\cdot}4629x(1+4x) - 1{\cdot}0368x^{4/3}\left(1 + \frac{15}{8}x\right) \\ xS^{(2)} &= -0{\cdot}0672x(1+3x) + 0{\cdot}1488x^{5/3}\left(1 + \frac{9}{5}x\right) \end{aligned}\right\} \quad x \leqslant 0{\cdot}02 \tag{25}$$

and for large x,

$$\left.\begin{aligned} xS^{(0)} &= 1 - \frac{1!}{x} + \frac{2!}{x^2} - \frac{3!}{x^3} + \frac{4!}{x^4}, \\ xS^{(1)} &= -0{\cdot}1728x^{1/3}\left\{1 - \frac{8}{(3x)} + \frac{70}{(3x)^2} - \frac{800}{(3x)^3} + \frac{11440}{(3x)^4}\right\}, \\ xS^{(2)} &= -0{\cdot}0496x^{2/3}\left\{1 - \frac{3}{(3x)} + \frac{32}{(3x)^2} - \frac{448}{(3x)^3}\right\} \end{aligned}\right\} \quad x \geqslant 20. \tag{26}$$

2. *Total recombination coefficients.*—The total rate coefficient for radiative recombination is

$$\alpha_{\text{tot}} = \sum_{n'=1}^{\infty} \alpha_{n'}. \tag{27}$$

For large n' the sum may be replaced by an integral. From

$$\sum_{n'=n}^{\infty} \alpha_{n'} \simeq \tfrac{1}{2}\alpha_n + \int_n^{\infty} \alpha_{n'}\,dn' \tag{28}$$

we obtain

$$\sum_{n'=n}^{\infty} \alpha_{n'} \simeq \tfrac{1}{2}\mathscr{D}Z\lambda^{1/2}\left\{\frac{x_n}{n}S_n(\lambda) + \sigma_n(\lambda)\right\} \tag{29}$$

where

$$\sigma_n(\lambda) = \int_0^{x_n} S_{n'}(\lambda)\,dx_{n'} \tag{30}$$

and, using (11),

$$\sigma_n(\lambda) = \sigma^{(0)}(x_n) + \lambda^{-1/3}\sigma^{(1)}(x_n) + \lambda^{-2/3}\sigma^{(2)}(x_n) + \ldots \tag{31}$$

TABLE II

x	$\sigma^{(0)}$	$\sigma^{(1)}$	$\sigma^{(2)}$	x	$\sigma^{(0)}$	$\sigma^{(1)}$	$\sigma^{(2)}$	x	$\sigma^{(0)}$	$\sigma^{(1)}$	$\sigma^{(2)}$
0·020	·0877	·0053	−·0012	0·20	·4611	·0218	−·0106	2·0	1·632	−·032	−·076
·022	·0944	·0057	−·0014	·22	·4903	·0225	−·0115	2·2	1·701	−·041	−·082
·024	·1010	·0061	−·0015	·24	·5182	·0231	−·0125	2·4	1·766	−·050	−·088
·026	·1074	·0065	−·0016	·26	·5451	·0235	−·0134	2·6	1·827	−·059	−·094
·028	·1137	·0069	−·0017	·28	·5709	·0239	−·0143	2·8	1·884	−·068	−·100
·030	·1199	·0073	−·0018	·30	·5958	·0242	−·0152	3·0	1·938	−·076	−·106
·032	·1259	·0076	−·0020	·32	·6198	·0244	−·0161	3·2	1·989	−·085	−·112
·034	·1318	·0080	−·0021	·34	·6431	·0245	−·0169	3·4	2·037	−·093	−·117
·036	·1376	·0083	−·0022	·36	·6656	·0245	−·0178	3·6	2·084	−·102	−·123
·038	·1434	·0086	−·0023	·38	·6875	·0245	−·0187	3·8	2·128	−·110	−·128
·040	·1490	·0089	−·0024	·40	·7088	·0245	−·0195	4·0	2·170	−·118	−·134
·045	·1627	·0097	−·0027	·45	·7595	·0241	−·0216	4·5	2·268	−·138	−·147
·050	·1759	·0104	−·0030	·50	·8070	·0235	−·0237	5·0	2·357	−·158	−·160
·055	·1886	·0111	−·0033	·55	·8519	·0227	−·0257	5·5	2·439	−·177	−·172
·060	·2010	·0118	−·0035	·60	·8944	·0217	−·0277	6·0	2·514	−·195	−·185
·065	·2130	·0124	−·0038	·65	·9348	·0206	−·0296	6·5	2·584	−·213	−·197
·070	·2247	·0130	−·0041	·70	·9733	·0193	−·0316	7·0	2·650	−·230	−·208
·075	·2361	·0135	−·0044	·75	1·0101	·0179	−·0335	7·5	2·711	−·247	−·220
·080	·2472	·0141	−·0046	·80	1·0454	·0164	−·0354	8·0	2·769	−·264	−·231
·085	·2581	·0146	−·0049	·85	1·0792	·0148	−·0372	8·5	2·824	−·280	−·243
·090	·2687	·0150	−·0051	·90	1·1119	·0131	−·0391	9·0	2·875	−·295	−·254
·095	·2791	·0155	−·0054	·95	1·1433	·0113	−·0409	9·5	2·924	−·311	−·268
·100	·2892	·0160	−·0057	1·00	1·1736	·0095	−·0427	10·0	2·971	−·326	−·275
·11	·3090	·0168	−·0062	1·1	1·231	·006	−·046	11	3·059	−·354	−·296
·12	·3281	·0176	−·0067	1·2	1·285	+·002	−·050	12	3·139	−·382	−·317
·13	·3464	·0183	−·0072	1·3	1·337	−·002	−·053	13	3·214	−·408	−·337
·14	·3642	·0189	−·0077	1·4	1·385	−·006	−·057	14	3·283	−·434	−·356
·15	·3815	·0195	−·0082	1·5	1·431	−·011	−·060	15	3·348	−·459	−·375
·16	·3983	·0201	−·0087	1·6	1·475	−·015	−·063	16	3·409	−·482	−·394
·17	·4146	·0206	−·0092	1·7	1·517	−·019	−·067	17	3·466	−·505	−·413
·18	·4305	·0210	−·0097	1·8	1·557	−·024	−·070	18	3·520	−·528	−·431
·19	·4460	·0214	−·0101	1·9	1·595	−·028	−·073	19	3·572	−·549	−·449
·20	·4611	·0218	−·0106	2·0	1·632	−·032	−·076	20	3·621	−·570	−·467

where

$$\sigma^{(p)}(x)=\int_0^x S^{(p)}(x')\,dx'. \tag{32}$$

Using (18) it may be shown that

$$\sigma^{(0)}(x)=S^{(0)}(x)+\ln x+\gamma. \tag{33}$$

The functions $\sigma^{(0)}$, $\sigma^{(1)}$ and $\sigma^{(2)}$ are given in Table II for $0{\cdot}02\leqslant x\leqslant 20$. For small x,

$$\left.\begin{aligned}\sigma^{(0)}&=x\left\{\left(1+\frac{1}{2}x\right)(-\ln x-0{\cdot}5772)+\left(1+\frac{3}{4}x\right)\right\},\\ \sigma^{(1)}&=x\left\{0{\cdot}4629(1+2x)-0{\cdot}7776x^{1/3}\left(1+\frac{15}{14}x\right)\right\},\\ \sigma^{(2)}&=x\left\{-0{\cdot}0672\left(1+\frac{3}{2}x\right)+0{\cdot}0893x^{2/3}\left(1+\frac{9}{8}x\right)\right\}\end{aligned}\right\}\quad x\leqslant 0{\cdot}02 \tag{34}$$

and for large x,

$$\left.\begin{aligned}\sigma^{(0)}&=S^{(0)}+\ln x+0{\cdot}5772,\\ \sigma^{(1)}&=0{\cdot}926-0{\cdot}5184x^{1/3}\left\{1+\frac{4}{(3x)}-\frac{14}{(3x)^2}+\frac{100}{(3x)^3}\right\},\\ \sigma^{(2)}&=0{\cdot}134-0{\cdot}0744x^{2/3}\left\{1+\frac{6}{(3x)}-\frac{16}{(3x)^2}+\frac{128}{(3x)^3}\right\},\end{aligned}\right\}\quad x\geqslant 20. \tag{35}$$

Table III gives values of x_1S_1, $x_2S_2/2$ and $\sum_1^\infty x_nS_n/n$ for various values of (T/Z^2).

As compared with the results obtained using the asymptotic expansion, the expression

$$\alpha_{\text{tot}}=\mathscr{Q}Z\lambda^{1/2}\{0{\cdot}4288+\tfrac{1}{2}\ln\lambda+0{\cdot}469\lambda^{-1/3}\} \tag{36}$$

is in error by less than 0·5 per cent for $(T/Z^2)\leqslant 10^5$, by 3 per cent for $(T/Z^2)=10^6$ and by 31 per cent for $(T/Z^2)=5\times 10^6$ °K.

TABLE III

(T/Z^2) °K	x_1S_1	$\frac{x_2S_2}{2}$	$\sum_{n=1}^{\infty}\frac{x_nS_n}{n}$
10^3	0·775	0·427	3·046
5×10^3	0·763	0·399	2·305
10^4	0·748	0·371	1·998
5×10^4	0·660	0·260	1·324
10^5	0·585	0·202	1·055
5×10^5	0·350	0·089	0·529
10^6	0·252	0·056	0·364
5×10^6	0·094	0·018	0·127

3. *The energy of electrons recombining on level n.*—Let $kT\beta_nN_eN_+$ be the kinetic energy, per unit volume per unit time, of the electrons recombining on level n. We obtain

$$\beta_n(Z,T)=\mathscr{Q}Z\frac{\lambda^{1/2}}{n}x_n^2R_n(\lambda) \tag{37}$$

where

$$R_n(\lambda)=\int_0^\infty \frac{g_{\text{II}}\,\mathrm{e}^{-x_nu}}{(1+u)}u\,du. \tag{38}$$

Using (10) we have

$$R_n(\lambda)=R^{(0)}(x_n)+\lambda^{-1/3}R^{(1)}(x_n)+\lambda^{-2/3}R^{(2)}(x_n) \tag{39}$$

TABLE IV

x	$xR^{(1)}$	$xR^{(2)}$	$\rho^{(1)}$	$\rho^{(2)}$	x	$xR^{(1)}$	$xR^{(2)}$	$\rho^{(1)}$	$\rho^{(2)}$
0·02	·139	−·044	·0029	−·0009	1·0	+·008	−·031	·054	−·035
·03	·134	−·043	·0043	−·0013	1·5	−·008	−·029	·054	−·050
·04	·129	−·043	·0056	−·0018	2·0	−·013	−·027	·049	−·064
·05	·124	−·042	·0069	−·0022	2·5	−·017	−·026	·041	−·078
·06	·120	−·042	·0081	−·0026	3·0	−·0204	−·0255	·032	−·091
·07	·116	−·042	·0093	−·0031					
·08	·112	−·041	·0104	−·0035	4	−·0234	−·0240	+·010	−·115
·09	·108	−·041	·0115	−·0039	5	−·0245	−·0230	−·014	−·139
·10	·105	−·041	·0126	−·0043	6	−·0247	−·0223	−·038	−·161
					7	−·0247	−·0216	−·063	−·183
·12	·099	−·040	·0146	−·0051	8	−·0244	−·0210	−·088	−·205
·14	·093	−·040	·0165	−·0059	9	−·0238	−·0205	−·112	−·225
·16	·088	−·039	·0184	−·0067	10	−·0232	−·0199	−·135	−·246
·18	·084	−·039	·0201	−·0075					
·20	·080	−·039	·0217	−·0083	12	−·0221	−·0190	−·181	−·285
					14	−·0211	−·0183	−·224	−·322
·25	·070	−·038	·0255	−·0102	16	−·0201	−·0177	−·265	−·359
·3	·062	−·037	·0288	−·0121	18	−·0191	−·0172	−·304	−·393
·35	·055	−·036	·0317	−·0139	20	−·0183	−·0168	−·342	−·427
·4	·049	−·035	·0343	−·0157					
·5	·038	−·034	·0377	−·0191					
·6	·030	−·034	·0411	−·0225					
·7	·023	−·033	·0445	−·0259					
·8	·018	−·032	·0477	−·0291					
·9	·013	−·031	·0509	−·0323					
1·0	+·008	−·031	·0540	−·0354					

where

$$xR^{(0)} = 1 - xS^{(0)}, \tag{40}$$

$$xR^{(1)} = -0{\cdot}1728x^{4/3}\frac{d}{dx}X_1(x), \tag{41}$$

$$xR^{(2)} = 0{\cdot}0496x^{5/3}\frac{d}{dx}X_2(x). \tag{42}$$

The functions $R^{(1)}$ and $R^{(2)}$ are given in Table IV for $0{\cdot}02 \leqslant x \leqslant 20$. For small x,

$$\left.\begin{aligned} xR^{(1)} &= 0{\cdot}1543(1-8x) + 1{\cdot}944x^{4/3} \\ xR^{(2)} &= -0{\cdot}0448\left(1-\frac{3}{2}x\right) - 0{\cdot}268x^{5/3} \end{aligned}\right\} \quad x \leqslant 0{\cdot}02, \tag{43}$$

and for large x,

$$\left.\begin{aligned} xR^{(1)} &= -0{\cdot}1728x^{-2/3}\left\{1 - \frac{16}{(3x)} + \frac{210}{(3x)^2} - \frac{3200}{(3x)^3} + \frac{57200}{(3x)^4}\right\} \\ xR^{(2)} &= -0{\cdot}0496x^{-1/3}\left\{1 - \frac{6}{(3x)} + \frac{96}{(3x)^2} - \frac{1792}{(3x)^3}\right\} \end{aligned}\right\} \quad x \geqslant 20. \tag{44}$$

For the total kinetic energy loss due to recombination we require

$$\beta_{\text{tot}} = \sum_{n'=1}^{\infty} \beta_{n'}. \tag{45}$$

For large n,

$$\sum_{n'=n}^{\infty} \beta_{n'} \simeq \tfrac{1}{2}\beta_n + \int_n^{\infty} \beta_{n'}\, dn' = \tfrac{1}{2}\mathscr{D}Z\lambda^{1/2}\left\{\frac{x_n^2}{n} R_n(\lambda) + \rho_n(\lambda)\right\} \tag{46}$$

where

$$\rho_n(\lambda) = \rho^{(0)}(x_n) + \lambda^{-1/3}\rho^{(1)}(x_n) + \lambda^{-2/3}\rho^{(2)}(x_n) + \ldots \tag{47}$$

and

$$\rho^{(p)}(x) = \int_0^x x' R^{(p)}(x')\, dx'. \tag{48}$$

We obtain

$$\rho^{(0)}(x) = (1-x)S^{(0)}(x) + \ln x + \gamma = \sigma^{(0)}(x) - xS^{(0)}(x). \tag{49}$$

The functions $\rho^{(1)}$ and $\rho^{(2)}$ are given in Table IV for $0{\cdot}02 \leqslant x \leqslant 20$. For small x,

$$\left.\begin{aligned} \rho^{(1)} &= 0{\cdot}1543x(1-4x) + 0{\cdot}833x^{7/3} \\ \rho^{(2)} &= -0{\cdot}0488x\left(1 - \tfrac{3}{4}x\right) \end{aligned}\right\} \quad x \leqslant 0{\cdot}02, \tag{50}$$

and for large x,

$$\left.\begin{aligned} \rho^{(1)} &= 1{\cdot}239 - 0{\cdot}5184x^{1/3}\left\{1 + \frac{8}{(3x)} - \frac{42}{(3x)^2} + \frac{400}{(3x)^3}\right\}, \\ \rho^{(2)} &= 0{\cdot}225 - 0{\cdot}0744x^{2/3}\left\{1 + \frac{12}{(3x)} - \frac{48}{(3x)^2} + \frac{512}{(3x)^3}\right\} \end{aligned}\right\} \quad x \geqslant 20. \tag{51}$$

Table V gives values of $x_1^2 R_1$ and $\sum_1^{\infty} x_n^2 R_n/n$ for various values of (T/Z^2). As compared with the results obtained using the asymptotic expansion, the expression

$$\beta_{\text{tot}} = \mathscr{D}Z\lambda^{1/2}\left\{-0{\cdot}0713 + \tfrac{1}{2}\ln\lambda + 0{\cdot}640\lambda^{-1/3}\right\} \tag{52}$$

is in error by less than 1 per cent for $(T/Z^2) < 5 \times 10^4$ and by 4 per cent for $(T/Z^2) = 10^5$ °K.

TABLE V

(T/Z^2) °K	$x_1^2 R_1$	$\sum_{n=1}^{\infty} \frac{x_n^2 R_n}{n}$
10^3	0·772	2·578
5×10^3	0·748	1·857
10^4	0·722	1·564
5×10^4	0·570	0·926
10^5	0·457	0·679

4. *Accuracy of the calculations.*—The asymptotic expansions will be accurate if the third term is much smaller than the sum of the first two terms. For a given temperature the accuracy will improve with increasing n and, for a given n, the accuracy will improve with decreasing temperature.

In Table VI some values of $x_n S_n$ calculated from the asymptotic expansion are compared with the results of more accurate calculations made by Burgess (**5**); the results of Burgess are exact in the limit of $T \to 0$. For $(T/Z^2) \leqslant 2 \times 10^4$ °K the maximum error in α_1 will be 2·5 per cent and the errors in α_n for $n > 1$ will be smaller than 1 per cent.

TABLE VI

(T/Z^2) (°K)	n	$x_nS^{(0)}(x_n)$	$\lambda-\frac{1}{2}x_nS^{(1)}(x_n)$	$\lambda-\frac{1}{2}x_nS^{(2)}(x_n)$	$x_nS_n(\lambda)$ (Asymptotic)	$x_nS_n(\lambda)$ (Burgess)	Difference
0	1	1	−·1728	−·0496	·7776	·7973	+·0197
	2	1	−·1089	−·0197	·8714	·8763	+·0048
	3	1	−·0831	−·0115	·9054	·9075	+·0021
10^4	1	·9434	−·1480	−·0470	·748	·763	+·015
	2	·8237	−·0645	−·0169	·742	·748	+·006
	3	·7001	−·0305	−·0089	·661	·660	−·001
2×10^4	1	·8970	−·1293	−·0451	·723	·726	+·003
	2	·7203	−·0436	−·0156	·661	·663	+·002
	3	·5708	−·0148	−·0081	·548	·549	+·001

From the magnitudes of the various terms in the expansions, it is estimated that our results for α_{tot} may be in error by about 10 per cent for $(T/Z^2)=10^6$ and by about 25 per cent for $(T/Z^2)=5\times10^6$ °K.

University College,
London, W.C.1:
1959 *February 2.*

References

(1) J. G. Baker and D. H. Menzel, *Ap. J.*, **88**, 52, 1938.
(2) J. G. Baker, D. H. Menzel and L. H. Aller, *Ap. J.*, **88**, 422, 1938.
(3) L. Spitzer, *Ap. J.*, **107**, 6, 1948.
(4) D. H. Menzel and C. L. Pekeris, *M.N.*, **96**, 77, 1935.
(5) A. Burgess, *M.N.*, **118**, 477, 1958.
(6) *Tables of sine, cosine and exponential integrals*, Vol. 1, Federal Works Agency, New York, 1940.
(7) Bateman Manuscript Project, *Higher Transcendental Functions*, Vol. 1, Ch. VI, McGraw Hill, 1953.

THE SOLUTION OF CAPTURE-CASCADE EQUATIONS FOR HYDROGEN

M. J. Seaton

(Received 1959 February 3)

Summary

Calculations are made for $T=2{\cdot}5\times10^3$, 5×10^3, 1×10^4 and 2×10^4 °K taking an infinite number of levels into account but assuming that $b_{nl}=[(2l+1)/n^2]\,b_n$. The results obtained by Baker and Menzel are shown to be in error by about 5 per cent for Case A and 20 per cent for Case B.

An improved method of calculation results from the introduction of the cascade matrix, the elements $C_{n'n}$ giving the total probability of the $n'\rightarrow n$ transition when all cascade routes are taken into account.

---

1. *Introduction.*—In Case A of Baker and Menzel (**1**), valid for an optically thin nebula, it is assumed that the excited states of hydrogen are populated by radiative capture and by cascade from higher states and that they are depopulated by radiative transitions to all lower states. In Case B, valid for a nebula which is optically thick in the Lyman lines, it is assumed that the rate of depopulation of excited states by emission of Lyman lines is exactly equal to the rate of population by absorption of Lyman lines. In Case B, for all $n>2$, one may equate the rate of population by capture and cascade to the rate of radiative transitions to all lower states n'' with $n''\geqslant 2$. For both cases the equilibrium equations may be written

$$N_eN_+\alpha_{nl}+\sum_{n'l'}N_{n'l'}A_{n'l',\,nl}=N_{nl}A_{nl} \tag{1}$$

where n' is greater than n. The number of electrons per unit volume is N_e, the number of protons N_+ and the number of hydrogen atoms in quantum states nl is N_{nl}. The radiative recombination coefficient for nl is α_{nl} and the radiative transition probability for $n'l'\rightarrow nl$ is $A_{n'l',\,nl}$. The total radiative transition probability for nl is

$$A_{nl}=\sum_{n''=n_0}^{n-1}\sum_{l''=l\pm1}A_{nl,\,n''l''} \tag{2}$$

where* $n_0=1$ for Case A and $n_0=2$ for Case B.

In conditions of thermodynamic equilibrium all quantum states of the same energy have equal populations. We then have

$$N_{nl}=\frac{(2l+1)}{n^2}N_n \tag{3}$$

where

$$N_n=\sum_l N_{nl}. \tag{4}$$

* It is, of course, to be understood that $A_{nl,\,n''l''}$ is identically zero for $n''<(l''+1)$; hence it is only for $l=1$ that the A_{nl} are different for Cases A and B.

Although the solutions of (1) will not satisfy (3) we consider the approximation of simplifying (1) by assuming (3). We then have, in place of (1),

$$N_e N_+ \alpha_n + \sum_{n'=n+1}^{\infty} N_{n'} A_{n',n} = N_n A_n \tag{5}$$

where

$$\alpha_n = \sum_l \alpha_{nl}, \tag{6}$$

$$A_{n',n} = \frac{1}{n^2} \sum_{l'l} (2l'+1) A_{n'l',nl}, \tag{7}$$

and

$$A_n = \sum_{n'=n_0}^{n-1} A_{n,n'} \quad \begin{pmatrix} n_0 = 1 \text{ for Case A} \\ n_0 = 2 \text{ for Case B} \end{pmatrix}. \tag{8}$$

Baker and Menzel (1) have considered equations (5) with an infinite number of levels. Burgess (2) has obtained solutions of the equations (1) in the approximation of considering only 12 levels and has then applied a correction obtained on comparing solutions of (5) for 12 levels and for an infinite number of levels. Searle (3) has obtained solutions of (1) for 10 levels.

Burgess has drawn attention to some errors in the work of Baker and Menzel. An error in the third term of the asymptotic expansion of the Kramers–Gaunt factor, as obtained by Menzel and Pekeris (4), gives rise to errors of a few per cent in the calculated hydrogen level populations. There are more serious errors in the Case B calculations of Baker and Menzel. Burgess notes that for $T = 2 \times 10^4$ °K, some of the N_n given by Baker and Menzel in the approximation of considering only 14 levels are greater than the corresponding N_n given for an infinite number of levels. This cannot be correct since the inclusion of more levels should increase the rate of population due to cascade and hence increase all of the N_n. Burgess checked the solutions for 14 levels and was able to conclude that there were errors in the Baker and Menzel Case B calculations for an infinite number of levels.

It may be shown that the solutions for hydrogenic ions of nuclear charge Z at temperature T may be obtained from the solutions for hydrogen at a temperature of (T/Z^2). In planetary nebulae T is usually between 1×10^4 °K and 2×10^4 °K. To obtain results for H I and He II we therefore require calculations for hydrogen in the range $2{\cdot}5 \times 10^3$ °K to 2×10^4 °K. The lowest temperature considered by Baker and Menzel is 5×10^3 °K. The need for calculations at lower temperatures has been emphasized by Wurm (5).

In the present paper we consider equations (5) for an infinite number of levels and obtain solutions for $T = 2{\cdot}5 \times 10^3$, 5×10^3, 1×10^4 and 2×10^4 °K. These calculations correct the errors in the work of Baker and Menzel and extend the solutions to lower temperatures. Our main interest in this work has been in the development of convenient methods for the solution of the infinite set of simultaneous linear equations for all values of n. Similar methods will later be used for the solution of exact equations of type (1), both for hydrogen and for complex atoms.

2. *Solution of the equilibrium equations.*—Let $P_{n',n}$ be the probability that population of n' is followed by a direct radiative transition to n. Then

$$P_{n',n} = \frac{A_{n',n}}{A_{n'}}. \tag{9}$$

Let $C_{n',n}$ be the probability that population of n' is followed by a transition to n *via* all possible cascade routes. We then have

$$\left.\begin{aligned} C_{n+1,n} &= P_{n+1,n} \\ C_{n+2,n} &= P_{n+2,n+1}C_{n+1,n} + P_{n+2,n} \\ C_{n+3,n} &= P_{n+3,n+2}C_{n+2,n} + P_{n+3,n+1}C_{n+1,n} + P_{n+3,n} \end{aligned}\right\}. \tag{10}$$

With the convention $C_{n,n} = 1$ we have, quite generally,

$$C_{n',n} = \sum_{p=n'-1}^{n} P_{n',p}C_{p,n}. \tag{11}$$

We shall refer to $C_{n',n}$ as the *cascade matrix*. Using (11) the cascade matrix may be generated once the matrix $P_{n',n}$ is known.

The solutions of equations (5) are given by

$$N_nA_n = N_eN_+\sum_{n'=n}^{\infty}\alpha_{n'}C_{n'n}. \tag{12}$$

The form of the solutions used by Baker and Menzel may be obtained by the following argument. We consider level n to be populated by: direct capture on n; captures on higher levels followed by direct radiative transitions to n; captures on higher levels followed by cascade transitions to n *via* one intermediate state; cascade transitions *via* two intermediate states, ... The solutions are then

$$N_nA_n = N_+N_e\left\{\alpha_n + \sum_{n'=n+1}^{\infty}\alpha_{n'}P_{n',n} + \sum_{n'=n+2}^{\infty}\sum_{p=n+1}^{n'-1}\alpha_{n'}P_{n',p}P_{p,n} + \ldots\right\}. \tag{13}$$

Re-arrangement of terms shows (12) and (13) to be identical. The particular advantage of (12) is that one may calculate the cascade matrix once and for all, this matrix being independent of the particular processes populating the excited states. It may then be used for radiative recombination at all temperatures and also for non-radiative processes such as collisional excitation from the ground state. The only assumption made* is that the excited states are depopulated by radiative transitions alone. The cascade matrices are, of course, different for Cases A and B, due to the difference in the definition of A_n.

It is usual to solve for b_n, defined as the ratio of N_n to the corresponding population for thermodynamic equilibrium at the same density and temperature. We then have

$$N_n = N_+N_en^2b_n\mathrm{e}^{x_n}\left(\frac{h^2}{2\pi mkT}\right)^{3/2} \tag{14}$$

where $x_n = I_n/kT$, I_n being the threshold ionization energy for level n. From (12) and (14),

$$\mathrm{e}^{x_n}b_n = \left(\frac{2\pi mkT}{h^2}\right)^{3/2}\frac{1}{n^2A_n}\sum_{n'=n}^{\infty}\alpha_{n'}C_{n',n}. \tag{15}$$

3. *Formulae for hydrogenic ions.*—For hydrogenic ions with nuclear charge Z the radiative transition probabilities are given by†

$$A_{n',n} = \left(\frac{8\alpha^4c}{3\pi a_0\sqrt{3}}\right)\frac{Z^4}{n'^5}t_{n',n} \tag{16}$$

* We here consider only the essential assumption made in our definition of the cascade matrix and disregard the incidental assumption implied by (3); one may easily define the cascade matrix when (3) is not assumed.

† Where possible we use a notation similar to that of Baker and Menzel.

where α is the fine structure constant, a_0 the Bohr radius, c the speed of light and

$$t_{n',n} = \frac{2n'^2 g_{n',n}}{n(n'^2-n^2)}, \tag{17}$$

$g_{n',n}$ being the Kramers–Gaunt factor of order unity. Defining

$$t_n = \sum_{n''=n_0}^{n-1} t_{n,n''} \tag{18}$$

we have

$$P_{n',n} = \frac{t_{n',n}}{t_{n'}}. \tag{19}$$

The ionization threshold for level n is

$$I_n = \frac{hRcZ^2}{n^2} \tag{20}$$

where R is the Rydberg wave number. We put

$$x_n = \frac{hRcZ^2}{n^2kT} = \frac{\lambda}{n^2} \tag{21}$$

where

$$\lambda = \frac{hRcZ^2}{kT} = \frac{15{\cdot}789\times 10^4 Z^2}{T} \qquad (T \text{ in } {}^\circ\text{K}). \tag{22}$$

The radiative recombination coefficients are given by

$$\alpha_n = \left(\frac{64}{3}\left(\frac{\pi}{3}\right)^{1/2}\alpha^4 c a_0^2\right) Z\lambda^{1/2}\frac{x_n S_n(\lambda)}{n} \tag{23}$$

where

$$S_n(\lambda) = \int_0^\infty \frac{g_{II}(n,\epsilon)e^{-x_n u}}{(1+u)}\,du \tag{24}$$

and where $hRcZ^2\epsilon$ is the energy of a free electron, g_{II} the bound–free Kramers–Gaunt factor and $u = n^2\epsilon$. From (15), (16) and (23) we obtain

$$e^{x_n} b_n = \frac{n^3}{t_n}\sum_{n'=n}^{\infty}\frac{S_{n'}C_{n',n}}{n'^3}. \tag{25}$$

In the notation of Baker and Menzel,

$$e^{x_n} b_n = \frac{(S_n + V_n)}{t_n}; \tag{26}$$

therefore

$$V_n = n^3\sum_{n'=n+1}^{\infty}\frac{S_{n'}C_{n',n}}{n'^3}. \tag{27}$$

4. *Methods of calculation and extrapolation procedures.*—Three-figure tables of the factors $g_{n',n}$ are given by Baker and Menzel for $n, n' \leqslant 30$. Accurate six-figure calculations have been made by Green, Rush and Chandler (**6**) for $n, n' \leqslant 20$. Spot checks show that most of the values of Baker and Menzel are correct to three figures. Errors which are larger, but not serious, occur for n, n' large and $(n'-n)$ small: thus $g_{29,19} = 0{\cdot}782$ according to Baker and Menzel compared with the exact value of $0{\cdot}7782\ldots$. In all of our calculations the Baker and Menzel $g_{n',n}$ were used.

Table I gives calculated values of t_n for Cases A and B and Tables II A and II B give the cascade matrices $C_{n+m,n}$ for $n \leqslant 10$, $m \leqslant 10$. For $5 \leqslant m \leqslant 10$ it is found that the calculated $C_{n+m,n}$ can be fitted accurately to

$$C_{n+m,n} = C_{\infty,n} + \frac{\Delta_n}{m}. \tag{28}$$

Tables II include the limiting values, $C_{\infty,n}$.

The functions $S_n(\lambda)$ may be calculated using the first three terms in the asymptotic expansion of the factor g_{II}. Tables for the calculation of S_n are given in the preceding paper (7). For n' large the sum in (25) may be replaced by an

TABLE I

n	t_n	
	A	B
2	1·911	—
3	3·084	1·363
4	3·929	2·265
5	4·589	2·951
6	5·132	3·507
7	5·590	3·973
8	5·989	4·378
9	6·339	4·731
10	6·657	5·051
11	6·943	5·340
12	7·205	5·604
13	7·442	5·841
14	7·668	6·068
15	7·876	6·277
20	8·740	7·144
25	9·410	7·814
30	9·956	8·360

integral and in this integral $C_{n',n}$ may be replaced by a mean value independent of n'. We then have

$$(S_n + V_n) = n^3 \sum_{n'=n}^{\infty} \frac{S_{n'} C_{n',n}}{n'^3}$$

$$\simeq n^3 \left\{ \sum_{n'=n}^{q-1} \frac{S_{n'} C_{n',n}}{n'^3} + \frac{1}{2} \frac{S_q C_{q,n}}{q^3} + \frac{1}{2} (C_{q,n} + C_{\infty,n}) \frac{\sigma_q(\lambda)}{2\lambda} \right\} \qquad (29)$$

where

$$\frac{\sigma_q(\lambda)}{2\lambda} = \int_q^{\infty} \frac{S_{n'}(\lambda)}{n'^3} \, dn'. \qquad (30)$$

TABLE II A

Values of $C_{n+m,n}$

(Case A)

m \ n	2	3	4	5	6	7	8	9	10
1	·4418	·2978	·2336	·1975	·1744	·1581	·1464	·1369	·1295
2	·4105	·2601	·1947	·1587	·1361	·1203	·1093	·1006	·0939
3	·3991	·2454	·1791	·1430	·1206	·1052	·0942	·0858	·0791
4	·3934	·2380	·1710	·1347	·1120	·0968	·0858	·0775	·0711
5	·3903	·2336	·1661	·1294	·1068	·0916	·0806	·0723	·0660
6	·3883	·2308	·1627	·1260	·1033	·0881	·0771	·0688	·0624
7	·3870	·2289	·1605	·1236	·1008	·0854	·0745	·0662	·0598
8	·3860	·2274	·1589	·1217	·0990	·0835	·0725	·0642	·0578
9	·3853	·2264	·1575	·1203	·0975	·0821	·0710	·0627	·0563
10	·3848	·2255	·1564	·1191	·0964	·0809	·0698	·0615	·0551
∞	·3796	·2174	·1468	·1088	·0860	·0703	·0590	·0505	·0441

TABLE II B

Values of $C_{n+m,\,n}$

(Case B)

m \ n	3	4	5	6	7	8	9	10
1	·5164	·3633	·2890	·2454	·2163	·1961	·1804	·1683
2	·4838	·3224	·2458	·2015	·1726	·1531	·1382	·1269
3	·4714	·3060	2282	·1836	·1550	·1351	·1206	·1094
4	·4651	·2975	·2187	·1737	·1451	·1253	·1107	·0997
5	·4614	·2923	·2128	·1676	·1389	·1190	·1045	·0936
6	·4591	·2888	·2090	·1635	·1346	·1148	·1003	·0894
7	·4575	·2866	·2062	·1605	·1315	·1117	·0971	·0863
8	·4564	·2848	·2041	·1584	·1292	·1094	·0948	·0840
9	·4555	·2833	·2025	·1567	·1274	·1076	·0930	·0822
10	·4547	·2822	·2012	·1553	·1260	·1062	·0916	·0808
∞	·4481	·2721	·1895	·1431	·1130	·0934	·0787	·0680

Tables for the calculation of $\sigma_q(\lambda)$ are given in the preceding paper. For $n \leqslant 10$ it was found that good accuracy was obtained with $q = n + 10$.

For $n > 10$, $(S_n + V_n)$ was obtained by extrapolation. This may be done quite accurately. Taking all Kramers–Gaunt factors equal to unity, Menzel and Baker (**8**) show that, in the limit of large n, $t_n \sim 3 \ln n$, $S_n \sim 2 \ln n$ and $V_n \sim \ln n$. Using the methods of Menzel and Baker it may be shown that the same results are obtained with the asymptotic expansions of the g-factors. It follows that $b_n \sim 1$ in the limit of large n. The values of t_n given in Table I may be fitted to $t_n = 3 \ln n + \text{const.}$ for $n \geqslant 20$.

For $5 \leqslant n \leqslant 10$ it was found that the calculated values of $(S_n + V_n)$ could be fitted accurately to

$$(S_n + V_n) = 3 \ln n + c + \frac{d}{n} + \frac{e}{n^2}. \tag{31}$$

These expressions were used for extrapolation to larger values of n.

5. *Results.*—Table III gives values of $e^{x_n} b_n$ for the four temperatures considered and Table IV the Balmer decrements (relative emission intensities), for $T = 1 \times 10^4$ and 2×10^4, calculated from

$$\mathscr{I}_n = 100 \left(\frac{4}{n}\right)^3 \frac{b_n e^{x_n} g_{n,2}}{b_4 e^{x_4} g_{4,2}}. \tag{32}$$

Our relative intensities are similar to those of Baker and Menzel but there is some change in the (H_α/H_β) ratio for Case B. In Table V we compare our values of b_4 with the values of b_4 obtained by Baker and Menzel and the values of $\bar{b}_4$ obtained by Burgess, $\bar{b}_n$ being the effective value of b_n for the calculation of Balmer intensities. The errors of order 5 per cent in Baker and Menzel's b_n for Case A may be explained in terms of the error in g_{II}. The larger errors, of order 20 per cent, in their b_n for Case B may be explained by assuming that the values of $(S_n + V_n)$ used in (26) were in error due to the error in g_{II} and in addition that the values of t_n used in (26) were calculated with $g_{n,n''} = 1$. This explanation seems plausible in view of the fact that Baker and Menzel made some calculations with $g_{n,n''} = 1$.

TABLE III

Values of $e^{x_n} b_n$

Case	A				B			
n \ $T=$	$2{\cdot}5\times10^3$	5×10^3	1×10^4	2×10^4	$2{\cdot}5\times10^3$	5×10^3	1×10^4	2×10^4
2	·0657	·114	·193	·315	—	—	—	—
3	·0770	·131	·213	·332	·257	·422	·668	1·013
4	·0939	·155	·244	·364	·218	·350	·540	·792
5	·1113	·179	·273	·394	·220	·346	·519	·739
6	·129	·201	·299	·421	·231	·355	·520	·725
7	·145	·222	·322	·443	·245	·369	·529	·722
8	·161	·241	·341	·463	·259	·384	·540	·725
9	·175	·258	·360	·480	·274	·398	·552	·730
10	·189	·274	·376	·494	·287	·412	·563	·735
11	·202	·288	·390	·507	·300	·425	·572	·739
12	·214	·301	·402	·519	·312	·436	·582	·744
13	·226	·313	·414	·529	·324	·447	·591	·748
14	·236	·324	·424	·538	·334	·457	·598	·752
15	·246	·335	·434	·547	·344	·466	·605	·756
20	·288	·377	·472	·580	·386	·503	·635	·772
25	·320	·407	·499	·603	·417	·531	·656	·785
30	·345	·431	·520	·621	·442	·552	·673	·795

TABLE IV

Balmer decrements (values of $\mathcal{F}_n$)

Case	A		B	
n \ $T=$	1×10^4	2×10^4	1×10^4	2×10^4
3	191	199	271	279
4	100	100	100	100
5	58·9	56·9	50·6	49·1
6	37·8	35·6	29·8	28·2
7	25·8	23·8	19·2	17·8
8	18·4	16·7	13·2	12·0
9	13·7	12·2	9·5	8·5
10	10·4	9·2	7·1	6·3
11	8·1	7·1	5·4	4·7
12	6·5	5·6	4·2	3·7
13	5·3	4·5	3·4	2·9
14	4·3	3·7	2·8	2·3
15	3·6	3·0	2·3	1·9
20	1·6	1·4	1·0	0·8
25	0·9	0·7	0·5	0·4
30	0·5	0·4	0·3	0·3

TABLE V

Case	A		B	
$T=$	1×10^4	2×10^4	1×10^4	2×10^4
b_4, Baker and Menzel	·096	·233	·166	·404
b_4, present results	·091	·222	·201	·484
b_4, Burgess	·132	·312	·200	·494

For Case B the calculations of Burgess (**2**) and of Searle (**3**), based on equation (1), are in fairly good agreement with the results of the present calculations. For Case A the agreement is less satisfactory. This is due to the fact that, in calculations using (1), transitions to the ground state take place only from the np states; equations (1) therefore give differences between Cases A and B which are smaller than the corresponding differences obtained using (5).

Department of Physics,
University College,
London, W.C.1:
1959 *February* 2.

References

(1) J. G. Baker and D. H. Menzel, *Ap. J.*, **88**, 52, 1938.
(2) A. Burgess, *M.N.*, **118**, 477, 1958.
(3) L. Searle, *Ap. J.*, **128**, 489, 1958.
(4) D. H. Menzel and C. L. Pekeris, *M.N.*, **96**, 77, 1935.
(5) K. Wurm, *Mém. Soc. Roy. Sci. Liège*, **14**, 387, 1954.
(6) L. C. Green, P. P. Rush and C. D. Chandler, *Ap. J. Suppl. Series*, **3**, 37, 1957.
(7) M. J. Seaton, *M.N.*, **119**, 81, 1959.
(8) D. H. Menzel and J. G. Baker, *Ap. J.*, **86**, 70, 1937.

THE OBSERVATION OF SOLAR GRANULATION FROM A MANNED BALLOON

I. Observational Data and Measurement of Contrast

D. E. Blackwell, D. W. Dewhirst and A. Dollfus

(Received 1959 February 25)

Summary

There appears to be a practical limit to the resolution attainable in solar photography from a ground station. In an attempt to obtain greatly improved resolution, photographs have been made with a 29 cm refracting telescope mounted underneath the nacelle of a manned balloon at a height of 18 000 ft. Two flights were made; during the second flight on 1957 April 1, 480 frames were exposed. Although the ground seeing during the flight was very poor, the photographs taken with the balloon-borne telescope during this second flight are superior to the best that have been secured at any ground station.

The complex structure of the photosphere is illustrated by photographs. Autocorrelation curves for two scans across the best photograph are given. The contrast transmission functions for the complete telescope (objective, eyepiece, photographic emulsion) have been measured using sinusoidal gratings, and the results used to correct microphotometric measurements of contrast. The corrected mean contrast between granules and intergranular regions is 40 per cent at a wave-length of 5300 A.

---

1. *Introduction.*—The fine structure of the solar photosphere, known as granulation, has received a great deal of attention during the last hundred years, but progress towards an understanding of its nature has been slow. Observations are greatly hindered by the daytime seeing, which is usually of poor quality: while some of this poor seeing has its origin in the upper atmosphere, much of the trouble is due to local heating near the ground or around the observing slit of a dome. Also, unless the telescope is carefully designed, instrumental imperfections arise, chiefly from the disturbing effects of the large flux of solar radiation through the apparatus. This is especially true of local heating near the prime focus.

In the past, good photographs have been taken by paying particular attention to the design of the telescope and to the selection of an observing site. We should mention here the early pioneering work of Janssen (**1**) and of Hansky (**2**). The well-known photograph taken by Janssen on 1885 July 5 has scarcely ever been improved upon, but it is not often mentioned that it has been selected as the best of an extensive collection of photographs taken at Meudon over a period of 20 years with a telescope of only 13·5 cm aperture. Better photographs, taken by Lyot at the Pic du Midi, were investigated by Macris (**3**); Lyot's techniques have been still further improved by Rösch (**4, 5**) using a refractor of 25 cm aperture. A smaller telescope, of 13 cm aperture only, has recently been designed and used by Bray, Loughhead and Burgess (**6, 7**) with good results. Other investigations of solar granulation will be referred to later.

Even under the best observing conditions at a good site the proportion of first-rate photographs has always been disappointingly small. In all of the work described above the theoretical resolution of a 25 cm objective has never been realized. As some of the bad seeing originates close to the ground we may reasonably expect that if photographs could be taken from a balloon at a height of a few thousand feet above the ground, better definition would result. The present experiments using a manned balloon were made to test this supposition and obtain photographs of still higher resolution. More recently, Schwarzschild and Rogerson have taken photographs from an unmanned balloon at heights of up to 80 000 ft (**8, 9**).

The expected scale of the fine structure is very close to the resolution limit of a telescope of about 25 cm aperture. If quantitative deductions about granulation are to be made from the photographs, the least that we can do is to test the laboratory performance of the telescope and use this information to correct the observed data as well as possible. This also has been done in the present investigation. The photometric measurement of granulation is closely analogous to the investigation of Fraunhofer line profiles with a spectrograph of rather low resolving power. It would be unwise to attempt to measure a line profile knowing almost nothing of the instrumental profile of the spectrograph; and almost as unwise to assume that the instrumental profile is that corresponding to simple diffraction, without aberration or scattering in the photographic emulsion. Similarly, it is unwise to deduce the photometric properties of granulation knowing that the resolution is only just sufficient to show the granulation, but not knowing the precise properties of the telescope.

2. *Apparatus.*—Two flights have been made. Accounts of the apparatus used on the first flight from the Meudon Observatory on 1956 November 22 have already been published and only a few notes will be given here. The telescope and balloon are described in ref. (**10**). The telescope was a refractor, with a visual doublet of 29 cm aperture and 294 cm focal length which had been figured by Schaer. The primary image was projected by an eyepiece of 2·5 cm focal length to give an image of diameter 46 cm in the second focal plane. This final image was photographed on Kodak Microfile Pan film through a Wratten No. 58 filter with a peak transmission of 5300 A and a bandwidth at half-peak transmission of 600 A. The shutter of a Contax camera was placed in the prime focus and set to a speed of $0{\cdot}8 \times 10^{-3}$ sec. It was later discovered to have given an exposure of about 2×10^{-3} sec because of the low temperature at altitude. The telescope was so supported on an altazimuth mounting underneath the balloon basket that it could be directed at the Sun by one of the two observers, whilst the second could control the mechanisms of the telescope (primary shutter, exposing shutter, camera wind, focusing, alteration of shutter speed) electrically from the basket. The automatic mechanism for operating the Contax is described in ref. (**11**). When the balloon is floating at equilibrium altitude and the observers in the basket are still, the telescope does not oscillate appreciably. The principal effect is an occasional slow rotation about the vertical axis. Under reasonably calm conditions it proved possible to keep the telescope directed at the Sun with an error not exceeding 20′–30′ for a few minutes at a time. On this first flight 390 photographs were taken at heights between 18 000 ft and 20 000 ft, but the photographs of granulation had a sheared structure caused by the movement of the telescope during the unexpectedly long exposure.

On 1957 April 1 a second flight was made from Meudon (**12**) with similar apparatus, but including a much improved shutter. This publication shows a photograph of the balloon and apparatus. The Contax shutter was replaced by a flying slit shutter of original design which gave a speed of about 2×10^{-4} sec. This was sufficiently fast to prevent the appearance of shear on practically every photograph even though the balloon was less stable than during the first flight. An outline drawing of the shutter mechanism is shown in Fig. 1. An essential requirement of the shutter was that it should be as nearly inertia-free as possible, to minimize vibrations transverse to the optical axis of the telescope just at the moment when the photograph is taken. The shutter proper consists of the framework A pivoted and balanced about a horizontal axis and containing in

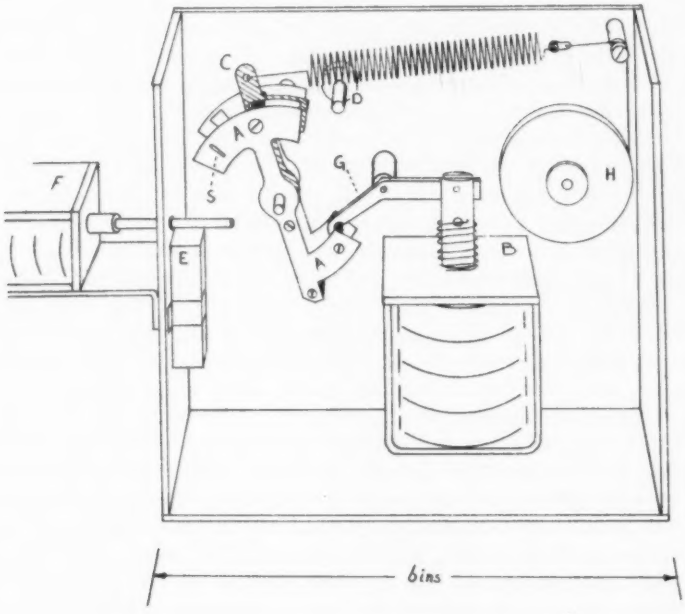

FIG. 1.—*Diagrammatic representation of components of flying slit shutter. For clarity the bearing that supports the nearer end of the horizontal axle of the shutter is not shown. The shutter is here loaded, ready to be released by raising the latch G.*

its upper part the adjustable slit, S, which makes the exposure. The slit is set to a width of about 0·4 mm. In operation, we require this slit frame A to be accelerated to the required angular speed and then to be allowed to continue its motion at constant speed whilst the slit which it contains moves across that part of the primary image which is being photographed. At the end of its run it must be stopped positively without any rebound. These operations are performed by the mechanism shown. The spring loaded arm C can rotate freely about the same axis as the slit frame A. The sequence is initiated by the solenoid B which lifts the latch G and so releases the slit frame. The arm C is then accelerated by the spring and carries the slit frame A with it, until the

slit is just before the area of prime focus to be photographed. Part C is then brought to rest by a cushioned stop, D, but the slit framework A continues in free motion at constant speed until it comes against the stop E. This stop is a small permanent magnet which, attracting a steel shoe on the slit frame A, prevents any rebound.

The shutter is reloaded by a solenoid at F, which pushes the whole shutter framework until it is caught by the latch G. The shutter is enclosed in a light-tight box which contains, however, an entrance aperture which is normally covered by a preliminary shutter. This shutter is moved out of the way by an electromagnet just before each 0·2 millisecond exposure is made.

In flight the speed of the shutter could be changed by altering the tension of the spring by means of the motor-driven wheel H. The speed was measured in the laboratory by illuminating the shutter with a neon lamp fed from a beat frequency oscillator. The light after passing through the shutter then shows a pattern of light and dark stripes, and the speed of the shutter can be calculated from a knowledge of the scale of this pattern and the width of the slit. There is a limit to the increase of speed that can be effected by diminishing the slit width. The reason for this is that during the flight the position of the shutter with respect to the primary focal plane is changed. The change in focus is very difficult to predict theoretically. It depends partly on the known change in refractive index of the air at altitude. But it depends also on thermal changes in the dimensions of the metal framework and the two components of the objective, and the temperature at which these attain thermal equilibrium with their surroundings is uncertain. It proved impossible to predict the position of focus with an accuracy better than ± 2 mm. We must evidently be careful that the shutter slit is not displaced so much from the focal plane that the whole of the objective cannot be seen through it at once, and, as the focal ratio of the objective is $f/10$, the slit must not be less than 0·2 mm in width.

For the second flight a smaller magnification was used, the image diameter being 14·4 cm and the scale $6''{\cdot}7 \equiv 1$ mm. During this flight 480 frames were exposed at an altitude of 18 000 ft. For the reasons just explained the position of focus is uncertain and the projection eyepiece was moved through 0·1 mm every ten photographs over a total range of ± 2 mm. During both flights a photoelectric photometer was used to estimate the exposure. The film was processed in strips and developed in Kodak D.19b for 5 minutes at a temperature of 70 °F. Photographs of a standardized step wedge, previously made on portions of the same batch of film, were developed with each strip to provide a calibration. The emulsion gave a contrast of $\gamma = 6{\cdot}1$.

3. *Measurement of contrast transmission functions of complete apparatus*

3.1. *Introduction.*—The photography of granulation is extremely difficult but the deduction of the photometric properties of granulation from calibrated photographs is even more difficult. Not only are we observing an extended object of low contrast, but we are also working near the resolution limit of a medium-sized objective. In visual tests with an eyepiece on a point object the objective may appear to perform well, showing clear and regular diffraction rings, but a test of this kind does not easily show how much spurious light there is in the outer parts of the image; such spurious light diminishes the contrast in the image of a complex object if the scale of its structure is of the

order of magnitude of the resolution. In all cameras there is the extra complication of scattering in the photographic emulsion and, in our apparatus particularly, the possible additional image defects introduced by an enlarging eyepiece. Although in our apparatus we should not expect these latter effects to be serious it seems desirable that such an optical system should be tested in its entirety on an extended low contrast object which has the same order of angular scale as solar granulation. To effect this we have measured the contrast transmission functions of the complete telescope—objective, eyepiece and photographic emulsion—and applied the results to the interpretation of the photographs.

3.2. *The contrast transmission functions.*—The contrast transmission function of an optical system, also known as the sine wave response factor, describes its response to various spatial frequencies in the object plane. It is a concept first suggested by Duffieux (**13**) and developed by Schade (**14**) and is now used increasingly to describe quantitatively the performance of an optical system in preference to the concept of resolution measured as lines/cm or as the " Rayleigh limit ". Analytically, it is the Fourier transform of the distribution of light in the image of a line object. An equivalent definition is that it is the ratio of contrast in the image plane to that in the object plane for each spatial frequency separately. The numerical value of the transmission function varies with spatial frequency, reaching zero at the " cut-off " frequency of the system. The significance of the cut-off frequency is that no greater spatial frequencies are passed by the optical system; if such spatial frequencies exist in the object they are completely suppressed in its image and cannot be restored in any way. At wave-length λ the cut-off frequency corresponds to an angular resolution limit of λ/d radians, where d is the linear diameter of the objective. If the optical system includes a photographic emulsion, it is necessary to include this as equivalent to an additional component.

3.3. *Measurement of the contrast transmission functions.*—The measurement of the transmission functions is not easy. It may be done directly by scanning the image of a line object and taking the Fourier transform afterwards, or by arranging a mechanical scanning device which will automatically measure the Fourier transform, as has been done by Ingelstam, Djurle and Sjogrën (**15**). This method has the advantage of measuring the phase as well as the amplitude. Alternatively, an extended test object may be used. For many years a square wave test object has been popular, but although this has the advantage of ease of construction it has the disadvantage of introducing uncertainty in going from the square wave response factor to the sine wave response factor (**16**). The use of a sinusoidal test object has been developed by Schade; for this work he uses film sound track (**17**).

In our tests we have used sinusoidal test objects which have been prepared photographically, starting with an accurate transmission grating of spacing 12 lines/mm and of square wave form. This grating has been reduced in size by projecting it with a high quality camera lens and photographing the slightly defocused image on a Kodak Maximum Resolution plate. For each of several reduction ratios this procedure is repeated using various exposures and different amounts of blurring, and the most suitable test object selected. Suitability is judged by two factors; contrast, or percentage modulation, and purity of waveform. These two characteristics are easily tested by viewing a distant

lamp through the grating; the amplitude of each modulation frequency is then proportional to the integrated brightness of the corresponding spectral order. Using this technique it is relatively easy to produce gratings of at least 170 lines/mm which attain such perfection of waveform that they show no trace of spectra above the first order. The brightness of the first order spectrum relative to the zero order depends upon the depth of modulation; this property provides a useful guide for the rapid selection of gratings suitable for further tests. This spacing of 170 lines/mm is near the cut-off frequency of an $f/10$ optical system.

The modulation of each grating was measured by scanning in a microphotometer at very slow speed, using a microscope objective of numerical aperture 0·28. Such an objective has a Rayleigh resolution of 1250 lines/mm and may be expected to measure the modulation of a 68 lines/mm grating to within 5 per cent. The modulation used increased with the grating frequency, being of the order of 15 per cent at the lower frequencies and up to 50 per cent at the higher frequencies.

In our tests of the telescope we have been obliged to use a collimator, as a sufficiently distant source would have introduced poor seeing in a long light path near the ground.

The collimator used was a chemically silvered paraboloid of diameter 46 cm and focal length 640 cm. As there is a reduction of image size by a factor $\times 2{\cdot}3$ it was necessary to use gratings of spacing up to 68 lines/mm only. The figure of the paraboloid was known to be of excellent quality. During the tests careful observations were made of the local seeing and a test was not made until the steadiness of the first diffraction ring of an artificial star source showed that the seeing was sufficiently good. Otherwise the identical optical system of the flight was used and the film was developed under exactly the same conditions as those of the flight film.

3.4. *Results of measurements.*—The results for the complete telescope are shown in Fig. 2. The curve for an aberration-free system in monochromatic light is also shown (**18**); the last point on this curve is the calculated cut-off limit of the telescope.

This is the first time that the contrast transmission functions have been measured for a complete photographic telescope. It is clear from the diagram that in spite of the apparently satisfactory results of conventional visual tests made on the objective before the flight, the performance of the whole telescope seems markedly inferior to that of an aberration-free system; the contrast transmission function at a spatial frequency corresponding to 1″, for example, being only about one-third of its value for an ideal telescope.

Although it is known from visual tests that its resolving power is good, as defined by the Rayleigh criterion, later examination in the light of the measured contrast transmission functions revealed spurious light in the outer parts of the image that had previously been thought unimportant. The only additional optical component is the chemically silvered paraboloid used as a collimator. It has been found by Lyot that such a mirror may form an image of a point object which contains excess light in its outer parts, the effect being ascribed to the variable thickness of the chemically deposited silver coating (**19**).

We attribute most of the fault to the objective. Other tests suggest that its defects are due partly to a rapid variation of spherical aberration with wave-length

and partly to disturbances in the wavefront produced by local figuring of the surfaces. Separate tests of the eyepiece show that it is almost free from defects.

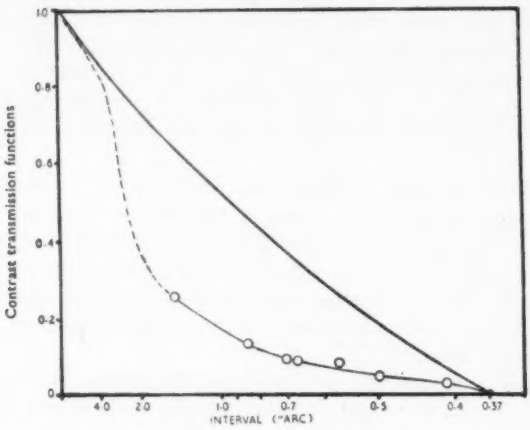

FIG. 2.—*Contrast transmission functions of complete telescope (objective, eyepiece, filter, photographic emulsion) as used on balloon flight (lower curve). The upper curve is the computed curve for an aberration-free optical system of the same size.*

4. *Preliminary discussion of the appearance of the photographs*

4.1. *Image quality.*—During the flight the focus setting was changed by 0·1 mm after every ten photographs. Two points now arise: first, that the ten photographs taken at the position of " best focus " are not all of equal quality, but one photograph in particular is somewhat superior to the others. Second, there is not a regular deterioration of image quality with change of focus: it sometimes happens that an isolated photograph taken as far as 0·3 mm from the " best focus " is of better quality than some taken nearer to this position. Even 2 mm from true focus there is an occasional photograph that shows a trace of fine structure of the order of size of the granulation. These observations show that the seeing is still not uniformly good even at 18 000 ft.

This kind of effect is not easily discerned at ground level with a large objective because the wavefront passing through the lower atmosphere is deformed by disturbed regions whose lateral dimensions are smaller than the telescope objective, and the resulting image is always confused. On the other hand, at high altitude the refractive index of air is smaller and the thickness of a disturbed region must be greater to produce the same phase change. We may expect these regions to be of greater lateral extent, and their principal effect to be a random change in the apparent focal length of the objective, without a necessary deterioration of image quality.

Whilst the flight was in progress, careful observations of the Sun were made at Meudon, the place of departure, by Mme d'Azambuja : the seeing throughout was of very poor quality. That we have obtained under these conditions photographs which are superior to the best previously secured from the ground confirms the supposition we set out to test, that there is undoubtedly a great improvement to be obtained by observing from a balloon at an altitude of about 18 000 ft.

4.2. *Shapes and dimensions of granules.*—Plate 1 shows enlargements of two parts of a good photograph taken near the centre of the solar disk. The resolution appears to be about 0″·5; it is clearly greater than the mean size of the granules so that the granules appear little altered in reproduction. The photograph clearly shows the individuality of each granule. Their mean size is about 1″·4. Few granules are larger than 2″ and few are smaller than 0″·8. When examined individually, the granules show a much less regular structure than that suggested by previous photographs. The granules are rarely circular. Their shape is often polygonal, elongated, or complex: many of them, but not all, are of uniform brightness with sharply defined edges.

4.3. *Large-scale variations of structure.*—The two photographs of Plate 2 are of regions where the granular structure is particularly irregular. Further comments are given in the legend.

4.4. *Associations of granules.*—It turns out that some granules are not completely separated but touch, or merge into each other, forming amorphous groups of greater size. In associations they can delineate complex shapes. Plate 3 (first row) gives three examples; left, the grouping of the granules traces a ring; middle, a crescent; right, a complex filament.

4.5. *Intergranular regions.*—The darker material between the granules is not of constant brightness. In some places granules seem to be missing, their place being taken by small areas whose material is generally darker than the neighbouring intergranular space. These are the " pores ". Plate 3 (second row) shows three examples of such formations.

4.6. *Striations.*—Curious alignments of the structure are sometimes revealed; the granules are drawn out in lines, isolated or in parallel arrangements over a distance of as much as 45″. These linear arrangements may be evident either in the granules themselves or in the dark intergranular material. Plate 3 (bottom) shows an example, and they may also be seen in parts of Plate 1 (top photograph). Similar structures which have been seen previously on other photographs have been interpreted as effects of atmospheric turbulence. Our photographs seem to confirm that these striae, although rather rare, are probably real.

4.7. *Isophotometric contours.*—We have drawn curves of equal intensity for different values of brightness, using the isophotometer of the Sacramento Peak Observatory, New Mexico, placed at our disposal by the Director, Dr J. Evans.

Three areas have been selected each of size 15″ × 20″ and are shown on Plate 4. In each of these areas five tracings have been made corresponding to five equal steps of brightness. The left column is a region of normal granulation. The region in the centre column contains a dark " pore " on the left and a particularly bright granule at the bottom. The right-hand column is selected from one of the regions referred to above which is darker and contains only granules smaller than the mean diameter.

Examination of the isophotes confirms the complexity and irregularity of the granules. As an example the photograph at the top left shows a particularly large granule right of centre. The isophotes in the bottom two photographs show its complex outline and its internal structure of three nuclei.

5. *Measurement of autocorrelation functions of brightness.*—We wish to obtain finally the power spectrum of the granulation. To derive this we have first measured the one-dimensional brightness distribution by scanning across

the negative with a very small spot of light. The scans were each made along a length of 24 mm with a square spot of 0·02 mm side ($\equiv 0''\cdot 14$), using a recording microphotometer. The resulting traces were measured at intervals of 0·021 mm ($\equiv 0''\cdot 142$). This value is within the interval required by the sampling theorem (**20**), which for a cut-off of $0''\cdot 37$ demands an interval not greater than $0''\cdot 18$ for the complete description of the microphotometer curve. With the Cambridge electronic computer (EDSAC II) the 1100 readings from each scan were converted into intensities using the calibration curve of the emulsion, and the autocorrelation function found for a shift of up to 100 measures, or $14''$. If the N successive brightness values are $I_1, I_2 \ldots I_n$, the autocorrelation function $\phi(j)$ for a shift j is defined as

$$\phi(j) = \frac{\sum_{k=1}^{k=N-j} (I_k - M)(I_{k+j} - M)}{\sum_{k=1}^{k=N-j} (I_k - M)^2}$$

where M is the mean brightness defined as

$$M = \frac{\sum_{k=1}^{k=N} I_k}{N}.$$

In all, six scans were made across different parts of the best negative (frame 221). The autocorrelation functions for each scan have been computed, and two of them are shown in Fig. 3 (*a*) and (*b*), plotted as a function of angular distance on the Sun. These curves show an initially steep descent followed by small fluctuations about the values $\phi = 0\cdot 2$ to $0\cdot 3$. Part of the long period fluctuation is probably instrumental in origin, but the fluctuations do not repeat from one scan to another and so are chiefly of a random nature. We emphasize that we have not used a moving average to eliminate the effects of slow changes of brightness across the photograph, real or spurious; had we done so the autocorrelation functions would have diminished to zero.

The " half-width " of the initial descent is a measure of the resolution of the photograph. The half-widths of the curves shown in Fig. 3 are $0''\cdot 50$ and $0''\cdot 72$. The half-width of the autocorrelation curves for the other four scans are $0''\cdot 75$, $0''\cdot 79$, $0''\cdot 79$ and $0''\cdot 97$. These results show that the average quality varies considerably over the area of the photograph. The best definition is along the line of scan of Fig. 3 (*a*) (half-width $0''\cdot 50$) but this autocorrelation function curve is a measure only of the average definition along this line. As the measurements were made with a small spot no appreciable contribution to these curves from photographic grain may be expected. Were there a contribution from grain a peak at the origin of the autocorrelation curve would be expected. Such a peak cannot be discerned on these curves.

Autocorrelation functions have been published by other investigators. Wlérick (**21**) has studied a photograph taken by W. A. Miller at the R.C.A. Laboratories with an 11·3 cm objective. The half-width of Wlérick's curve is $1''\cdot 23$. One photograph taken at Mount Wilson, " of exceptionally fine definition ", has been analysed by Frenkiel and Schwarzschild (**22**). This photograph was taken with the 60 ft solar tower diaphragmed to 10 cm aperture, the effective wave-length being 5800 A. The half-width of their curve is $0''\cdot 91$,

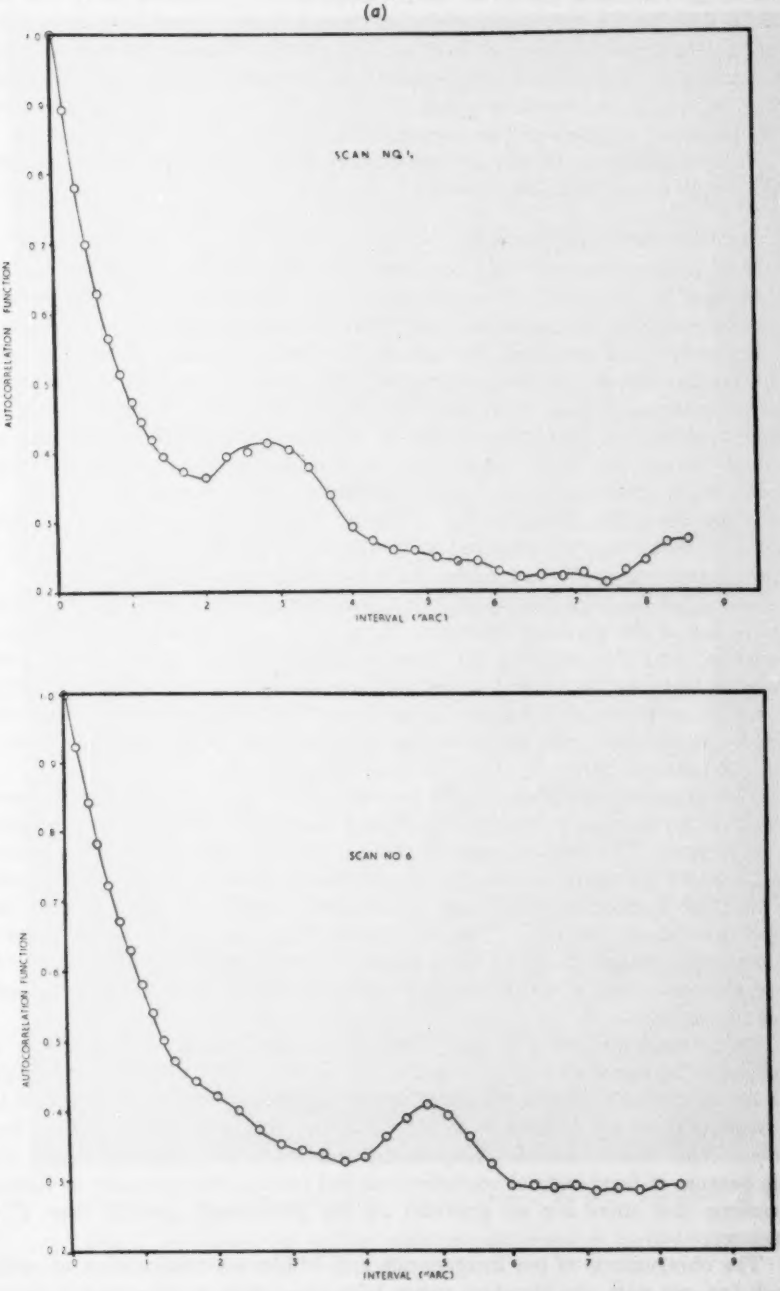

FIG. 3.—*Autocorrelation functions computed from two scans across the best negative.*

but as the calculated cut-off of the telescope is 1″·11, it seems likely that much of the first part of their autocorrelation curve is instrumental in origin. Uberoi (**23, 24**) has also analysed a high quality Mount Wilson photograph. This photograph, taken with the same 10 cm aperture and also at a wave-length of 5800 A, yields an autocorrelation curve of half-width 0″·76. For the same reason, much of this curve is instrumental in origin, as the author shows.

The significance of the autocorrelation curve found in this investigation will be discussed in a later paper.

6. *Measurement of contrast*

6.1. *Introduction.*—In the measurement of contrast a large instrumental correction is inevitable. Even if the optical system is free from aberration the correction is a considerable one, while aberrations too small to be noticed in ordinary visual tests will increase the correction greatly. In the absence of information about the optical quality of a telescope and the photographic emulsion the magnitude of the correction is very uncertain. The method usually used to obtain the correction is that of Wanders (**25**) which involves scanning radially across the limb. This must be done on separate photographs taken with longer exposures and almost inevitably gives erroneous results. In addition, the curve given in Fig. 2 for an ideal telescope shows that a great loss of contrast may be expected at frequencies near the cut-off. Probably all the observations made so far have been undercorrected.

6.2. *Previous observations.*—Two quantities characterize the brightness properties of the granular structure. One is the root mean square brightness variation, and the other is the mean contrast between granular and intergranular regions. In Table I we list previous determinations of these quantities. In the last two columns the upper figure for each determination is the uncorrected direct measurement, and the lower figure, in brackets, is the value as corrected for instrumental effects by the individual investigators.

We may reconsider these data in the light of the known contrast transmission functions for an ideal telescope, assuming a correction appropriate to the mean granule size. This would appear to be a minimum correction if only because no allowance has been made for the smaller transmission function corresponding to the first harmonic, which may be supposed to exist if there is light–dark asymmetry in granulation. The correction to the observed contrast must be at least that indicated for an ideal telescope and in practice will be larger by an unknown amount which depends upon the properties of the instrument and the seeing.

As an example, we take the observations of Keenan. In obtaining his correction he assumed a mean granule size of 1″·1. But the transfer function for an aberration-free objective of this size is only 0·37. This means that the correction must be at least a factor of ×2·7, giving a contrast of at least 28 per cent. The correction may be expected to be considerably bigger than this because of instrumental imperfections and seeing, and especially as Keenan mentions that there are no granules on his photograph smaller than 1″ in diameter.

The observations of ten Bruggencate and Müller—a continuation of earlier work (**29, 30**) with the Potsdam tower telescope—gave a value that is superficially in good agreement with that of Keenan. We have, however, already

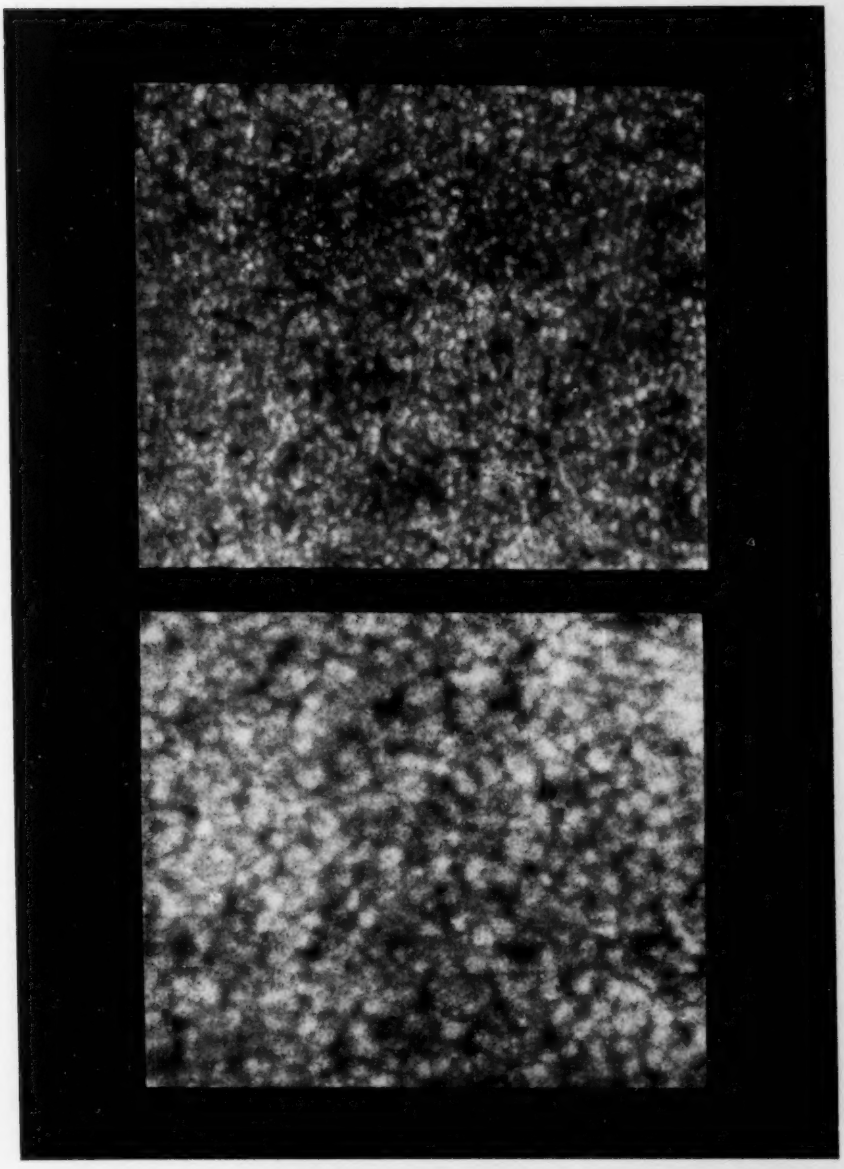

Above: *A part of the solar surface near the centre of the disk. Dimensions of field* $90'' \times 75''$.
Below: *Enlargement of field in which the granulation is particularly uniform. Dimensions of field* $48'' \times 40''$.

D. E. Blackwell, D. W. Dewhirst and A. Dollfus, Solar granulation observed from a manned balloon

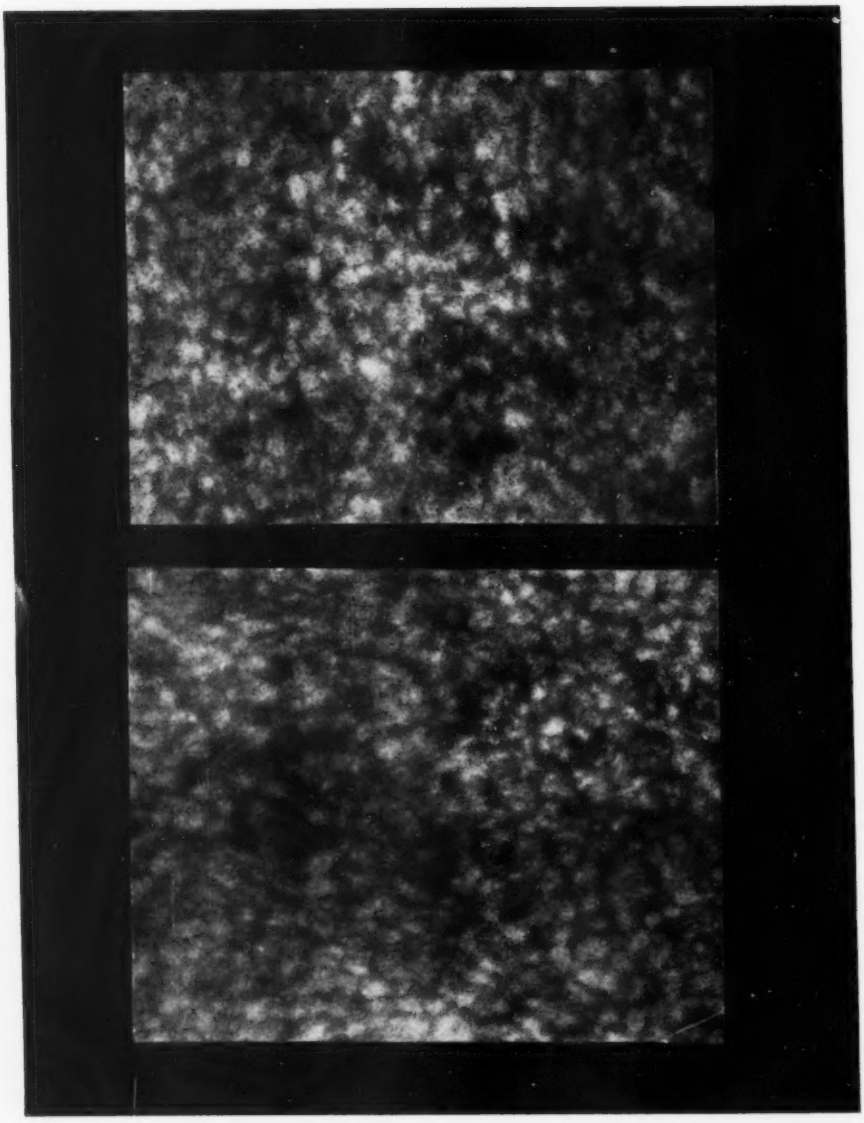

Enlargements of regions in which the granulation is noticeably irregular.
Top: *In the centre is a region where the granules are particularly bright. To the right a dark region where the granules are of unusually low contrast.*
Bottom: *At the top right a region where the granules are small; on the left, dark spots and "pores".*
Each field has dimensions 50″ × 40″.

D. E. Blackwell, D. W. Dewhirst and A. Dollfus. Solar granulation observed from a manned balloon.

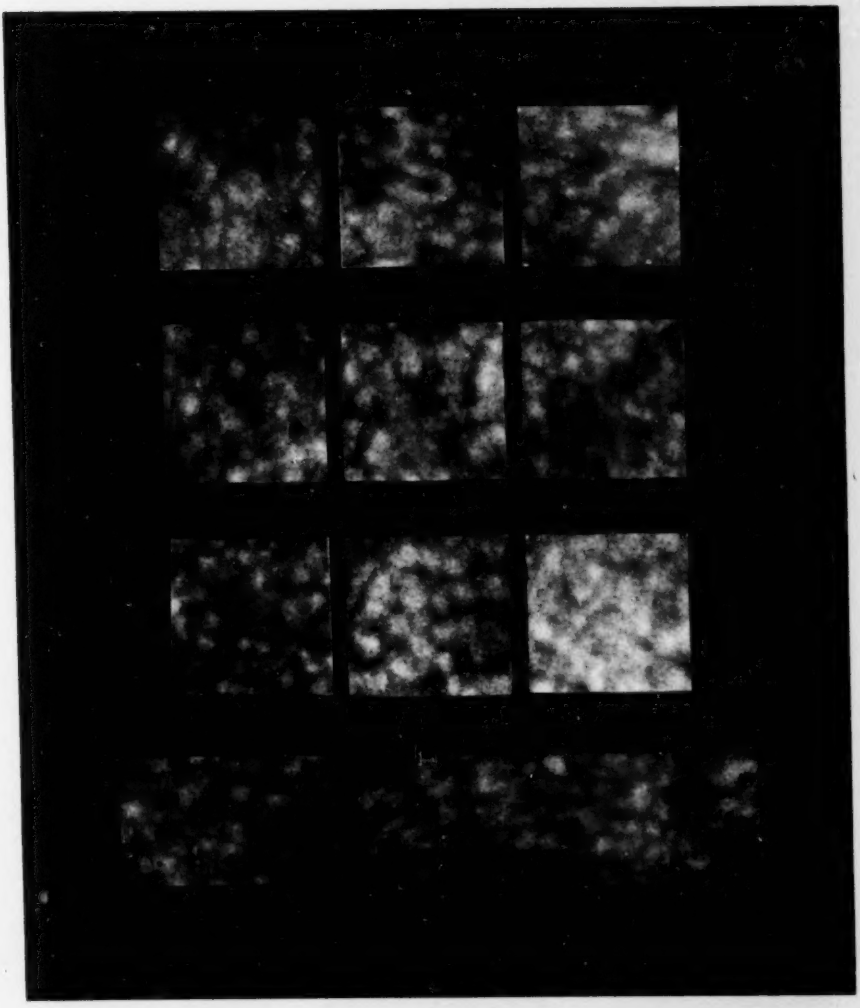

Top row: *Examples of granules of complex shapes.*
Second row: *Examples of small dark areas and "pores".*
Third row: *Left, a region of high contrast.*
Centre, a region of normal contrast.
Right, a region of low contrast.
Bottom: *Example of structures aligned in parallel streaks.*
(All the same scale; dimension of the squares: 12″ × 12″.)

D. E. Blackwell, D. W. Dewhirst and A. Dollfus, Solar granulation observed from a manned balloon.

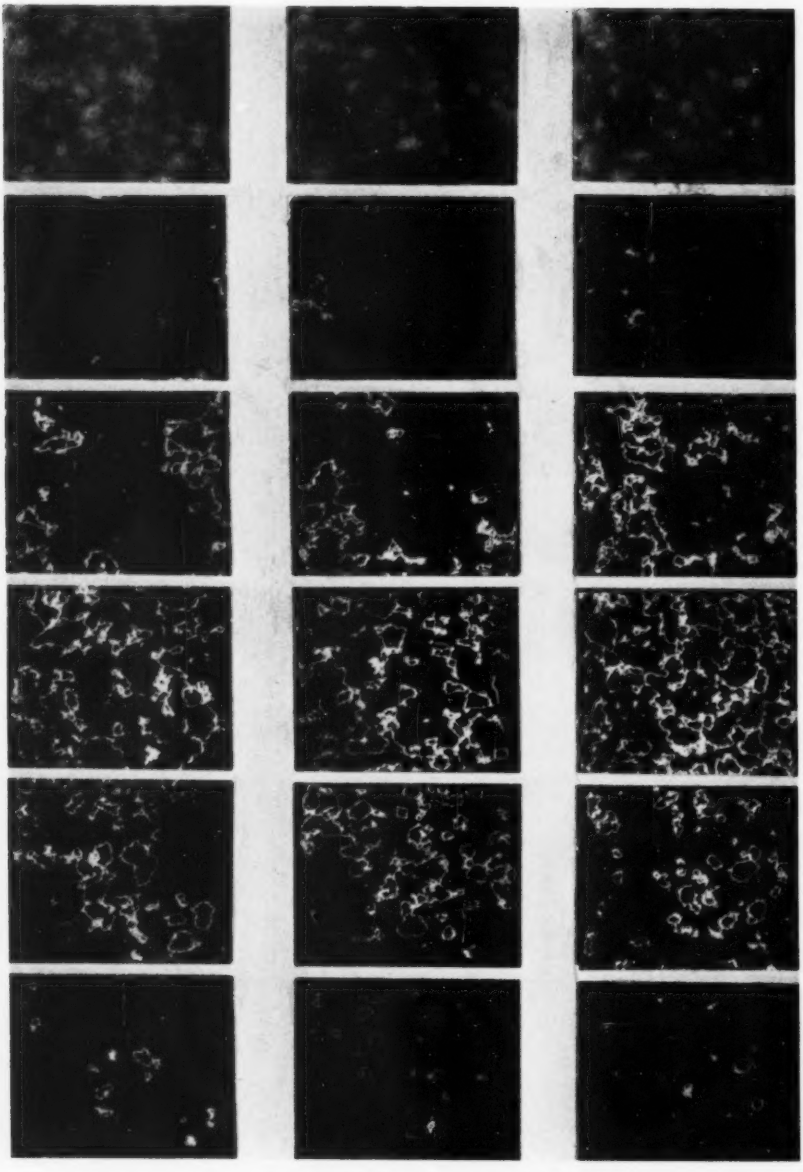

Contours of lines of equal brightness for three regions. The isophotes correspond to equal increments of brightness.
Left column: Normal region.
Centre column: Region containing a small dark area (on the left) and a particularly bright granule (at the bottom).
Right column: A region with unusually small granules.
Dimensions of each field: $20'' \times 15''$.

D. E. Blackwell, D. W. Dewhirst and A. Dollfus, Solar granulation observed from a manned balloon.

TABLE I

Author	Refs.	Aperture (cm)	Wave-length (A)	R.m.s. observed (r.m.s. corrected)	Contrast observed (contrast corrected)
ten Bruggencate and Müller	28	12	4350	–	9 (18)
Keenan	26, 27	19	5550	–	10·3 (15·0)
Thiessen	33, 34	60	5650	–	25 (35)
Richardson and Schwarzschild	31	10	5800	5·4 (–)	–
Frenkiel and Schwarzschild	22	10	5800	3·3 (–)	–
Leighton	32	30	5850	–	14 (–)
Richardson and Schwarzschild	31	30	6300	3·2 (–)	–
Waldmeier	35	(–)	(–)	–	– (30 to 40)
Krat	36	24	(–)	–	– (13)

pointed out that Keenan's value is undercorrected, and in addition the correction for the large wave-length difference is quite unknown.

The Mount Wilson photograph used by Frenkiel and Schwarzschild can tell us little about the contrast of the small scale granulation because the cut-off of the telescope is at 1″·1 and even at 1″·5 the contrast transmission function of an ideal telescope at 5800 A is only 0·15.

The r.m.s. value of 3·2 per cent obtained by Richardson and Schwarzschild was measured on a spectrogram and no instrumental correction can be estimated because of the possibility, for example, of astigmatism in the grating. The r.m.s. value of 5·4 per cent derived by these authors is for an average element size near 2″, and as the contrast transmission function for structure of this size is 0·36 for an aberration-free system, this means that the r.m.s. brightness fluctuation is probably at least 15 per cent.

The contrast given by Leighton is substantially a peak to peak brightness measurement over a scan of length 120″.

Thiessen's observations were made visually with the 60 cm refractor of the Hamburg Observatory and his value of contrast agrees well with that found by Waldmeier, who does not, however, give details of the method of observation.

The work of Plaskett (**37**) gave a total amplitude variation of 8 per cent on his best plates; however, this work refers to brightness variations in a large scale structure with elements about 5″ in diameter.

6.3. *Present results.*—On our photographs, taken with a 29 cm objective at a wave-length of 5300 A, the r.m.s. fluctuation of brightness measured on a microphotometer tracing is 4·6 per cent. Taking an effective transmission function of 0·25 appropriate to a mean granule size of 1″·4 (see Section 4.2) we obtain a corrected r.m.s. fluctuation of 18 per cent, without any additional correction for seeing.

The same microphotometer scans show that areas with an observed contrast of up to 7 per cent occur frequently, while a contrast of 9 per cent is not

uncommon (excluding those areas where there are known sunspots or pores). The isophotometer tracings show that the mean contrast between granular and intergranular regions is 11 per cent. This value is slightly higher than that indicated by the microphotometer scans probably because it refers to small regions selected for their good definition, while the microphotometer scans were made at random along the larger dimensions of the photograph. For further discussion we take the observed mean contrast between granule and intergranular space to be 10 per cent. This gives the ratio of mean contrast to r.m.s. brightness fluctuation of 2·2, which seems reasonable. Applying the same correction for a contrast transmission function of 0·25 we get a corrected value of 40 per cent. However, this correcting factor is a lower limit not only because the seeing will reduce the effective contrast transmission function (although because of the nature of our observational material we suppose that any further correction will be small), but also because the effective width of the intergranular regions is probably much less than 1″·4.

Our final result of a contrast of 40 per cent is not inconsistent with most of the values previously obtained by other investigators, provided that the observed values quoted in Table I are corrected anew by the larger factors indicated by the discussion in Section 6.2. However, the corrections that we have made to our own observed contrast are minimal. Simply interpreted this contrast implies a difference of temperature between mean granule and mean intergranular space of 520°K.

Acknowledgments

We particularly wish to acknowledge our debt to Professor R. O. Redman, who initiated this investigation and encouraged us throughout. The work was financed chiefly by a Royal Society Government Grant with help from French special funds, the balloon being placed at the disposal of Meudon Observatory by the French Air Ministry. We are especially grateful to M. Charles Dollfus of Paris who gave invaluable help and advice about the aeronautical problems. Dr P. B. Fellgett and Dr E. H. Linfoot gave advice at all times; the former also computed the autocorrelation functions on EDSAC II in the Cambridge University Mathematical Laboratory. We are indebted to Dr W. H. Steavenson who provided part of the optical apparatus, and also to T. I. Aluminium Ltd. who gave the aluminium tubing used in constructing the telescope tube.

The Observatories,
Madingley Road,
Cambridge:
1959 *February* 24.

References

(1) Janssen, J., *Ann. Obs. Paris, Meudon*, **1**, 91, 1896.
(2) Hansky, A., *Mitt. Pulkowo*, **1**, 81, 1905.
(3) Macris, C., *Ann d'Astrophys.*, **16**, 19, 1953.
(4) Rösch, J., *C.R. Acad. Sci.*, **243**, 478, 1956.
(5) Rösch, J., *L'Astronomie*, **71**, 129, 1957.
(6) Bray, R. J. and Loughhead, R. E., *The Observatory*, **77**, 201, 1957.
(7) Loughhead, R. E. and Burgess, V. R., *Australian Journal of Physics*, **11**, 35, 1958.
(8) Rogerson, J. B., *Sky and Telescope*, **17**, 112, 1958.
(9) Schwarzschild, M., Rogerson, J. B. and Evans, J. W., *A.J.*, **63**, 313, 1958.

(10) Blackwell, D. E., Dewhirst, D. W. and Dollfus, A., *The Observatory*, **77**, 20, 1957.
(11) Blackwell, D. E. and Dewhirst, D. W., *J. Sci. Instr.*, **34**, 274, 1957.
(12) Blackwell, D. E., Dewhirst, D. W. and Dollfus, A., *Nature*, **180**, 211, 1957.
(13) Duffieux, P. M., *L'Intégrale de Fourier et ses applications à l'optique*, Rennes 1946.
(14) Schade, O. H., Nat. Bur. Standards Circular 526, p. 231, 1954.
(15) Ingelstam, E., Djurle, E. and Sjögren, B., *J.O.S.A.*, **46**, 707, 1956.
(16) Coltman, J. W., *J.O.S.A.*, **44**, 468, 1954.
(17) Schade, O. H., Nat. Bur. Standards Circular 526, p. 231, 1954.
(18) Linfoot, E. H., *Optica Acta*, **4**, 12, 1957.
(19) Lyot, B., *L'Astronomie*, **67**, 3, 1953.
(20) See, for example, Goldman, S., *Information Theory*, London, 1953, p. 67.
(21) Wlérick, G., *Smithsonian Contributions to Astrophysics*, **2**, 25, 1957.
(22) Frenkiel, F. N. and Schwarzschild, M., *Ap. J.*, **121**, 216, 1955.
(23) Uberoi, M. S., *Ap. J.*, **121**, 400, 1955.
(24) Uberoi, M. S., *Ap. J.*, **122**, 466, 1955.
(25) Wanders, A. J. M., *Z. f. Astrophys.*, **8**, 108, 1934.
(26) Keenan, P. C., *Ap. J.*, **88**, 360, 1938.
(27) Keenan, P. C., *Ap. J.*, **89**, 604, 1939.
(28) ten Bruggencate, P. and Müller, H., *Z. f. Astrophys.*, **21**, 198, 1942.
(29) ten Bruggencate, P., Grotrian, W. and v. d. Pahlen, E., *Z. f. Astrophys.*, **16**, 51, 1938.
(30) ten Bruggencate, P., *Z. f. Astrophys.*, **16**, 374, 1938.
(31) Richardson, R. S. and Schwarzschild, M., *Ap. J.*, **111**, 351, 1950.
(32) Leighton, R. B., *P.A.S.P.*, **69**, 497, 1957.
(33) Thiessen, G., *Naturwiss.*, **37**, 427, 1950.
(34) Thiessen, G., *Z. f. Astrophys.*, **35**, 237, 1955.
(35) Waldmeier, M., *Helv. Phys. Acta*, **13**, 13, 1940.
(36) Krat, W. A., *Mitt. Astr. Hauptobs. Pulkowo*, **19**, No. 5 (152), 1, 1954.
(37) Plaskett, H. H., *M.N.*, **96**, 402, 1936.

MAIN-SEQUENCE STARS

C. B. Haselgrove and F. Hoyle

(Received 1959 March 9)

Summary

Integrations have been carried out for uniform stars of Types I and II. It appears likely that the separation at the zero-age main-sequence of the different populations does not exceed 0·1 magnitude, provided a correct effective temperature scale is used.

---

1. *Introduction.*—Models for main-sequence stars—i.e. stars of uniform chemical composition in which the outflow of energy is determined by nuclear processes—have been computed for the following cases:

Type I stars, $X=0{\cdot}75$, $Y=0{\cdot}24$, $A=8\times10^{-5}$, $\odot \lesssim M \lesssim 125\odot$.

Type II stars:

Case IIa, $X=0{\cdot}99$, $Y=0{\cdot}009$, $A=4\times10^{-6}$, $\odot \lesssim M \lesssim 4\odot$.

Case IIb, $X=0{\cdot}75$, $Y=0{\cdot}249$, $A=4\times10^{-6}$, $\odot \lesssim M \lesssim 3\odot$.

M = mass of the star, X = hydrogen concentration by mass, Y = helium concentration by mass, AX^{-1} = abundance of metal atoms by number relative to hydrogen.

The integrations were performed on the IBM 704. The method of integration was the same in principle as that described in a former paper (**1**), but with the increased speed and storage capacity available to us it was possible to use formulae of a more accurate kind for the opacity and for the nuclear energy generation. Account was taken of the appropriate surface boundary conditions.

2. *The opacity.*—The opacity per gram κ may be written in the form

$$\kappa=(\kappa_r^{-1}+\kappa_c^{-1})^{-1}, \tag{1}$$

where κ_r is the radiative opacity and κ_c is the conduction opacity. Formulae for κ_r, κ_c were constructed to give representations of the tabular values worked out by Keller and Meyerott for the radiative opacity (**2**) and by Mestel (**3**) for the conduction opacity. The following quite simple expression was found to represent Mestel's values with adequate accuracy (5 per cent in the important range of ρ, T)

$$\kappa_c^{-1}=\frac{T}{3018}\left\{1+\left[0{\cdot}1478(1+X)\frac{\rho}{T^{3/2}}\right]^{1{\cdot}685}\right\}, \tag{2}$$

where ρ is the density in gm cm^{-3}, and the temperature T is in units of 10^6 °K. The situation is much more complicated for the Keller–Meyerott tables. Because of the absorption edges of the various elements, the values do not run in any very simple way, so that empirical formulae must of necessity appear awkward.

The following were found to represent the tabular values within an accuracy of ~10 per cent in nearly all cases:

$$\left.\begin{aligned} 0{\cdot}1 \leqslant T < 10, &\quad \kappa_r = 0{\cdot}19(1+X) + \xi\rho(1+X), \\ 10 \leqslant T \leqslant 20, &\quad \kappa_r = 0{\cdot}19(1+X) + \xi\rho(1+X) + \rho(1-0{\cdot}1T)(\xi\overline{1+X} - \zeta), \\ 20 < T, &\quad \kappa_r = 0{\cdot}19(1+X) + \zeta\rho, \end{aligned}\right\} \quad (3)$$

the units for ρ, T being the same as in (2). The quantities ξ, ζ are given by

$$\left.\begin{aligned} \xi = 6{\cdot}5 \times 10^4 \frac{(1-X-Y)(1-0{\cdot}05T)}{T^2 + 2{\cdot}5T^4} \exp\left[-7{\cdot}75\frac{\rho(1+X)}{T^3}\right] \\ + 4{\cdot}15 \times 10^4 \left[\frac{X}{250T^4 - T^2} + \frac{Y}{250T^4}(1 + 5{\cdot}5\exp(-|\tfrac{2}{3} - 2{\cdot}873T|))\right] \\ \times \exp\left[-\frac{2\rho(1+X)}{T^3}\right], \\ \zeta = \frac{225 - 155X - 190Y}{T^{3{\cdot}5}}. \end{aligned}\right\} \quad (4)$$

These formulae enable κ to be computed when X, Y, ρ, and T are specified.

Considerable simplifications could be effected if no attempt were made to represent the tabular values over the whole of the ranges of ρ and T. If separate formulae were used in different parts of these ranges no doubt each formula could be given a straightforward structure. It must be emphasized, however, that unless care were taken to preserve strict continuity at the joins of the separate formulae severe difficulties in the iterative procedure for the numerical solutions would be encountered sooner or later (at any rate in the computational method we have used). The present formulae do preserve continuity.

The question arises as to how far the formulae can safely be extrapolated outside the range of the tables from which they were constructed. At low densities or high temperatures such an extrapolation can be made, since in these cases the formulae have a correct asymptotic form. But extrapolation at high density and low temperature would be most unsafe. The limitation is important, since the latter case arises for dwarf states with $M < \sim 0{\cdot}5\odot$. The present series of integrations were in fact carried down to $M \sim 0{\cdot}2\odot$. Results are not given below at this low mass, however, since doubts about the opacity make them of uncertain value.

Nor can the above formulae be used for the low values of T occurring at and near the photosphere. Here a quite different procedure must be followed. When ρ, T, X, Y, A, a_i, b_i, c_i ($i = 1, 2, \ldots$) are specified, the electron pressure P_e and the quantities Θ, x, y, z, u_i ($i = 1, 2, \ldots$) are determined by the following system of equations:

$$P_e = \mathfrak{R}\rho T\Theta, \quad (5)$$

$$\left.\begin{aligned} \log x &= -13{\cdot}54\theta + \tfrac{5}{2}\log T - 0{\cdot}48 - \log P_e, \\ \log y &= -24{\cdot}48\theta + \tfrac{5}{2}\log T + 0{\cdot}12 - \log P_e, \\ \log z &= -54{\cdot}17\theta + \tfrac{5}{2}\log T - 0{\cdot}48 - \log P_e, \\ \log u_i &= -a_i\theta + \tfrac{5}{2}\log T + b_i - \log P_e, \\ \theta &= \frac{5040}{T}, \end{aligned}\right\} \quad (6)$$

$$\Theta = \frac{Xx}{1+x} + \frac{Yy(1+2z)}{4(1+y+yz)} + A\sum_i \frac{c_i u_i}{1+u_i}, \qquad (7)$$

where $\mathfrak{R}$ is the gas constant, the logarithms are to base 10, and T is now in °K. The physical meanings of the symbols appearing in these equations are:

x = (ionized H density)/(neutral H density),

y = (singly ionized He density)/(neutral He density),

z = (doubly ionized He density)/(singly ionized He density),

u_i = (singly ionized density of constituent i)/(neutral density of constituent i),

a_i = ionization potential of constituent i (eV),

b_i = weight factor for constituent i,

c_i is proportional to the number density of constituent i, the constant of proportionality being chosen so that $\sum_i c_i = 1$,

$$AX^{-1} = \frac{\sum_i (\text{number density of constituent } i)}{(\text{number density of hydrogen})}.$$

Multi-stage ionization of constituent i has been neglected for all i in equation (7), Θ having the simple interpretation

$$\Theta/m_H = \text{number of electrons per gram of material},$$

where m_H is the mass of the hydrogen atom. This approximation can be made because the contribution to Θ of all elements except hydrogen and helium is always very small unless $x, y, z \ll 1$, and these inequalities require T to be low, in which case multi-stage ionization can be neglected. Indeed at low T we can neglect all elements except the metals, and of these only magnesium, silicon, iron, aluminium, sodium, and potassium are important. The above summation over i can therefore be taken as referring to these six metals only. The appropriate ionization potentials a_i, weight factors b_i, and relative abundances c_i are

	a_i (eV)	b_i	c_i
Magnesium	7·61	0·04	0·3750
Silicon	8·11	−0·42	0·3450
Iron	7·86	−0·08	0·2250
Aluminium	5·96	−0·98	0·0370
Sodium	5·12	−0·64	0·0167
Potassium	4·32	−0·92	0·0013

The relative abundances have been taken from Suess and Urey (**4**). The quantity A in equation (7) represents the overall abundance of the six metals. The tables of Suess and Urey give $A \cong 8 \times 10^{-5}$, and this can be regarded as typical for Type I stars. The value for Type II stars was taken to be twenty times less, viz. $A = 4 \times 10^{-6}$.

A satisfactory approximation for the opacity is given by

$$\kappa = 0{\cdot}38\Theta + \frac{XP_e}{(1+x)T^{5/2}} \exp\left[-6{\cdot}378 + \frac{0{\cdot}8704}{T}\right] + \frac{X \exp[15{\cdot}94 - 11{\cdot}61/T]}{(1+x)(1+0{\cdot}05T^3)}$$
$$+ \frac{Y}{4(1+y+yz)}\left(\exp\left[13{\cdot}81 - \frac{23{\cdot}22}{T}\right] + y\exp\left[13{\cdot}81 - \frac{62{\cdot}66}{T}\right]\right), \qquad (8)$$

T in units of 10^4 °K. The first term on the right-hand side of (8) gives the effect of electron scattering, the second term gives the contribution of the negative hydrogen ion, the third is the photoelectric contribution of neutral hydrogen, and the remaining term in Y represents the combined effect of neutral and singly ionized helium. Formula (8) was used at all temperatures below 10^5 °K. No attempt was made to preserve strict continuity between (3) and (8). Special provision was made to ensure that no computational difficulty could arise from a lack of strict continuity in this particular case.

3. *The nuclear energy generation.*—The following formula was used for the energy production

$$10^{-5}\rho X^2 T^4 + \rho X(1-X-Y)\left(\frac{T^8}{1 \cdot 5 \times 10^9}\right)^2 \text{ erg per gm,} \tag{9}$$

T in 10^6 °K. The first term represents the contribution of the P–P chain, and the second that of the C–N cycle.

The numerical coefficient used for the P–P chain is greater by a factor 1·5 than the rate given by Burbidge, Burbidge, Fowler and Hoyle (BBFH, **5**). This increase takes account of the recent radical change in ideas concerning the mode of completion of the P–P chain, viz.

$$\mathrm{He^3(He^4,\gamma)Be^7(e^-,\nu)Li^7}(p,\gamma)\mathrm{He^4}$$

$$\hookrightarrow (p,\gamma)\mathrm{B^8}(\beta^+,\nu)\mathrm{Be^{8*}}(\alpha)\mathrm{He^4},$$

competing strongly with $\mathrm{He^3(He^3}, 2p)\mathrm{He^4}$ whenever the concentration of $\mathrm{He^4}$ is appreciable and the temperature is above 13 m. °K. According to Fowler (**6**) the present increase of the rate by 1·5 should give a good approximation to the effect of the somewhat complicated competition between these different reactions, *provided that we are not concerned with dwarf stars appreciably fainter than the Sun.* The rate falls off at temperatures below 13 m. °K, at first slowly, and then rather steeply for temperatures below 8 m. °K, because the P–P chain then ends at $\mathrm{He^3}$. The effect is to reduce the energy production rate by a factor ~ 3 in faint dwarfs with $M \sim \odot/3$.

The coefficient chosen for the C–N cycle rate takes into consideration the enhanced rate of the $\mathrm{O^{16}}(p,\gamma)\mathrm{F^{17}}$ reaction, as discussed by BBFH. This has the effect of augmenting the nitrogen abundance through $\mathrm{F^{17}}(\beta^+,\nu)\mathrm{O^{17}}(p,\alpha)\mathrm{N^{14}}$. The carbon and nitrogen abundances were estimated from the tables of Suess and Urey (**4**) and the prescription of adding half the $\mathrm{O^{16}}$ abundance to the $\mathrm{N^{14}}$ abundance was used in order to take reasonably satisfactory account of these conversion reactions. It is true that this procedure exaggerates the coefficient of the C–N cycle for stars with central temperatures < 20 m. °K, but in such stars the main contribution to the energy generation comes in any case from the P–P chain. The situation is that the coefficient must be increased in all stars in which the C–N cycle is important.

In accordance with this prescription the concentration by mass X_{CN} of the group of elements that promote the C–N cycle is given by

$$X^{-1}X_{CN} \simeq 12C + 14(N + 0 \cdot 5O),$$

where C, N, O are abundances of $\mathrm{C^{12}}$, $\mathrm{N^{14}}$, $\mathrm{O^{16}}$ *by number* relative to hydrogen. We can rewrite:

$$X_{CN} = \left[\frac{12C + 14(N + 0 \cdot 5O)}{X^{-1}(1-X-Y)}\right](1-X-Y).$$

The point of expressing X_{CN} in this way is that we expect the *absolute* concentration of carbon, nitrogen, and oxygen in primaeval stellar material to be proportional to $1-X-Y$, so that the concentrations *relative to hydrogen* are proportional to $X^{-1}(1-X-Y)$. The value of the quantity in the square brackets should therefore be the same in all primaeval samples of stellar material. The value of this constant quantity was estimated from the tables of Suess and Urey, so that

$$X_{CN} = (\text{known quantity})(1-X-Y). \tag{10}$$

Assuming that the non-resonant reaction $N^{14}(p,\gamma)O^{15}$ is the determining step of the cycle, the formula for the rate of C–N energy production is (cf. (**5**))

$$7{\cdot}86\times 10^{27}\rho X X_{CN} f_{CN} T^{-2/3}\exp(-152{\cdot}3T^{-1/3}), \tag{11}$$

T in 10^6 °K, where f_{CN} is an electronic shielding factor $\sim 1{\cdot}5$ under conditions where the C–N cycle is important. For $20<T<45$, the range of T under consideration in this paper, (11) can be well represented by

$$(\text{known constant})\rho X X_{CN} T^{16}. \tag{12}$$

Combining (12) with (10) yields the second term in (9).

It is particularly to be noticed that when written in this way the contribution of the C–N cycle needs no change when we pass from Type I to Type II stars. The proportionality on $1-X-Y$ ensures that the coefficient of the C–N cycle changes in a correct way when $X+Y$ changes. For Type I stars $1-X-Y\cong 0{\cdot}01$, whereas for Type II stars $1-X-Y$ is probably $\leqslant 0{\cdot}001$.

4. *The surface condition.*—The method described by Hoyle and Schwarzschild was used (**7**), except that the differential equations were integrated numerically —i.e. the approximate integrals of Hoyle and Schwarzschild were not employed. A slight change was also made in the formulae used for the convective energy flux. In place of formula (84) of Hoyle and Schwarzschild

$$\beta\rho\left[Iy+\frac{1}{2}\frac{kT}{H}(1+y)\right]\left(\frac{5}{3}\frac{kT}{H}\right)^{1/2} \tag{13}$$

was used, again with $\beta=0{\cdot}3$.

5. *The homology relations.*—Although homology relations cannot be used for determining strict numerical results, they are of value in showing the approximate dependence of the radius and luminosity on the opacity and energy generation coefficients, and on the mass and mean molecular weight. The relevant formulae were obtained by Hoyle and Lyttleton (**8**) and are:

$$\left.\begin{aligned} L_{Bol} &\propto E^{-\frac{1}{2\eta+5}}\kappa^{\frac{2\eta+6}{2\eta+5}}\mu^{\frac{14\eta+45}{2\eta+5}}M^{\frac{10\eta+31}{2\eta+5}},\\ R_s &\propto E^{\frac{2}{2\eta+5}}\kappa^{-\frac{2}{2\eta+5}}\mu^{\frac{2\eta-15}{2\eta+5}}M^{\frac{2\eta-7}{2\eta+5}}, \end{aligned}\right\} \tag{14}$$

where L_{Bol}, R_s, μ represent the bolometric luminosity, radius, and mean molecular weight, where the opacity per unit mass approximates to the Kramer's form $\kappa\rho/T^{3{\cdot}5}$, and where the nuclear energy generation has the form $E\rho T^{\eta}$ per unit mass per unit time.

When on the other hand the opacity is due mainly to electron scattering the corresponding expressions are:

$$\left.\begin{aligned} L_{Bol} &\propto \mu^4 M^3, \\ R_s &\propto E^{\frac{1}{\eta+3}} \mu^{\frac{\eta-4}{\eta+3}} M^{\frac{\eta-1}{\eta+3}}. \end{aligned}\right\} \tag{15}$$

6. *Results.*—The relevant quantities for determining a stellar model (with composition specified) are L_{Bol}, R_s, the central pressure P_c and the central temperature T_c. Results for these quantities, and also for the effective surface temperature T_s, are given in Tables 1, 2, and 3. The surface temperatures were obtained from

$$L_{Bol} = \pi a c R_s^2 T_s^4,$$

where a is Stefan's constant and c is the velocity of light.

TABLE 1

Type I stars; $X=0{\cdot}75$, $Y=0{\cdot}24$, $A=8\times10^{-5}$ ($M_\odot=1{\cdot}985$, $L_\odot=3{\cdot}780$, $R_\odot=0{\cdot}6951$)

Mass (10^{33} gm)	L_{Bol} (10^{33} erg sec^{-1})	T_s (°K)	P_c (10^{16} dyne cm^{-2})	T_c (10^6 °K)	R_s (10^{11} cm)
247·78	$6{\cdot}9899\times10^5$	57400	2·0195	44·746	9·5184
165·19	$3{\cdot}5443\times10^5$	54250	2·1175	43·365	7·5875
110·13	$1{\cdot}6694\times10^5$	50320	2·2819	41·806	6·0517
73·417	$7{\cdot}1938\times10^4$	45670	2·5543	40·046	4·8228
59·945	$4{\cdot}5490\times10^4$	43130	2·7529	39·086	4·3012
39·963	$1{\cdot}6792\times10^4$	37760	3·3479	37·003	3·4081
26·642	$5{\cdot}5664\times10^3$	32290	4·3685	34·709	2·6839
17·761	$1{\cdot}6594\times10^3$	26950	6·1275	32·225	2·1043
11·841	$4{\cdot}4020\times10^2$	21850	9·1019	29·576	1·6479
7·7384	$1{\cdot}2027\times10^2$	18410	15·047	27·686	1·2141
6·8342	$7{\cdot}4701\times10^1$	16960	17·090	26·698	1·1268
5·7407	$3{\cdot}8363\times10^1$	15090	20·197	25·349	1·0204
3·9037	$7{\cdot}7211\times10$	11110	25·900	21·631	0·84462
3·0168	$2{\cdot}3215\times10$	8640	26·046	18·457	0·76553
2·8976	$1{\cdot}8930\times10$	8240	25·054	17·795	0·75986
2·7817	$1{\cdot}5332\times10$	7840	23·886	17·124	0·75483
2·5592	9·8896	7030	21·283	15·838	0·75482
2·3545	6·3535	6565	18·723	14·667	0·69379
2·1699	5·1202	6390	16·462	13·632	0·62352
1·9963	2·6958	5880	14·480	12·687	0·56299

TABLE 2

Type IIa; $X=0{\cdot}99$, $Y=0{\cdot}009$, $A=4\times10^{-6}$

Mass (10^{33} gm)	L_{Bol} (10^{33} erg sec^{-1})	T_s (°K)	P_c (10^{16} dyne cm^{-2})	T (10^6 °K)	R_s (10^{11} cm)
7·9430	$5{\cdot}7808\times10^2$	16720	28·147	27·836	1·0199
6·8750	$3{\cdot}3822\times10^2$	15100	30·074	26·154	0·95705
5·7750	$1{\cdot}7033\times10^2$	13080	30·098	23·692	0·90541
5·3130	$1{\cdot}2034\times10^2$	12095	29·026	22·367	0·88939
4·8879	$8{\cdot}3758\times10$	11120	27·400	20·992	0·87723
4·1059	$3{\cdot}7543\times10$	9200	23·103	18·143	0·85854
3·4489	$1{\cdot}6009\times10$	7500	18·613	15·526	0·84318
3·1730	$1{\cdot}0516\times10$	6820	16·603	14·402	0·82727
2·9192	6·8727	6410	14·745	13·362	0·75623
2·6856	4·4923	6060	13·072	12·408	0·68388
2·4751	2·9802	5730	11·631	11·560	0·62370
2·3761	2·4401	5580	10·988	11·169	0·59572
2·0986	1·3547	5095	9·3061	10·095	0·53171

TABLE 3

Type IIb; $X=0{\cdot}75$, $Y=0{\cdot}249$, $A=4\times10^{-6}$

Mass (10^{33} gm)	L_{Bol} (10^{33} erg sec^{-1})	T_s (°K)	P_c (10^{16} dyne cm^{-2})	T_c (10^6 °K)	R_s (10^{11} cm)
6·0614	$5{\cdot}5458\times10^2$	17800	29·818	29·083	0·88171
4·8260	$2{\cdot}3544\times10^2$	15220	34·884	26·730	0·78574
3·8423	$9{\cdot}3541\times10$	12580	36·128	23·662	0·72440
3·2014	$4{\cdot}1533\times10$	7000	32·391	20·043	0·70036
3·0170	$3{\cdot}1409\times10$	6950	30·563	19·630	0·69539
2·8337	$2{\cdot}3205\times10$	6910	28·497	18·575	0·69086
2·6523	$1{\cdot}6743\times10$	6865	26·268	17·496	0·68653
2·3128	8·3721	6860	21·813	15·443	0·68642
2·0168	4·1327	6370	17·870	13·640	0·59426
1·9579	3·5526	6240	17·121	13·289	0·57322

From the point of view of stellar structure, low metal content and presumably low carbon, nitrogen, and oxygen content are the essential characteristics of Type II stars. In the Type II models integrated, the metal content was reduced to 1/20 of that of the Type I stars and the carbon, nitrogen, and oxygen content was reduced to 1/10. It is uncertain whether the helium content should also be reduced. Two cases were therefore considered: the more likely case where the helium content was also very markedly lowered, and a less likely case in which the Type II helium concentration was taken to be the same as for Type I. These cases are shown in Tables 2 and 3 respectively and are described as IIa and IIb.

7. *Discussion.*—The dependence of L_{Bol} on the mass M changes quite markedly over the range given in Table 1 for the Type I stars. For M in the neighbourhood of $\odot$ we have $L_{Bol}\propto\sim M^5$; for $M\sim2\odot$ the dependence is already reduced to $L_{Bol}\propto\sim M^4$; for $3\odot<M<30\odot$ we have $L_{Bol}\propto\sim M^3$; and for $30\odot<M<125\odot$ radiation pressure reduces the dependence still further to $L_{Bol}\propto\sim M^2$. Apart from the latter effect of radiation pressure, these changes are determined by the opacity which alters from an essentially Kramers type of dependence at $M\sim\odot$ to an electron scattering dependence for $M>3\odot$.

The mass range of the integrations for Type II stars is not large enough to show such marked opacity effects. Indeed $L\propto M^4$ is a tolerable approximation for these stars over the whole of the mass ranges given in Tables 2 and 3. The reduced effect of the metals weakens the Kramers type of dependence at $M\sim\odot$.

Although there is no precise value of M at which the nuclear energy generation may be said to change from the P–P chain to the C–N cycle, as a general statement it can be said that the P–P chain dominates in stars with $T_c<21$ m. °K (Type I), $T_c<22$ m. °K (Type II). Maximum values of P_c occur at these temperatures. *It is also at these temperatures that convective cores first appear.*

Reference to (13) shows that when the Kramers type of opacity is dominant $R_s\propto M^{\frac{2\eta-7}{2\eta+5}}$. Now when Kramers opacity is dominant M is sufficiently small for the P–P chain to be more important than the C–N cycle. Thus we must put $\eta\sim4$, so that $R_s\propto\sim M^{1/13}$—i.e. the radius depends only very weakly on the mass. This effect is shown very clearly in Table 1, where the values of R_s decrease with M until a value $\sim0{\cdot}75$ is reached. Then $R_s\sim0{\cdot}75$ is maintained very closely for a while as M decreases.

A further consideration of the dependence of R_s on M shows, however, that R_s does not continue to stay nearly constant as M continues to decrease. Thus R_s declines markedly below 0·75 for the last three entries of Table 1. This behaviour cannot be understood in terms of the simple homology relations. It arises from the surface boundary condition. As T_s decreases with decreasing M the ionization of hydrogen at the photosphere also declines. This causes a marked decrease of photospheric opacity as T_s falls below 7000 °K. The consequent rise of the photospheric density produces an important effect on the structure of the outer regions of the star, causing the surface zone of convective instability to penetrate downwards to deeper and deeper levels. The decline in R_s due to this cause was first considered by Osterbrock (**9**).

8. *Accuracy of the integrations.*—For computations performed on a digital computer, questions of purely numerical accuracy scarcely arise. Accuracy is determined by the physical approximations that have been introduced in setting up the problem.

The Sun provides a valuable check on the physical theory used for stars on or near the main-sequence. The mass, luminosity and radius are known. Since moreover there is no reason to believe that mixing has ever taken place between the central energy producing regions of the Sun and the surface, spectroscopic analysis of the outer solar layers presumably determines the values of X, Y and of the carbon, nitrogen, and oxygen concentrations as they existed within the primaeval solar material.

Against these advantages, the Sun is not a "zero-age" main-sequence star. Geophysical evidence suggests that the Sun is probably about 5×10^9 years old. During this time the luminosity, radius, and the composition of the central regions must have changed appreciably. To allow for this, an evolutionary run was obtained by one of the present authors. This was done as a part of the investigation of the ages of Type I and II stars (cf. following paper). The results will be given here, however, since they are of more immediate application to the present paper than to the following one. The actual present-day solar values are given in brackets in the last line of Table 4. The Kelvin–Helmholtz contraction time has not been included in the age estimates.

TABLE 4

$M = 1{\cdot}985 \times 10^{33}$ gm, $X = 0{\cdot}75$, $Y = 0{\cdot}24$, $A = 8 \times 10^{-5}$.

Evolution of the Sun

L_{Bol} (10^{33} erg sec^{-1})	R_s (10^{11} cm)	Age (10^9 years)
2·620	0·5630	0·000
2·733	0·5665	0·700
2·919	0·5740	1·750
3·213	0·5875	3·150
4·016	0·6310	5·950
(3·780)	(0·6951)	(~5·000)

Interpolation between the last two entries yields an age $\sim 5{\cdot}2 \times 10^9$ years at $L_{Bol} = 3{\cdot}78 \times 10^{33}$ erg sec^{-1}, in excellent agreement with the geophysically estimated age. It may be noted that no allowance has been made for the loss of energy by neutrino emission from B^8 (cf. following paper). According to Fowler (**6**), this effect is not likely to be important for stars with internal

temperatures $\leqslant \sim 13$ m. °K, but might well amount to a 3 or 4 per cent effect —in the sense that the calculated age must be reduced to this extent.

This age agreement means that, subject to the ratio Y/X having been chosen correctly, the opacity values used in the present calculations must also be correct. In this connection it may be noted that an opacity error can be compensated (falsely!) in the luminosity calculation by a corresponding error in Y/X. Thus a calculation in which Y/X is taken as a free parameter scarcely has much value —one error may be cancelling another. In the present case the Y/X ratio indicated by the spectroscopic data was used, however.

The situation concerning the opacity is less complicated in the other stars we have considered than it is in the Sun. Hence the opacity values in the other stars are expected to be at least as reliable as they are for the Sun—and indeed the latter seem to be correct within a few per cent.

It is of interest that the luminosity of the Sun has increased by about 0·4 magn. during geologic time. By hand computation Schwarzschild, Howard and Härm obtained an increase of 0·5 magn. (**10**).

The position concerning R_s is more complicated. If the convective surface boundary condition had not been used in the present calculations, the value of R_s at zero-age would have been close to 0·75, in accordance with the simple homology conditions discussed above (i.e. if we had used the old-fashioned boundary condition $\rho, T \to 0$ at the surface, R_s would have been $\sim 0{\cdot}75$ at zero-age). Subsequent evolution would have again increased R_s by about 10 per cent—i.e. to $\sim 0{\cdot}83$. Thus the boundary condition formerly used (by Eddington for example) would have given a present-day radius some 20 per cent *too high*. By introducing a physically realistic boundary condition we have reduced the radius but have apparently overswung the correct value by about 10 per cent.

There are two ways of viewing the situation. In the broad sense it is satisfactory that the same rather simple analysis of the surface zone, found by Hoyle and Schwarzschild to be appropriate for giant stars (**7**), should also give tolerable results for dwarf stars. On this basis it appears that the analysis can probably be applied over the whole H–R diagram provided very accurate results are not required.

If really accurate values are required, the matter needs closer attention however. One possibility is to reduce the convective efficiency of material in the sub-photospheric levels. Thus the factor β in (13) could be reduced from the value 0·3, used by Hoyle and Schwarzschild for the giants, until R_s came into agreement with the required solar value. This in fact was the procedure used by Schwarzschild, Howard and Härm (**10**), and more recently by Sears (**11**).

A second way of resolving the discrepancy lies in an adjustment of the energy generation constant for the P–P chain. Reference to (14) shows that for $\eta = 4$, $R_s \propto E^{2/13}$. The radius can therefore be increased by 10 per cent through an increase of 2 in E—i.e. by a doubling of the rate of energy production at fixed ρ, T, X. In this connection it may be pointed out that within the last two years the nuclear energy estimates have in fact changed by factors of this general order on two occasions. In these circumstances it seems somewhat dangerous to take up the error in the calculated value of R_s by an adjustment of the surface condition. Until the nuclear situation becomes certain beyond any possible question it has seemed to us that the original value of the convection efficiency

should be adhered to, and that the error in R_s should be left in abeyance for the time being.

From one important point of view it would be preferable if it should ultimately prove to be the P–P energy generation rate that still is in error. The lithium abundance observed at the solar photosphere is extremely low. This has been interpreted by Greenstein and Richardson (**12**) to mean that at some stage during the history of the Sun the sub-photospheric convection zone penetrated inwards to regions where the temperature was as high as 2 m. °K. On the other hand Greenstein and Tandberg-Hanssen (**13**) find the solar beryllium abundance to be normal, implying that convection never extended inwards to a temperature of 3 m. °K (lithium is destroyed by nuclear reactions at 2 m. °K and beryllium at 3 m. °K).

Now convection turns out to be deepest at the beginning of the solar evolution. At the last solution of Table 4, convection extends inwards to $T \cong 1{\cdot}5$ m. °K, whereas at the first solution (zero-age) convection extended to $T \cong 2$ m. °K, exactly as is required by the lithium–beryllium data. In contrast to this, Schwarzschild, Howard and Härm found that after weakening the surface convective transport sufficiently to secure agreement in R_s the convection zone only extended down to $T \cong 1$ m. °K, even at zero-age. These authors suggested that lithium may have been destroyed during the Kelvin–Helmholtz contraction that preceded the main-sequence era.

9. *The main-sequence as a calibration standard.*—Fitting to the lower part of the main-sequence provides a powerful tool for determining the distance moduli of distant star groups. The procedure is to secure a standard zero-age main-sequence from nearby stars that are either young enough or faint enough to be regarded as essentially unchanged by evolution. Faint stars of large trigonometrical parallax delineate the lowest part of the main-sequence, as also do the stars of nearby clusters when a group parallax can be determined (as in the case of the Hyades). Young clusters yield the higher portions of the main-sequence simply by fitting at the faint end of the main-sequence to that given by the trigonometric stars. The distance modulus of any star group can then be determined by a simple superposition of its main-sequence on to the standard sequence (provided that main-sequence stars within the group can be resolved to a magnitude faint enough for them to be regarded as essentially unevolved).

This method would plainly be seriously upset if the zero-age main-sequence were sensitive to the composition of the stars. The degree to which the main-sequence is changed by quite drastic alterations of composition is shown in Fig. 1. Because of uncertainty in the value of Y for Type II stars both cases have been given: IIa for $Y = 0{\cdot}009$, IIb for $Y = 0{\cdot}249$. The very satisfactory result emerges that irrespective of this uncertainty *the main-sequence for Types I and II stars cannot differ by more than* 0·25 *magnitude.* Much greater differences have been claimed by observers. Indeed sub-dwarf Type II sequences as much as 1 magnitude below the Type I sequence have been described in the literature. It now seems certain, however, that errors have been made in the estimation of T_s due to line-blanketing effects (**14**).

The position concerning the coincidence of the main-sequences is probably much better than is suggested by Fig. 1. Although observational uncertainty

exists concerning the helium abundance of Type II stars it appears very probable on theoretical grounds (cf. following paper) that the helium abundance was initially very low. This suggests we should adopt case IIa. Now by an oversight (9) was used for the energy generation rate in all cases. This means that in case IIa the P–P energy production rate was overestimated by a factor 1·5, since Be^7 is not formed in the absence of He^4. The situation is easily corrected, however, since the resulting changes are small, and for small changes the homology relations (14) can be used. These relations show that for stars in which the P–P chain is dominant ($\eta = 4$) the radius R_s is proportional to the 2/13 power of the P–P energy generation rate. Thus the values of R_s in Table II should be

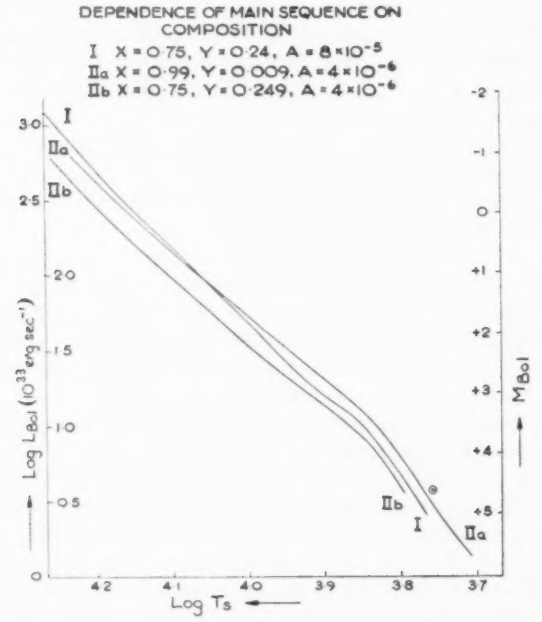

FIG. 1

decreased by $1{\cdot}5^{2/13}$ in all except the first four solutions (the C–N cycle dominates in these). Fig. 2 gives a revised plot incorporating this correction. The important result now emerges:

The separation of the lower main-sequences of Type I and II stars is not likely to exceed 0·1 magn.

On this basis the main-sequence can be used as an excellent calibration standard, provided line-blanketing effects are properly allowed for. It is particularly to be noted that a change of the surface boundary condition or of the overall P–P energy generation rate (cf. Section 8) would not change this result since both types of star would be affected in the same way.

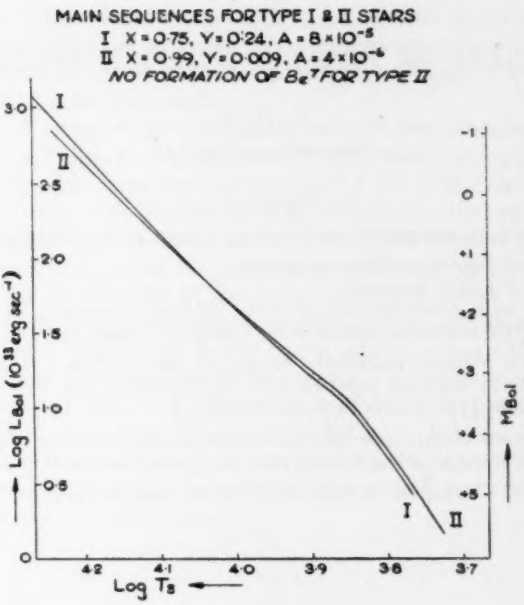
MAIN SEQUENCES FOR TYPE I & II STARS
I X = 0·75, Y = 0·24, A = 8 × 10⁻⁵
II X = 0·99, Y = 0·009, A = 4 × 10⁻⁶
NO FORMATION OF Be⁷ FOR TYPE II
Log L_Bol (10³³ erg sec⁻¹)
M_Bol
Log T_S
I
II

FIG. 2.

The authors wish to thank the Rockefeller Foundation for support of this work. Their thanks are also due to Dr H. Bratman of the Lockheed Aircraft Corporation for help in the early stages of programming; to the Rand Corporation where the calculations were begun; to the Atomic Energy Research Establishment, Aldermaston and to the I.B.M. Corporation (Great Britain) who provided facilities for their completion.

The University,
Manchester, 13:
1959 *March* 6.

St John's College,
Cambridge.

References

(1) Haselgrove, C. B. and Hoyle, F., *M.N.*, **116**, 515, 1956.
(2) Keller, G. and Meyerott, R. E., *Ap. J.*, **122**, 32, 1955.
(3) Mestel, L., *Proc. Camb. Phil. Soc.*, **46**, 331, 1950.
(4) Suess, H. E. and Urey, H. C., *Rev. Mod. Phys.*, **28**, 53, 1956.
(5) Burbidge, E. M., Burbidge, G. R., Fowler, W. A. and Hoyle, F., *Rev. Mod. Phys.* **29**, 547, 1957.
(6) Fowler, W. A., *Ap. J.*, in press, 1959.
(7) Hoyle, F. and Schwarzschild, M., 1955, *Ap. J. Suppl.*, **2**, 1, 1955.
(8) Hoyle, F. and Lyttleton, R. A., *M.N.*, **102**, 177, 1942.
(9) Osterbrock, D. E., *Ap. J.*, **118**, 529, 1953.
(10) Schwarzschild, M., Howard, R. and Härm, R., *Ap. J.*, **125**, 233, 1957.
(11) Sears, R. L., *Ap. J.*, in press, 1959.
(12) Greenstein, J. L. and Richardson, R. S., *Ap. J.*, **113**, 536, 1951.
(13) Greenstein, J. L. and Tandberg-Hanssen, E., *Ap. J.*, **119**, 113, 1954.
(14) Sandage, A. R. and Eggen, O. J., *M.N.*, **119**, in press.

Note.—For models of main-sequence stars, computed by a similar method, but with different formulae for the opacity and for the nuclear energy generation, see
(15) Blackler, J. M., *M.N.*, **118**, 37, 1958.

THE AGES OF TYPE I AND TYPE II SUBGIANTS

F. Hoyle

(Received 1959 March 9)

Summary

Evolutionary sequences corresponding closely to the lower portions of

(i) the globular cluster sequences,
(ii) the M67 sequence,

have been worked out with the aid of the IBM 704 computer. These lower portions of the sequences determine the ages of the Type I and Type II stars.

By using observed magnitudes for certain nearby Type I stars of large trigonometrical parallax, together with the condition that Type II stars be older than Type I stars, it is concluded:

(1) that the cluster-type variables cannot be brighter than $M_V = +0{\cdot}6$,
(2) that the age of the Galaxy must be greater than 10^{10} years.

Evidence is also given that the initial helium content of Type II stars was low.

---

1. *Introduction.*—On the basis of hand computation Hoyle and Schwarzschild (**1**) obtained an age of $6{\cdot}2 \times 10^9$ years for the Type II stars. This value was confirmed by Haselgrove and Hoyle (**2**), who obtained $6{\cdot}5 \times 10^9$ years from calculations carried out on a digital computer (EDSAC I). These estimates were based on $C^{12}(p,\gamma)N^{13}$ as the determining reaction of the carbon–nitrogen cycle. It now appears, however, that the non-resonant reaction $N^{14}(p,\gamma)O^{15}$ must be taken as the determining step of the cycle (**3**), and that the overall C–N energy production rate (at given X, X_{CN}, ρ, T) must be taken lower than the rates assumed in former work by a factor 10 to 10^2 (cf. preceding paper). The question accordingly arises as to whether the former age estimates stand in need of appreciable revision.

The lowering of the C–N energy generation rate enhances the importance of the P–P chain. It turns out that during the early stages of evolution of stars in the mass range $\odot$ to $1{\cdot}5\odot$ (the range in question for Type II stars) the energy generation is essentially due to the P–P chain. This introduces an important increase in the time required for evolution to carry stars away from the main-sequence—an increase that comes about for the following reason.

Because of the much lower temperature sensitivity of the P–P chain ($\sim T^4$ as compared with $\sim T^{16}$ for the C–N cycle) hydrogen is burned more uniformly throughout the central regions of a main-sequence star. Hence $d\bar{X}/dX_0$ is appreciably larger for the P–P chain than it is for the C–N cycle, where $\bar{X}$ is the mean hydrogen concentration for the whole star, and X_0 is the concentration at the centre. Now soon after X_0 declines to zero a star always moves to the right in the H–R diagram away from the main-sequence. At this evolutionary stage, $\bar{X}$ must be appreciably less when the P–P is dominant than it would be if the C–N cycle were dominant. At a given luminosity level this greater decline of $\bar{X}$ requires a greater length of time to elapse before the star departs from the

main-sequence. Thus on simple grounds it can be seen that stars evolving off the main-sequence at a given luminosity level must have a greater age if the energy is mainly generated by the P–P chain than they would have if the energy were mainly generated by the C–N cycle.

2. *Results.*—A sequence of evolutionary models was determined for a star of mass $2{\cdot}6856 \times 10^{33}$ gm, with initial hydrogen concentration 0·99, initial helium concentration 0·09, and metal concentration $A = 4 \times 10^{-6}$ (for the meaning of A, see preceding paper). The formulae used for the opacity, the energy generation, and for the surface condition were the same as in the preceding paper.

The important parameters determining the solutions are given in Table 1. The relation of these solutions to the main-sequence is shown in Fig. 1. The way in which the hydrogen concentration changes from one solution to another is given in Fig. 2. The abscissa in this figure, M_r/M, changes from zero at the centre of the star ($M_r = 0$) to unity at the surface ($M_r = M$), M_r being the mass interior to a sphere of radius r ($\leqslant R_s$). Curves of M_r/M are given in Fig. 2 only for those solutions marked by an asterisk in Table 1. It has not been thought necessary to mark which particular X-curve belongs to which solution since the solutions run down the table in the sense of decreasing $\bar{X}$, so that their respective association with the curves is obvious.

TABLE 1

Evolution of Type II star

$M = 2{\cdot}6856 \times 10^{33}$ gm; initially $X = 0{\cdot}99$, $Y = 0{\cdot}009$, $A = 4 \times 10^{-6}$

L_{Bol} (10^{33} erg sec^{-1})	T_s (°K)	P_c (10^{16} dyne cm^{-2})	T_c (10^6 °K)	Age (10^{17} sec)	R_s (10^{11} cm)
4·4920*	6065	12·986	12·378	0	0·68387
5·0088*	6135	14·646	12·901	0·5189	0·70523
5·6538*	6210	16·870	13·523	1·0378	0·73118
6·5068*	6290	20·117	14·312	1·5567	0·76434
7·0693	6335	22·453	14·814	1·8162	0·78549
8·1542*	6410	27·468	15·751	2·2054	0·82468
9·0953	6460	32·456	16·540	2·4648	0·85700
10·004	6505	37·844	17·289	2·6594	0·88676
10·721*	6535	42·563	17·875	2·7891	0·90942
12·473	6600	56·149	19·326	3·0486	0·96186
14·277*	6650	72·803	21·023	3·2432	1·0133
17·193*	6665	103·84	25·024	3·5026	1·1077
19·071	6655	176·52	22·474	3·5810	1·1690
22·468*	6550	325·82	23·782	3·7216	1·3095
24·525	6425	540·09	24·431	3·7799	1·4223
26·363*	6250	1007·5	25·321	3·8218	1·5599
27·720	5975	2437·8	27·128	3·8526	1·7499
27·657	5630	8438·9	30·700	3·8753	1·9677
30·619*	5490	24911	34·059	3·8945	2·2544

The curves of Fig. 2 demonstrate quantitatively the point that was mentioned at the end of the previous section. It is immediately clear that at the stage where X_0 declines to zero $\bar{X}$ has declined from the initial 0·99 to less than 0·85—i.e. some 15 per cent of the original hydrogen has been burned. This may be compared

with the integrations of Haselgrove and Hoyle (**2**) which gave a burning of about 11 per cent at the corresponding evolutionary phase.

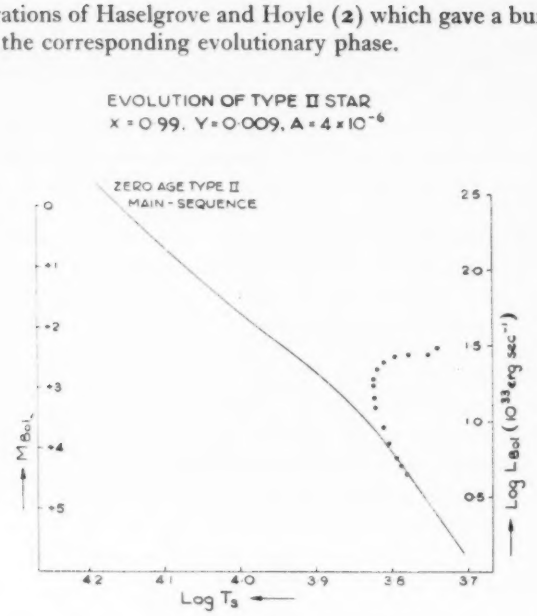

FIG. 1

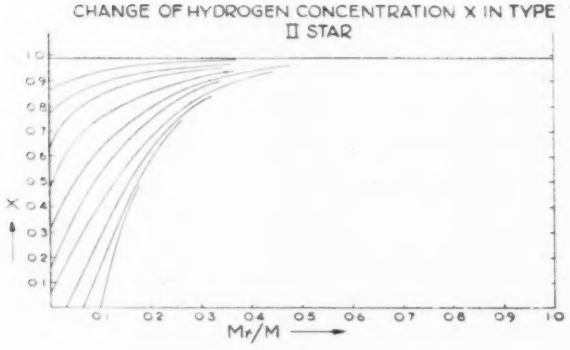

FIG. 2

The last solution given in Table 1 has a well-marked significance. It lies at the second turning point of the Type II evolutionary sequence; the point where the sequence mounts parallel to the magnitude axis of the H–R diagram at a colour index of about +0·6. It is emphasized that this solution can readily be recognized in performing the integrations because at this point the surface condition first begins to exercise a dominating influence on the structure of the star (**1**). It might also be added that even if an error were made in the identification of this particular point the effect on the calculated age would be very small indeed. The values given in the age column of Table 1 show that the main contribution

to the age comes overwhelmingly from the early stages when the star lies very near the main-sequence.

According to Sandage (**4**) this second turning point lies about 2·1 magn. below the cluster-type variables (RR Lyrae stars). Thus since the bolometric luminosity at the last solution of Table 1 is +2·4 it follows that the integrations are applicable to a Type II sequence with RR Lyrae stars at bolometric absolute magnitude +0·3. The relevant age is $1{\cdot}23 \times 10^{10}$ years. The bolometric correction to be used for the RR Lyrae stars (surface temperature ~8000 °K) is about 0·2 magn. We can conclude therefore that for a sequence with

$$M_V \cong +0{\cdot}5$$

the age $\sim 1{\cdot}2 \times 10^{10}$ years.

The absolute visual magnitude of the RR Lyrae stars has in the past been set, somewhat conventionally, at 0·0. Evidence has been put forward, however, that +0·5 is a more correct value (**5, 6**). Indeed recent work by Eggen and Sandage requires these stars to be fainter still by about 0·2 magn. (**7**).

If we assume that for small changes of the starting point on the main-sequence the whole evolutionary sequence is changed homologously, it is easy to estimate the age for other values of M_V at the RR Lyrae "gap". Under homologous conditions, age is simply proportional to M/L_i, where L_i is the initial main-sequence luminosity. For Type II stars on the main-sequence $L_i \propto \sim M^4$ (cf. preceding paper) so that the age t varies as $L_i^{-0{\cdot}75}$. Under homologous conditions there must also be a constant ratio between the starting luminosity L_i and the luminosity of the RR Lyrae variables, so that M_V for these stars is given by

$$M_V = -2{\cdot}5 \log_{10} L_i + \text{constant}.$$

Thus

$$\log_{10} t = -0{\cdot}75 \log_{10} L_i + \text{constant} = 0{\cdot}3 M_V + \text{constant}.$$

Combining this equation with the age result obtained above, viz. $t = 1{\cdot}23 \times 10^{10}$ years at $M_V = +0{\cdot}5$, we have

$$\log_{10}\left(\frac{t}{1{\cdot}23 \times 10^{10}}\right) = 0{\cdot}3(M_V - 0{\cdot}5), \qquad t = 10^{9{\cdot}94 + 0{\cdot}3 M_V} \text{ years.} \qquad (1)$$

The age estimate determined by Haselgrove and Hoyle (**2**) referred to $M_V = 0{\cdot}0$. It is seen that with this same value of M_V we now obtain $t = 8{\cdot}7 \times 10^9$ years. This gives the extent of the correction introduced by the lower efficiency of the C–N cycle. *It is particularly to be noticed that these age estimates assume no energy loss by neutrino emission from the decay of* B^8 (cf. preceding paper). This question will be discussed later.

3. *The age of M*67.—The significance of the comparison between the evolutionary sequences of the globular cluster stars (Type II) and of the stars of M67 (Type I) has been discussed by Sandage (**4**). A set of integrations ($M = 2{\cdot}1699$ gm, $X = 0{\cdot}75$, $Y = 0{\cdot}24$, $A = 8 \times 10^{-5}$) giving a theoretical sequence close to the observed sequence of M67 was computed. Results are set out in Table 2. The relation of these solutions to the Type I main-sequence is shown in Fig. 3.

At the last solution of Table 2 the bolometric magnitude is +2·67. This agrees quite closely with Sandage's value $M_{Bol} = +2{\cdot}9$ taken at the corresponding surface temperature of the M67 sequence. The age is $9{\cdot}23 \times 10^9$ years.

We again assume that Type I stars with slightly different values of the initial main-sequence luminosity L_i follow homologous evolutionary sequences. Writing

TABLE 2

Evolution of Type I star

$M = 2{\cdot}1699$ gm; initially $X = 0{\cdot}75$, $Y = 0{\cdot}24$, $A = 8 \times 10^{-5}$

L_{Bol} (10^{33} erg sec^{-1})	T_s (°K)	P_c (10^{16} dyne cm^{-2})	T_c (10^6 °K)	Age (10^{17} sec)	R_s (10^{11} cm)
5·1202	6390	16·462	13·632	0	0·62352
6·2003	6455	27·378	15·868	1·2256	0·70920
9·0576	6620	47·194	19·124	2·0427	0·81472
11·409	6655	73·216	20·518	2·4136	0·90511
13·633	6645	118·14	20·937	2·5852	0·99118
15·521	6605	175·30	21·350	2·6834	1·0717
17·170	6535	252·46	21·738	2·7463	1·1512
18·619	6445	360·60	22·135	2·7896	1·2312
19·876	6350	517·64	22·587	2·8207	1·3124
20·987	6230	774·23	23·194	2·8447	1·3995
21·867	6095	1203·8	24·034	2·8631	1·4929
22·406	5945	1928·8	25·169	2·8772	1·5897
22·517	5815	3278·5	26·660	2·8888	1·6652
22·402	5740	4234·8	27·421	2·8935	1·7044
22·229	5660	5444·2	28·178	2·8978	1·7454
22·055	5580	7001·4	28·934	2·9019	1·7892
21·974	5495	9091·2	29·701	2·9059	1·8412
22·140	5425	11465	30·227	2·9099	1·8957
22·413	5375	13494	30·607	2·9126	1·9444
22·783	5335	15439	30·783	2·9152	1·9876

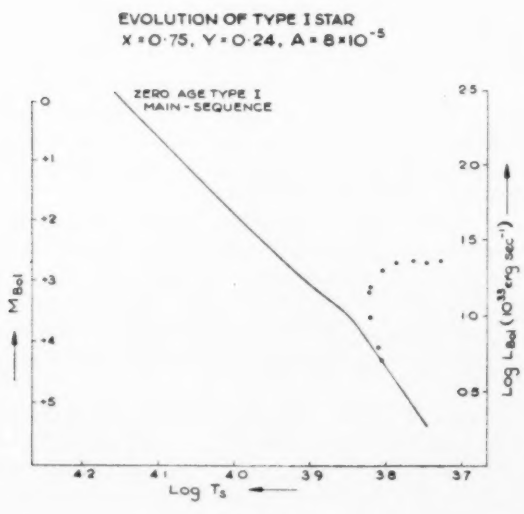

FIG. 3

M_{Bol} for the bolometric magnitude at any particular stage of the evolution we have

$$M_{Bol} = -2{\cdot}5 \log_{10} L_i + \text{constant}. \qquad (2)$$

The constant in this equation depends of course on the particular evolutionary stage that happens to be chosen, but the important point emerges from Table 2 that the constant is very insensitive to the evolutionary stage provided that it is chosen at the almost constant luminosity level at which the evolutionary track moves markedly to the right in the H–R diagram.

We can again argue that the age t is proportional to M/L_i. For Type I stars with masses of solar order we have $L_i \propto \sim M^5$ (cf. preceding paper) so that $t \propto L_i^{-0{\cdot}8}$. Using equation (2) this proportionality becomes

$$t = (\text{constant}) \,.\, 10^{0{\cdot}32 M_{Bol}}. \qquad (3)$$

The constant here is also very insensitive to the precise stage of the evolution provided that it is chosen at the almost constant luminosity level of Table 2. Thus since we have already obtained $t = 9{\cdot}23 \times 10^9$ years for $M_{Bol} = +2{\cdot}67$ at this almost constant level, we have

$$t = 10^{9{\cdot}11 + 0{\cdot}32 M_{Bol}}, \qquad (4)$$

where M_{Bol} must be taken as the bolometric absolute magnitude of subgiants at the almost constant luminosity level in the H–R diagram at which the evolutionary track first moves markedly to the right.

4. *δ Erid. and μ Herc. A.*—In a survey of nearby subgiants Eggen (**8**) obtained $M_V = +3{\cdot}67$, $B-V = +0{\cdot}94$ ($T_s \cong 4650$ °K) for the star δ Erid. Since the trigonometrical parallax is very large (0·109″) the value of M_V cannot be seriously doubted. The bolometric correction for such a Ko IV star is probably about 0·37 magn. (**9**), yielding $M_{Bol} = \cong +3{\cdot}3$. Substitution in (2) gives $t = 1{\cdot}47 \times 10^{10}$ years.

The same result follows for the G5 IV star μ Herc. A. The appropriate values are $M_V = +3{\cdot}58$, $B-V = +0{\cdot}75$ ($T_s \cong 5100$ °K), bolometric correction $\cong 0{\cdot}28$, $M_{Bol} \cong +3{\cdot}3$. This star has parallax 0″·108.

A fair number of Type I subgiants are also known at comparable values of M_{Bol}, but the determinations of M_V are somewhat less certain than they are for δ Erid. and μ Herc. A.

5. *The B^8 problem.*—The question now arises as to how far the above age estimates must be modified to take account of recent changes in our understanding of the termination of the P–P chain, viz.

$$\mathrm{He^3}(\alpha,\gamma)\mathrm{Be^7}(e^-,\nu)\mathrm{Li^7}(p,\gamma)\mathrm{He^4}$$
$$\hookrightarrow (p,\gamma)\mathrm{B^8}(\beta^+,\nu)\mathrm{Be^{8*}}(\alpha)\mathrm{He^4}$$

competing with $\mathrm{He^3}(\mathrm{He^3}, 2p)\mathrm{He^4}$. If the P–P chain were always completed through B^8 all estimates of lifetimes would be reduced by the factor 0·73. The reason for this is simply that the effective energy output from hydrogen burning is then reduced by 0·73, so that the time required for a star to burn a given quantity of hydrogen at a specified luminosity is reduced by the same factor.

According to an analysis by Fowler (**10**), the situation is much more complex than this, however. The energy loss by neutrino emission from B^8 depends on the temperature and on the concentration of He^4. The numerical values given by Fowler show that little correction is needed up to, and including, the fourth solution of Table 1 for the Type II stars—the central temperature and the

helium concentration are both too low for the correction to be appreciable, even for the largest reasonable cross-section for the reaction $Be^7(p,\gamma)B^8$. Likewise little correction is required for central temperatures above 20 m. °K, since the main energy generation then comes from the C–N cycle. This leaves only the range of solutions where the central temperature ranges from ~14 m. °K to ~20 m. °K.

The following prescription should give a reasonably accurate estimate for the corrections to be applied for the Type II stars:

$T_c < 14$ m. deg., no correction (Y small),

$14 < T_c < 20$ m. deg., 20 per cent reduction,

$T_c > 20$ m. deg., no correction.

This prescription amounts to an overall reduction of age by ~0·90. Probably the reduction is then somewhat exaggerated, but the uncertainty in the final age is probably less than 5 per cent—the factor could scarcely be as low as 0·85 or as high as 0·95, although it might well be as high as 0·92 or 0·93. Formula (1) then becomes

$$t = 10^{9\cdot90+0\cdot3M_V} \text{ years.} \tag{5}$$

The reduction factor must be greater for Type I stars, because the initial helium concentration is almost certainly higher in Type I stars. Also the central temperatures in Table 2 are systematically higher than in Table 1. Against this latter point, however, it must be remembered that the solutions of Table 2 refer to an evolutionary sequence more luminous by about 0·7 magn. than the sequences of δ Erid. and μ Herc. A. Thus the central temperatures along the sequences of the latter stars would probably fall closer to Table 1 than to Table 2.

As a reasonable estimate for old Type I stars, a reduction factor of 0·85 may be used, again probably correct to within 5 per cent. Then formula (4) becomes

$$t = 10^{9\cdot04+0\cdot32M_{Bol}} \text{ years,} \tag{6}$$

where M_{Bol} is the absolute bolometric magnitude of the old Type I subgiants —e.g. δ Erid. and μ Herc. A at $M_{Bol} \cong +3\cdot3$.

6. *Conclusion.*—If we accept the inference that the stars of the globular clusters are older than the oldest Type I stars (an inference that can be based either on dynamical arguments or on considerations of nucleogenesis) the value of t given by (6) must be less than the value given by (5). Immediately we have

$$0\cdot30(M_V)_{\text{RR Lyrae}} > 0\cdot32(M_{Bol})_{\delta\text{ Erid}} - 0\cdot86.$$

Setting $M_{Bol} = +3\cdot3$ for δ Erid. (or for μ Herc. A) we obtain

$$(M_V)_{\text{RR Lyrae stars}} > +0\cdot6,$$

in agreement with the recent work of Eggen and Sandage (7). And with $M_V > +0\cdot6$ in (5) we have $t > 1\cdot2 \times 10^{10}$ years. *The age of the Galaxy is in excess of* 10^{10} *years.*

In view of the cosmogonical significance of these conclusions it is of interest to consider what errors might possibly influence the above arguments. A change in the calculated age of the Galaxy could come about from:

(*a*) errors in the observed apparent magnitudes of δ Erid. and μ Herc. A,

(*b*) errors in the parallaxes of these stars,

(*c*) errors in the bolometric corrections,

(*d*) errors in the assumed initial helium–hydrogen ratio,

(*e*) an error in estimating the effect of neutrino emission from B^8.

Before considering these possibilities it may be noticed that an error in the opacities used in the calculations would not affect the age calculation in an appreciable measure. An error of opacity would change the theoretical estimate of the masses of the stars. In this connection it may be noted that the present calculations give a mass $1{\cdot}093\odot$ at subgiant bolometric magnitude $+2{\cdot}67$. For other values of M_{Bol}, the homology relation (with $L_i \propto \sim M^5$ on the main-sequence—M is the mass of the star) gives

$$\log_{10}\frac{M}{\odot} = 0{\cdot}2523 - 0{\cdot}08 M_{Bol}.$$

Thus for δ Erid. and μ Herc. A at $M_{Bol} \cong +3{\cdot}3$ we obtain $M \cong 0{\cdot}97\odot$.

Likewise a moderate error in the overall energy generation coefficient for the P–P chain would not affect the age estimates. Such an error would change the radius R_s slightly (cf. preceding paper) and would hence alter T_s somewhat. But M_{Bol} for the subgiants is substantially independent of T_s, as can be seen from Table 2. Hence such an error would be of no real consequence in the present considerations.

Of the possibilities listed above, (*a*) and (*b*) are too improbable to be seriously considered. A bolometric correction of 0·28 magn. was used for μ Herc. A at $B-V=+0{\cdot}75$. It seems most unlikely that this correction is significantly too small—which it would have to be to change the above estimate for the age of the Galaxy at all appreciably. Nor can the age estimate be much reduced by (*e*). We have already noticed that 0·73 gives the greatest possible factor of reduction in the ages, corresponding to the extreme case where the P–P chain always proceeds through B^8. In our estimates for Type I stars the factor used was 0·85. If instead the factor 0·73 had been used the age inequality for the Galaxy would have been $t > 1{\cdot}07 \times 10^{10}$ years. This estimate is certainly too low since the P–P chain does not always pass through B^8.

The initial helium–hydrogen mass ratio of the old Type I stars was taken as $\frac{1}{3}$. This falls close to the value given by Suess and Urey (**11**), and is close to the value associated with the primaeval solar material. Since the Sun is apparently much younger than the old Type I subgiants it would indeed be surprising if the solar helium–hydrogen ratio were less than the value appropriate to the latter stars (as it would have to be to reduce the calculated age of the Galaxy). Rather should the reverse be the case.

It may be remarked that an increase in the helium–hydrogen ratio would decrease the calculated masses of δ Erid. and μ Herc. A below the value $0{\cdot}97\odot$ obtained above. Accurate mass determinations would provide a test of this question.

Turning now to the value of M_V appropriate to the RR Lyrae stars, we ask: how would the above conclusion ($M_V > +0{\cdot}6$) be affected if the Type II stars were taken to have initial composition $X=0{\cdot}75$, $Y=0{\cdot}249$, instead of $X=0{\cdot}99$, $Y=0{\cdot}009$ (the metal abundance remaining unchanged at $A=4\times10^{-6}$)? A qualitative answer can be given at once. Since the amount of hydrogen is thus reduced, the corresponding evolutionary development at a given luminosity level proceeds more quickly. Thus to obtain the *same* age for two evolutionary sequences, one with $X=0{\cdot}99$ (IIa) and the other with $X=0{\cdot}75$ (IIb), the general

luminosity level for IIb must be lower than for IIa. Hence the condition that the ages of Type II stars be greater than the ages of Type I stars demands a lower luminosity level in case IIb than in case IIa. Hence for case IIb the RR Lyrae stars must have M_V fainter than for case IIa.

To examine this effect quantitatively an evolutionary sequence for case IIb was computed at mass $2{\cdot}3128 \times 10^{33}$ gm. Results are given in Table 3. Unfortunately the value of M used in the calculations was too large, causing the

TABLE 3

Evolution of Type II star

$M = 2{\cdot}3128 \times 10^{33}$ gm: initially $X = 0{\cdot}75$, $Y = 0{\cdot}249$, $A = 4 \times 10^{-6}$

L_{Bol} (10^{33} erg sec^{-1})	T_s (°K)	P_c (10^{16} dyne cm^{-2})	T_c (10^6 °K)	Age (10^{17} sec)	R_s (10^{11} cm)
8·3730	7070	21·717	15·417	0	0·68643
10·674	7465	29·071	16·949	0·4110	0·69536
11·770	7605	33·002	17·632	0·5480	0·70332
13·127	7765	38·294	18·451	0·6850	0·71312
17·060	8120	56·293	20·805	0·9590	0·74261
19·854	8295	70·784	22·818	1·0960	0·76803
23·442	8420	94·316	24·994	1·2331	0·81051
25·277	8475	116·49	24·326	1·2744	0·83015
27·642	8520	146·49	24·566	1·3207	0·85886
29·773	8545	179·55	24·898	1·3562	0·88663
31·968	8545	218·31	25·095	1·3830	0·91820
33·931	8535	261·80	25·334	1·4044	0·94861
37·549	8475	368·83	25·800	1·4215	1·0123
40·820	8370	512·62	26·270	1·4472	1·0816
44·077	8210	736·23	26·832	1·4660	1·1682
47·151	7990	1083·6	27·550	1·4800	1·2759
49·973	7700	1630·4	28·530	1·4909	1·4135
52·638	7300	2595·3	29·952	1·4991	1·6139
54·636	6785	4260·3	31·262	1·5077	1·9053

general luminosity level to be too high. By applying the homology condition the relevant results can readily be extracted, however. The luminosity level in Table 3 is higher than the level in Table 1 by about 0·7 magn. Remembering that the level for the RR Lyrae stars fell at $M_V \cong +0{\cdot}5$ for the sequence of Table 1, the level for the sequence of Table 3 must fall at $M_V \cong -0{\cdot}2$ according to the homology assumption. The corresponding age is $4{\cdot}78 \times 10^9$ years.

An argument exactly similar to that leading to (1) now gives the following general relation between the age t and the luminosity level M_V of the RR Lyrae stars:

$$t = 10^{9{\cdot}74+0{\cdot}3M_V} \text{ years.} \tag{7}$$

Once again a correction must be made for neutrino emission by B^8. In the present case the correction factor must be closely the same as for the Type I stars, since the helium–hydrogen ratio is closely the same. Thus we now apply the correction factor 0·85 instead of the factor 0·90 used formerly for case IIa. This gives

$$t = 10^{9{\cdot}67+0{\cdot}3M_V} \text{ years.} \tag{8}$$

The requirement that the age (8) for the case IIb be greater than the age (6) of old Type I stars (with $M_{Bol} = +3{\cdot}3$, as for μ Herc. A and δ Erid.) leads immediately to

$$M_V > +1{\cdot}3.$$

This is the condition imposed on the visual magnitude of the RR Lyrae stars. Such a low value of M_V makes it appear unlikely that Type II stars correspond to case IIb, the upper limit $+1{\cdot}3$ being significantly fainter than the value suggested by observation (7).

It is a pleasure to acknowledge my gratitude to the Rockefeller Foundation and to the I.B.M. Corporation for the support and facilities that were given to me during the course of this work.

St John's College,
Cambridge:
1959 *March* 6.

References

(1) Hoyle, F. and Schwarzschild, M., *Ap. J. Supp.*, **2**, 1, 1955.
(2) Haselgrove, C. B. and Hoyle, F., *M.N.*, **116**, 515, 1956.
(3) Burbidge, E. M., Burbidge, G. R., Fowler, W. A. and Hoyle, F., *Rev. Mod. Phys.*, **29**, 547, 1957.
(4) Sandage, A. R., *Ap. J.*, **126**, 326, 1957.
(5) Parenago, P. P., *Per. Zvezd.*, **10**, 193, 1954.
(6) Sandage, A. R., *Semaine D'etude sur le Problème des Populations Stellaires* (Pontificia Academia Scientiarum), 41, 1958.
(7) Eggen, O. J. and Sandage, A. R., *M.N.*, **119**, in press.
(8) Eggen, O. J., *P.A.S.P.*, **67**, 315, 1955.
(9) Hoyle, F. and Wilson, O. C., *Ap. J.*, **128**, 604, 1958.
(10) Fowler, W. A., *Ap. J.*, in press, 1959.
(11) Suess, H. E. and Urey, H. C., *Rev. Mod. Phys.*, **28**, 53, 1956.

A NOTE ON THE RR LYRAE VARIABLES

T. D. Kinman

(Communicated by the Radcliffe Observer)

(Received 1958 December 19)

Summary

The pulsation criterion $P\sqrt{\rho}=Q$ is used to derive the absolute magnitudes of the RR Lyrae variables as a function of their colour and period; an error in a similar derivation by Sandage is corrected. According to this model the observed difference in mean periods of the variables in M3 and ω Cen is due to a difference of 0·3 absolute visual magnitude between the stars in the two clusters.

Rough agreement is found between the predicted absolute magnitudes and those derived from trigonometrical parallaxes for four field variables with $P<0{\cdot}2$ days.

The pulsation model predicts a difference of $0^{m}{\cdot}7$ between the abnormal short period *ab* types found by Gaposchkin at the galactic centre and the normal *ab* and *c* types in the same field. Since this is not observed, either the model or the periods of the abnormal variables are incorrect.

A list is given of 16 stars of *ab* type and $P<0{\cdot}36$ days in the general field. These stars are shown to lie closer to the galactic plane than a sample of normal *c* type variables of the same period, in agreement with Detre's observation of a relatively smaller solar motion for these stars. Further observations are required for such stars both at the galactic centre and in the general field.

In 1940, Schwarzschild (**25**) showed that the RR Lyrae stars in M3 were restricted to a definite zone in the colour magnitude diagram and that the pulsations of those variables of Bailey type *ab* obeyed the period–density pulsation criterion $P\sqrt{\rho}=Q$*. Recently, Roberts and Sandage (**21**) determined colours and magnitudes for 47 RR Lyrae stars in M3 on a photoelectric scale. They showed that both Bailey types *ab* and *c* obeyed the pulsation criterion with $Q_{ab}/Q_c \sim 1{\cdot}5$, so that type *ab* probably vibrate in the fundamental mode and type *c* in the first overtone. Sandage (**24**) has further suggested that the pulsation model may explain the distribution of mean period ($\bar{P}$) of these variables in globular clusters which was found by Oosterhoff (**18**). For one group of clusters (e.g. ω Cen, M15, M53 and M92) $\bar{P}_{ab} \sim 0{\cdot}63$ and $\bar{P}_c \sim 0{\cdot}37$, while for the other group (e.g. M3, M4 and M5) $\bar{P}_{ab} \sim 0{\cdot}55$ and $\bar{P}_c \sim 0{\cdot}31$. Sandage's calculations are repeated here because, in obtaining his relation between absolute magnitude and period (viz. $\Delta M_v = -2{\cdot}8\Delta \log P$), he used an incorrect sign in the expression for the mass–luminosity relation. His corresponding calculation for galactic cepheids (**23**) is however correct.

* This relation holds for homologous stellar models. It was first found by A. Ritter (*Wied. Ann.*, **8**, 172, 1879) for a homogeneous star, and H. Shapley (*Ap. J.*, **40**, 448, 1914) first applied it quantitatively to the cepheid variables. Later, Eddington (*M.N.*, **79**, 2, 177, 1918) found that the relation also holds approximately for stars of a non-uniform density distribution.

The pulsation criterion may be written as

$$\log P + \tfrac{1}{2}\log\frac{\mathfrak{M}}{\mathfrak{M}_\odot} + 0{\cdot}3(M_{\text{bol}} - M_{\text{bol}\odot}) + 3\log\frac{T_e}{T_{e\odot}} = \log Q. \qquad (1)$$

From Morgan and Keenan (**17**) and Johnson and Morgan (**9**), we have:

$$\log T_e = 3{\cdot}983 - (0{\cdot}332 \pm 0{\cdot}030)(B-V) \quad \text{for} \quad 0{\cdot}17 < (B-V) < 0{\cdot}40 \qquad (2)$$

and from Kuiper (**13**) and Eggen (**2**), we have:

$$M_{\text{bol}} = M_V - 0{\cdot}23 + (0{\cdot}28 \pm 0{\cdot}16)(B-V) \quad \text{for} \quad 0 < (B-V) < 0{\cdot}7 \qquad (3)$$

while assuming that the slope of the main-sequence mass–luminosity relation (Kuiper (**14**)) may be applied as in (**23**), we have:

$$\log\frac{\mathfrak{M}}{\mathfrak{M}_\odot} = \text{const.} - (0{\cdot}122 \pm 0{\cdot}014)M_{\text{bol}}. \qquad (4)$$

Substituting (2), (3) and (4) in (1), we have:

$$M_V = (+3{\cdot}89 \pm 0{\cdot}41)(B-V) - (4{\cdot}18 \pm 0{\cdot}12)\log P + (4{\cdot}18 \pm 0{\cdot}12)\log Q + \text{const.} \qquad (5)$$

The quoted errors are merely the uncertainties in obtaining linear relations from the data; the actual errors of the coefficients in equation (5) may be somewhat larger because the relations (2), (3) and (4) do not apply exactly to RR Lyrae stars. This error of application is likely to be quite small for the bolometric correction in equation (3). Iwanowska (**8**) has deduced from a mass–luminosity relation of Parenago and Masevitch (**19**) that the coefficient of M_{bol} in (4) varies from $-0{\cdot}100$ for pulsation stars of Population I to $-0{\cdot}086$ for all Population II stars. These values lead to an error in the coefficient of $\log P$ and $\log Q$ in equation (5) of $\pm 0{\cdot}32$. The colour–temperature relation in equation (2) is derived from main-sequence stars. According to Sandage (**22**), however, RR Lyrae stars have a surface gravity 0·03 that of main-sequence stars of the same T_e, and the electron pressure is reduced by a factor 5. The application of the slope of the plot of $(B-V)$ against T_e for main-sequence stars to RR Lyrae stars (see Fig. 2 of (**22**)) will therefore introduce errors which will show up as an error in the coefficient of $(B-V)$ in equation (5) which it is difficult to estimate. The uncertainty in the coefficient of $(B-V)$ is therefore likely to be somewhat larger than that quoted above.

The zone of instability in M3 is $0{\cdot}17 < (B-V) < 0{\cdot}23$ for *c* type variables and $0{\cdot}23 < (B-V) < 0{\cdot}39$ for type *ab*. Sandage (**24**) has assumed that this is true for all globular clusters, i.e. the zone is vertical on a c-m diagram. There is no observational evidence for this because of the unknown amounts of reddening in different clusters. For W Virginis stars and classical cepheids it is known that the zone has a slope of $\Delta(M_V)/\Delta(B-V) \sim 11$. The adoption here of a vertical zone does not materially affect the arguments in this paper.

Fig. 1 shows a colour–magnitude diagram for RR Lyrae stars in the form given by Sandage (**24**). Lines of constant period are drawn calculated from equation (5) assuming $Q_{ab}/Q_c = 1{\cdot}5$ (Roberts and Sandage, *loc. cit.*). The M3 variables with known photoelectric colours and periods (further than 180″ from the cluster centre) are plotted in the figure, *using their colours and periods alone*. Plotted in this way, a range of 0·4 in absolute visual magnitude is predicted; it must be noted that the ordinate in the figure (M_V) has an arbitrary zero. The predicted range must be diminished when allowance is made for errors in colour; it could in fact be produced entirely by a maximum error of $\pm 0{\cdot}05$ in the observed

colour. The directly observed spread in visual magnitude for the selected *ab* stars in M3 is 0·23 magnitude.

The ratio P_{ab}/P_c of the periods of *ab* type and *c* type variables with the same M_v in any cluster is found from equation (5) to be:

$$\log \frac{P_{ab}}{P_c} = 0{\cdot}93[(B-V)_{ab} - (B-V)_c] + \log \frac{Q_{ab}}{Q_c}. \qquad (6)$$

It would be desirable to see if Q_{ab}/Q_c is the same for the ω Cen group of clusters ($\bar{P}_{ab} = 0^d{\cdot}63$ and $\bar{P}_c = 0^d{\cdot}37$) as for the M3 group ($\bar{P}_{ab} = 0^d{\cdot}55$ and $\bar{P}_c = 0^d{\cdot}31$), but sufficient variables of known colour are not available for the

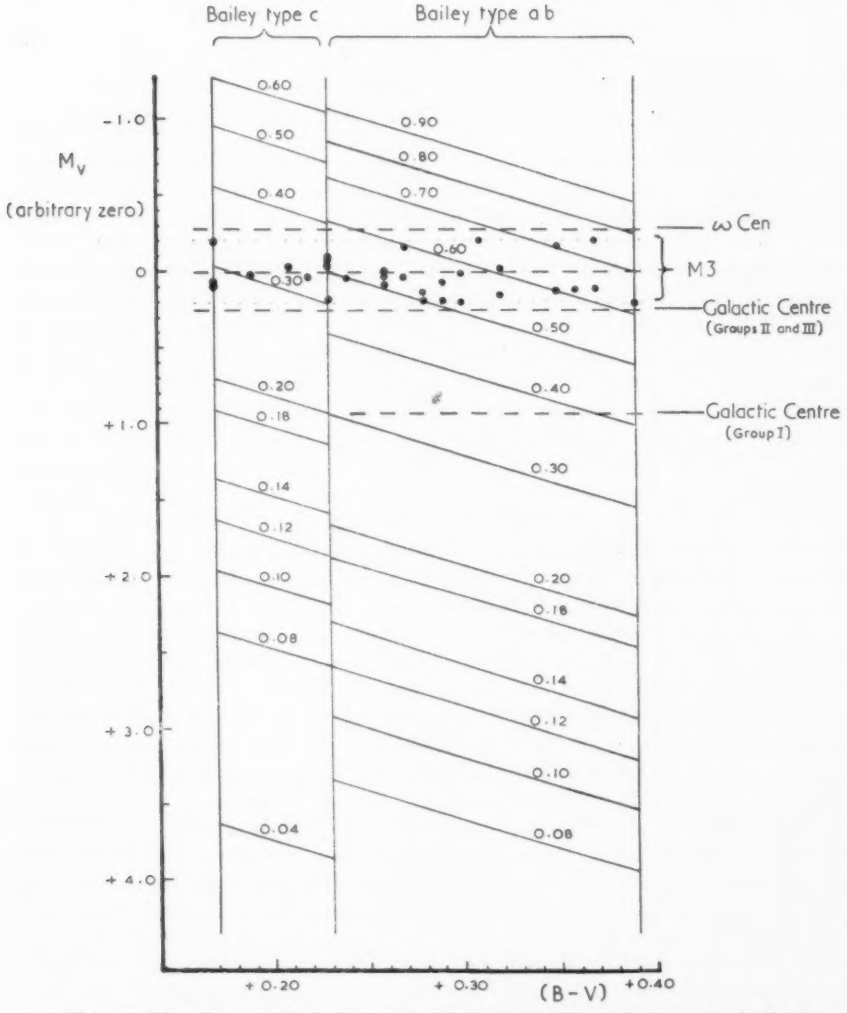

FIG. 1.—*The colour-magnitude diagram for RR-Lyrae variables in the form given by Sandage* (24). *The ordinate* M_v *is computed from the colour and period by equation* (5) *with* $Q_{ab}/Q_c = 1{\cdot}5$ *and is adjusted so that the variables in M3 have zero mean magnitude.*

ω Cen group. If we assume that the mean colours of the *ab* type and the *c* type variables are the same for all clusters and further if Q_{ab}/Q_c is constant, we should expect $\bar{P}_{ab}/\bar{P}_c$ to be constant. The values of $\bar{P}_{ab}/\bar{P}_c$ for the ω Cen group and the M3 group are 0·170 and 0·177 respectively, suggesting that Q_{ab}/Q_c is in fact constant. In this case, equation (5) predicts that the variables of the ω Cen group are $\sim 0^{m}\cdot 3$ brighter than those in M3. Also, it can be seen from the figure that the ω Cen variables should be bluer than those of the same period in M3, when absorption effects have been removed; it is therefore very necessary to obtain colours for the variables in a cluster of the ω Cen group to check this prediction. At present we can only conclude that the pulsation model is consistent with the available observations of the RR Lyrae variables in globular clusters.

Additional checks on the model may be obtained by considering its implications for the short period variables in the general field and this is discussed in the following sections.

Variables with $0{\cdot}05 < P < 0{\cdot}2$ *days.*—About 30 of these stars are known and they are often distinguished from RR Lyrae stars for which $0{\cdot}2 < P < 1{\cdot}0$ days. Absolute magnitudes from trigonometric parallaxes are known for four of them and Woltjer (**27**) has attempted to estimate absolute magnitudes for SX Phe and AI Vel from radii determined from phase shifts in the light curves. The absolute photographic magnitude (M_{pg}) has been calculated for these stars by equation (5) using Eggen's colours (**3**) for SX Phe, ρ Pup and δ Sct, while the colour of AI Vel has been deduced from the mean spectral type. M_{pg} was *assumed* to be zero for the variables in M3 in order to determine the constant in equation (5). The values found are compared with those found from parallaxes and by Woltjer in Table I. It may be noted that the values derived from parallaxes and from the pulsation model will be similarly affected by a small unknown amount of reddening ϵ: the parallax magnitude will be too bright by 4ϵ and the pulsation model magnitude by $4{\cdot}9\epsilon$. The assigned Bailey type can be no more than a guess, in view of the variable nature of the light curves of these very short period stars; this considerably strains the applicability of a simple model with one pulsation period. Considering this and the likely errors in the parallaxes, the discrepancies found for individual stars might have been expected. Both model and trigonometrical parallaxes however give a mean M_{pg} for the group of $+2{\cdot}5$ which suggests that the coefficient of $\log P$ in equation (5) is roughly correct.

TABLE I

The absolute photographic magnitude (M_{pg}) *for stars with* $0{\cdot}05 < P < 0{\cdot}20$ *days*

Star	Assumed Bailey type	Period (days)	$B-V$	M_{pg} Pulsation model	M_{pg} Trigonometrical parallaxes	M_{pg} Woltjer (**27**)
SX Phe	*ab*	0·056	+·20 (**3**)	+3·7	+4·1 ± 0·9 (**27**)	+4·5
AI Vel	*ab*	0·111	+·26 (**27**)	+2·7	+4·3 ± 0·4 (**26**)	+2·2
ρ Pup	*c*	0·141	+·42 (**3**)	+2·4	−0·4; +0·3; +1·6 (**3**)	—
δ Sct	*c*	0·194	+·34 (**3**)	+1·4	+1·7; +1·6 (**3**)	—

RR Lyrae variables at the galactic centre.—It is found that in globular clusters the variables with periods $\sim 0{\cdot}3$ days always have symmetrical light curves

(Bailey type *c*). Greenstein (**6**) noticed, however, that there are a few stars of type *ab* of this period in the general field. Recently Gaposchkin (**4**), in studying a field near the galactic centre, has found that about one-half of the stars of this period are of type *ab*. Pavlovskaya (**15**), however, claims that some of Gaposchkin's short periods should be 0·5 instead of 0·3 days.

A comparison of Gaposchkin's stars with a sample from the general field (on a plot of the period (P) against the asymmetry ($M-m$)) shows that the greatest difference for the two samples is for stars with $0{\cdot}20 \leqslant P \leqslant 0{\cdot}36$ days and $(M-m) \leqslant 0{\cdot}22$; ~30 per cent of Gaposchkin's stars lie in this region compared with ~1 per cent in the general field. Ninety-three of Gaposchkin's stars taken from the General Catalogue (**5**) are divided into three groups according to period and asymmetry in Table II.

TABLE II

Stars at the galactic centre (Gaposchkin)

Group	Bailey type	Period range	Mean period	$M-m$	Mean $(M-m)$	Mean apparent pg magnitude	No.
I	*ab*	$0{\cdot}20<P<0{\cdot}36$	0·32	$<0{\cdot}22$	0·17	$17{\cdot}62\pm0{\cdot}08$	36
II	*c*	$0{\cdot}20<P<0{\cdot}36$	0·28	$>0{\cdot}22$	0·34	$17{\cdot}57\pm0{\cdot}06$	32
III	*ab*	$P>0{\cdot}36$	0·43		0·19	$17{\cdot}63\pm0{\cdot}15$	25

Asymmetry ($M-m$) is the time of brightness increase for the variable expressed as a fraction of the period.

Each group of Gaposchkin's stars shows the same mean apparent magnitude with only a small scatter; it may be inferred therefore, following Baade, that they all occupy the same volume in space and have the same absolute photographic magnitude within 0·1 magnitude. If we assume that the mean colour of the *ab* variables is about 0·1 magnitude redder than for the type *c*, then the M_V for all groups is practically the same. The horizontal dashed lines in the figure labelled Galactic Centre (Groups II and III) and Galactic Centre (Group I) indicate the approximate absolute magnitude (M_V) which the pulsation model predicts for these groups *as judged from their mean periods and Bailey types alone* since no colours are available. It may be seen that the stars of Groups II and III have the same absolute visual magnitude, which is $\sim 0^{m}{\cdot}25$ fainter than for the variables in M3, and which agrees with the observation that the mean apparent magnitude of the two groups is the same. The asymmetrical short period stars of Group I are however anomalous on the pulsation model, since this predicts that they should be about 0·7 magnitudes fainter than the other two groups and this is contrary to Gaposchkin's observations. In the light of this discrepancy and also the results of Pavlovskaya's re-analysis, it seems very desirable that new observations should be made to check the periods, colours and light-curves of these galactic centre stars.

RR Lyrae stars with $0{\cdot}20 \leqslant P \leqslant 0{\cdot}36$ *days.*—As Greenstein noted (*loc. cit.*) some RR Lyrae stars of short period (~0·3 days) and type *ab* do occur in the general field. Baade (**1**) has suggested the possibility that RR Lyrae stars of this type may be present in the Galaxy with a disk-like distribution. A list of 69 stars was therefore made from the General Catalogue (**5**) of all RR Lyrae stars with $0{\cdot}20 \leqslant P \leqslant 0{\cdot}36$ days and with known asymmetries ($M-m$). Sixteen of these for which $(M-m)<0{\cdot}22$ may be considered to be of type *ab* and are listed in Table III.

TABLE III

Stars in the general field with $0{\cdot}20 < P < 0{\cdot}36$ *and* $(M-m) < 0{\cdot}22$

Star	$M-m$	P	l	b	m_p or m_v	*R.A.* (1900)	Dec.
v672 Aql	0·20	0·346	14°	−10°	12·6–13·5p	19h 40m 49s	+07° 46′·9
v753 Aql	0·07	0·299	18	−12	14·8–15·5p	19 55 21	+09 59
IU Car	0·18	0·298	237	−22	10·4–11·5p	06 51 40	−59 28·1
QR Cas	0·20	0·323	82	− 6	14·0–15·4p	23 46 12	+55 08
SW Cru	0·18	0·328	264	+ 2	11·9–12·7p	11 54 03	−59 44·8
IV Cyg	0·10	0·334	37	+ 3	13·6–14·9p	19 46 28	+34 04·2
RV Del	0·20	0·332	25	−13	12·9–13·8v	20 16 04	+14 56·3
BK Del	0·14	0·360	23	−17	13·0–14·6p	20 24 38	+11 33·7
CP Del	0·15	0·345	25	−14	14·4–15·6p	20 21 18	+14 28
DQ Del	0·17	0·348	28	−17	13·9–15·3p	20 36 30	+14 23·4
XX Hya	0·15	0·337	213	+22	10·5–12p	09 05 08	−15 11·8
TV Lib	0·13	0·270	321	+38	10·8–12·3p	15 13 00	−08 05·8
AQ Lyr	0·16	0·357	23	+14	12·0–13·3v	18 30 48	+26 28·8
DD Lyr	0·19	0·271	25	+10	12·7–13·8v	18 49 07	+26 56·4
v413 Oph	0·16	0·310	332	+25	11·8–13·6p	16 19 42	−10 18·4
v1176 Sgr	0·16	0·355	338	− 6	12·0–12·9p	18 18 24	−21 38

For some of these stars the periods are doubtful on the basis of large residuals between the observations and the quoted light curves; on the other hand, SW Cru for example has a period which has been well determined over a number of years.

A plot of asymmetry against galactic latitude (b) for all 69 stars appears to show that the asymmetrical stars do occur at lower latitudes than the remainder. If the sky is divided into two zones of equal solid angle—an equatorial zone ($|b| < 30°$) and a polar zone ($|b| > 30°$), then the distribution into these zones according to $(M-m)$ is as given in Table IV. Application of Fisher's exact

TABLE IV

Distribution in galactic latitude of short period variables according to asymmetry $(M-m)$

	$(M-m) < 0{\cdot}22$	$(M-m) > 0{\cdot}22$
Equatorial zone ($\|b\| < 30°$)	15	35
Polar zone ($\|b\| > 30°$)	1	18

method for a 2×2 table gives these two populations as significantly different at the 5 per cent level. The mean perpendicular distance ($|\bar{Z}|$) from the galactic plane was found for each group assuming zero absolute magnitude for all stars. The interstellar absorption for a group of 270 B stars at a mean distance of 2 kpc has a mean value of $1{\cdot}9\, m_{pg}$ and shows no correlation with distance (cf. Hiltner (7)). This value was therefore adopted for the 13 stars which have $|b| < 8°$ and the cosecant law of absorption, $A_{pg} = 0{\cdot}28 \operatorname{cosec} b$ (12), was used for the remainder. The following values were found for the mean height from the plane ($|\bar{Z}|$), the r.m.s. dispersion in Z about the plane (σ_Z) and the mean distance from the Sun projected on to the plane ($\bar{R}$) in kiloparsecs:

$(M-m) < 0{\cdot}22$ $\quad |\bar{Z}| = 0{\cdot}65, \quad \sigma_Z = 0{\cdot}8 \pm 0{\cdot}2, \quad \bar{R} = 2{\cdot}7,$

$(M-m) > 0{\cdot}22$ $\quad |\bar{Z}| = 1{\cdot}49, \quad \sigma_Z = 2{\cdot}6 \pm 0{\cdot}3, \quad \bar{R} = 3{\cdot}2.$

The mean period of the 16 stars with $(M-m)<0\cdot22$ is 0·326 days. On the pulsation model, an absolute magnitude of +0·9 relative to the M3 stars would be predicted. On this hypothesis and *assuming* the M3 stars to have zero absolute magnitude, the group of stars with $(M-m)<0\cdot22$ will have:

$$|\bar{Z}|=0\cdot43, \qquad \sigma_Z=0\cdot6\pm0\cdot1, \qquad \bar{R}=1\cdot8.$$

In either case the asymmetrical group has a more flattened distribution with respect to the plane than the normal *c* type variables. The approximate equality of $(\bar{R})$ when the same absolute magnitude is assumed for each group suggests that observational selection has not produced this result—as it might if the asymmetrical type stars were much nearer to the Sun than the others.

Joy (**10**, **11**) has given radial velocities for two of the stars with $(M-m)<0\cdot22$ (XX Hya and TV Lib); both have the same low velocity (−10 km/s) which is in accord with a disk-like distribution. Pavlovskaya (**20**) reports that Detre* has investigated RR Lyrae stars with $0\cdot20<P<0\cdot40$ days of Bailey type *a* and has found a solar motion of 48 km/s which is appreciably less than for *c* type variables of the same period. This is to be expected if the asymmetrical group (type *a*) has a more flattened distribution than type *c* stars of the same period.

Iwanowska (**8**) has separated RR Lyrae stars into two sequences according to her observed mean spectral types and period, and shown that stars with $P<0\cdot5$ days form a sequence of later spectral type than those with $P>0\cdot5$ days. Repeating this with additional stars for which a reliable spectral type is available, the effect, although small, is confirmed for type *ab* stars, as is shown in Table V.

TABLE V

Mean spectral type and mean period for type ab variables

Period range	Mean period	Mean spectral type
$0\cdot20<P<0\cdot50$	0·442	A 7·4
$P>0\cdot50$	0·589	A 5·0

On the pulsation model the group of larger mean period should be nearly $0^m\cdot5$ brighter in absolute visual magnitude. Lubienska-Iwaniszewska (**16**) has shown that the group of shorter mean period has a smaller height above the plane and lower mean velocity than the other group. This suggests that the properties which we have found for the group of short period asymmetric stars in the present paper are an extreme example of a general tendency for the *ab* variables in which their space distribution, space motion and spectral type are a function of their period; presumably a similar relationship holds for the type *c* variables. In this case the sixteen stars listed in the present paper would be expected to have a later mean spectral type than type *ab* variables of longer period or type *c* variables of the same period.

There is no indication for the stars with $0\cdot20<P<0\cdot36$ days that the type *ab* variables exist preferentially in the galactic centre hemisphere compared with those of type *c*. A preponderance of type *ab* stars of short period would not therefore be expected at the galactic centre on this meagre evidence. The well-known increase of RR Lyrae stars of all types towards the galactic centre is however shown in Table VI.

To summarize, the pulsation model has some success in relating the different mean periods of the type *ab* and type *c* variables found in globular clusters and in

* Paper unavailable to author.

TABLE VI

Concentration to galactic centre as function of asymmetry $(M-m)$

	$(M-m)<0\cdot22$	$(M-m)>0\cdot22$
Galactic centre hemisphere	13	42
Anti-centre hemisphere	3	9

predicting the absolute magnitudes of very short period variables within the observational errors and likely theoretical limitations. The disagreement with Gaposchkin's observations together with the results of Pavlovskaya's re-analysis make further observations of RR Lyrae stars at the galactic centre desirable. The short period variables of type *ab* in the general field lie closer to the plane than the type *c* variables of the same period and have a smaller solar motion.

It would seem worth while to check on the periods of the 16 stars listed in Table III and also discover if they differ from the type *c* variables of the same period or type *ab* variables of longer period in physical properties (such as colour variation through the cycle or spectrum). To this end, spectra are now being secured at the Radcliffe Observatory of SW Cru and IU Car; the remaining stars are within reach of Northern Observatories.

I should like to thank the Radcliffe Observer (Dr A. D. Thackeray) for suggesting some of these problems to me and for his advice in writing this paper. I am also grateful to Drs A. R. Sandage and M. W. Feast for several most helpful discussions.

This work was carried out partly with the aid of a Radcliffe Travelling Fellowship and partly with the aid of a grant from the Department of Scientific and Industrial Research to the Radcliffe Trustees.

Radcliffe Observatory,
Pretoria:
1958 *December.*

References

(1) W. Baade, *Pont. Acad. Sci. Scripta Varia*, **16**, 303, 1958.
(2) O. J. Eggen, *A.J.*, **61**, 361, 1956.
(3) O. J. Eggen, *P.A.S.P.*, **68**, 238, 1956.
(4) S. Gaposchkin, *Variable Stars*, **10**, 337, 1956.
(5) *General Catalogue of Variable Stars*, B. V. Kukarkin, P. P. Parenago, Yu. I. Efremov and P. N. Khopolov, Moscow, 1958.
(6) J. L. Greenstein, *A.N.*, v. 257, 301, 1935.
(7) W. Hiltner, *Ap. J. Supplement* No. 24, Vol. I, 1956.
(8) W. Iwanowska, *Torun Bulletin*, III, No. 2, 1, 1953.
(9) H. L. Johnson and W. W. Morgan, *Ap. J.*, **117**, 313, 1953.
(10) A. H. Joy, *P.A.S.P.*, **50**, 302, 1938.
(11) A. H. Joy, *P.A.S.P.*, **62**, 60, 1950.
(12) T. D. Kinman, *M.N.A.S.S.A.*, XVII, No. 3, 1958 (Radcliffe Observatory Reprint No. 9)
(13) G. P. Kuiper, *Ap. J.*, **88**, 429, 1938.
(14) G. P. Kuiper, *Ap. J.*, **88**, 472, 1938.
(15) B. V. Kukarkin, X Gen. Assembly I.A.U. Draft Report, p. 226, 1958.
(16) C. Lubienska-Iwaniszewska, *Torun Bulletin*, III, No. 2, 25, 1953.
(17) W. W. Morgan and P. C. Keenan, *Astrophysics* (Hynek), p. 20, McGraw Hill, 1951.
(18) P. Th. Oosterhoff, *Observatory*, **62**, 104, 1939.
(19) P. Parenago and A. Masevitch, *Rus. Astr. J.*, XXVII, 137, 1950.

(20) E. D. Pavlovskaya, X Gen. Assembly I.A.U. 1958. (Joint discussion on luminosity of cepheids).
(21) M. Roberts and A. R. Sandage, *A. J.*, **60**, 185, 1955.
(22) A. R. Sandage, *Ap. J.*, **123**, 278, 1956.
(23) A. R. Sandage, *Ap. J.*, **127**, 513, 1958.
(24) A. R. Sandage, *Pont. Acad. Sci. Scripta Varia*, **16**, 41, 1958.
(25) M. Schwarzschild, *Harvard Obs. Circ.*, No. 437, 1940.
(26) J. B. G. Turner, *M.N.A.S.S.A.*, **16**, 29, 1957.
(27) L. Woltjer, *B.A.N.*, **13**, 62, 1956.

THE SYSTEM OF ζ PHOENICIS

G. Hagemann

(Received 1959 January 1)

Summary

Radial velocities have been measured from 71 new spectrograms of ζ Phoenicis, taken at Mt Stromlo.

The spectroscopic orbit of the primary star has been computed, and the semi-amplitude, K_2, of the secondary star has been determined from differential measures. Absolute dimensions of the two components have been derived by combining the spectroscopic figures with the photometric results of A. R. Hogg, and the spectral type of the secondary star has been computed. Certain difficulties of the system seem to be solved.

---

1. *Introduction.*—The system of ζ Phoenicis ($\alpha = 01^h 06^m.3$, $\delta = -55° 31'$ (1950), HD 6882) belongs to the class of double-line spectroscopic binaries that are eclipsing variables as well. It was reported as a spectroscopic binary by Wilson from four plates obtained at Santiago (**1**). Altogether 16 plates were secured at Santiago, from which Colacevich (**2**) determined provisional orbital elements. The lines of the fainter component were found on but five plates and then only with difficulty. The system was reported as an eclipsing variable by Hogg from photoelectric measurements taken at Mt Stromlo between the years 1947–49. His results and certain discrepancies between the photometric and spectroscopic solutions were discussed in this journal (**3**). Spectroscopic observations with the Cassegrain spectrograph were made at Mt Stromlo during the years 1954–57 at the suggestion of W. Buscombe.

2. *Observations, spectral lines, measurements.*—Altogether 80 plates of the spectrum of ζ Phoenicis were taken at Mt Stromlo. During the years 1954–56 mostly Kodak 103a–O were used, but during the observing period of 1957 Kodak IIa–O were used at the author's suggestion, as the finer grain of these plates enhanced the very faint lines of the weaker component. The linear dispersion was about 35 A/mm at Hγ. The slit-width used from 1954–56 was 0·04 mm, and was changed later to 0·06 mm. This corresponded to a projected slit-width of 0·01 resp. 0·015 mm. The spectra show the following lines between λ3922 to λ4528, the range used for radial velocity measurements: He 4026, 4388, 4471; H 3970 (Hε), 4102 (Hδ), 4340 (Hγ); Mg 4481. From the available 80 plates, 71 were measured for radial velocities by the author; 9 plates were rejected as too weak. The quality of the lines for radial velocity determinations was poor. Lines due to He and Mg were faint and diffuse, and not visible on some plates because of variations of the density of the plates. The H-lines, although strong, were broad; H 3970, moreover, showed as a heavy blend on all spectra, and was unusable. Accordingly the lines H 4102 and H 4340 were mostly the only ones to be used for the determination of radial velocities. The measurements were made with a Zeiss-Abbe Comparator, the advantages of which will be described later.

TABLE I

Radial velocity observations of ζ Phoenicis

No.	Date (U.T.)		Phase	Obs.	Velocity 1	Velocity 2
			d			
1	1954 Sept.	6·69	1·26	WH	+ 38	
2		12·67	·56	WB	− 65	
3		14·57	·79	WH	−106	+246
4		·58	·80	WH	−104	+278
5	Oct.	5·57	·09	WB	+116	−240
6		8·51	1·36	AP	+ 64	
7		·61	1·46	AP	+ 85	
8		·71	1·56	AP	+126	
9		9·50	·68	WB	−103	
10		·60	·78	WB	−116	+274
11		·68	·86	WB	−106	+253
12		10·50	·01	HG	+138	−242
13		·59	·10	HG	+122	−242
14		·68	·19	HG	+118	
15		11·49	1·00	WH	− 82	
16		·60	1·11	WH	− 36	
17		12·50	·34	AP	+ 32	
18		·52	·36	AP	+ 39	
19		·58	·42	AP	+ 26	
20		·68	·52	AP	− 42	
21		13·50	1·34	WB	+ 40	
22		·60	1·44	WB	+ 87	
23		·67	1·51	WB	+117	
24	Nov.	12·45	1·23	AP	+ 12	
25		·54	1·32	AP	+ 44	
26		14·48	1·60	HG	+132	−208:
27		·62	·07	HG	+133	−213
28		15·43	·87	AP	−111	+251
29		·49	·93	AP	− 99	+287
30		·58	1·02	AP	− 65	
31		16·40	·17	WH	+110	
32		·49	·26	WH	+ 87	
33	Dec.	6·43	·16	WB	+ 98	
34		·54	·27	WB	+ 85	
35		8·42	·49	WH	− 14	
36		9·43	1·50	WB	+109	
37		·49	1·56	WB	+123	
38		14·44	1·50	WB	+110	
39		·48	1·54	WB	+123	
40	1955 Aug.	1·57	1·20	WB	+ 2	
41		5·66	·28	AP	+ 82	
42		·72	·34	AP	+ 54	
43	Sept.	10·77	1·33	WH	+ 48	
44		29·55	·07	WB	+141	−225:
45	Oct.	4·07	·08	HG	+132	−222:
46	1957 Sept.	8·67	·54	AP	− 41	
47		·68	·55	AP	− 40	
48		·68	·55	AP	− 44	
49	Oct.	2·64	1·14	AP	− 36	
50		4·49	1·31	AP	+ 42	
51		·57	1·39	AP	+ 87	
52		·65	1·47	AP	+117	
53		7·50	·99	AP	− 69	
54		14·56	1·37	AP	+ 88	

TABLE I (*continued*)

No.	Date (U.T.)		Phase	Obs.	Velocity 1	Velocity 2
			d			
55	1957 Oct.	·66	1·46	AP	+114	
56		·76	1·56	AP	+132	
57		16·58	·04	AP	+127	−209
58		·65	·11	AP	+128	−230
59		·76	·22	AP	+106	
60	Nov.	13·45	1·20	HG	− 18	
61		·50	1·25	HG	+ 24	
62		·55	1·30	HG	+ 44	
63		14·44	·52	AP	− 60	
64		·48	·56	AP	− 65	
65		·52	·60	AP	− 83	
66		·57	·65	AP	− 89	
67		·59	·67	AP	− 83	
68		·62	·70	AP	− 96	
69		·68	·76	AP	− 86:	+285:
70	Dec.	2·58	·29	AP	+ 57	
71		·66	·37	AP	+ 43	

Observers: W. Buscombe (WB), H. Gollnow (HG), W. D. Heintz (WH), A. Przybylski (AP).

3. *Period.*—Colacevich determined a period $P = 1^{d}\cdot66958$ from the early spectroscopic observations; Hogg from the photometric observations found $P = 1^{d}\cdot66990$. A new period $P = 1^{d}\cdot6697597$ was derived, using the old and

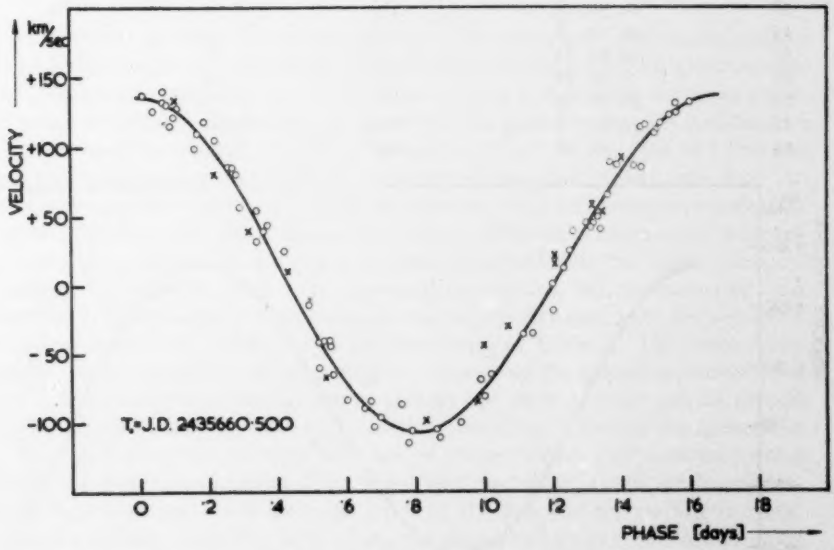

FIG. 1.—*All individual radial velocities of the primary star of ζ Phoenicis plotted against the radial-velocity curve drawn according to the final elements. Lick observations are indicated by crosses.*

new spectroscopic observations. This period represented all observations, spectroscopic and photometric, with the exception of the first observation listed by Colacevich in his Table I (**2**, p. 85). According to a private communication

from G. H. Herbig, the published J.D. should read ...39·93 instead of ...31·93. This correction removed the discrepancy. Between the first and last observation the system has completed 10 800 revolutions. Fig. 1 shows the radial velocity curve with all observations for the main star. The epoch of maximum radial velocity is given by J.D. 2435660·50 + 1^{d}·6697597*E*.

TABLE II

Normal places

No.	Observation Nos.	Mean phase	Mean R.V.	Residuals
1	12, 57, 27	·04	+133	− 2
2	44, 45, 5	·08	+130	− 1
3	13, 58, 33	·12	+115	− 9
4	31, 14, 59	·19	+111	+ 5
5	32, 34, 41	·27	+ 85	+ 8
6	70, 17, 42	·32	+ 48	− 7
7	18, 71, 19	·38	+ 36	+ 9
8	35, 20, 63	·51	− 39	− 4
9	46, 47, 48	·55	− 42	+10
10	64, 2, 65	·57	− 70	−10
11	66, 67, 9	·67	− 92	− 1
12	68, 69, 10	·75	−102	+ 2
13	3, 4, 11	·82	−106	0
14	28, 29, 53	·93	− 93	0
15	15, 30, 16	1·04	− 61	+ 5
16	49, 60, 40	1·18	− 17	− 8
17	24, 61, 1	1·25	+ 25	+ 4
18	62, 50, 25	1·31	+ 44	− 2
19	43, 21, 6	1·34	+ 51	− 8
20	54, 51, 22	1·40	+ 87	+ 5
21	7, 55, 52	1·46	+104	+ 3
22	36, 38, 23	1·50	+112	− 1
23	39, 37, 8	1·55	+124	0
24	56, 26	1·58	+132	+ 3

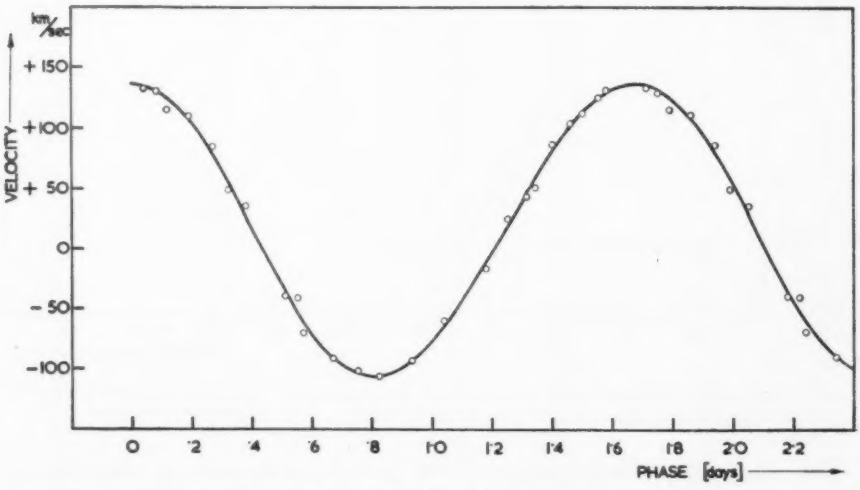

FIG. 2.—*The 24 normal points from Mt Stromlo observations of the primary star of ζ Phoenicis shown against the radial velocity curve from the final elements.*

4. *Orbital elements.*—Orbital elements for the main star were derived from Mt Stromlo observations only, as this material is homogeneous and the Lick observations are not numerous. In such a case Schlesinger suggests the omission of early observations, because the residuals of these observations depend largely upon the adopted period (4). The period was adopted as final and omitted from the solution. Preliminary elements found graphically confirmed Hogg's result that the eccentricity was very small, and hence in a first solution a circular orbit was assumed and corrections to the elements deduced by Sterne's method (5). The observations were formed into 24 normal places given in Table II and Fig. 2. A second, and final, solution was made for an elliptic orbit, using also Sterne's method. The results are shown in Table III.

TABLE III

Orbital elements of ζ Phoenicis

Element	Circular	Elliptical (adopted)
P	d 1·6697597	
T		·44 ± ·12
e	·033	·034 ± ·015
ω	94°	97° ± 25°
K_1	121·5 km/s	121·4 ± 1·9
γ	15·2 km/s	15·4 ± 1·1

Note.—The time T is the date of periastron passage, as usual. Sterne uses the " epoch of the mean longitude " instead, but the dates can easily be converted into each other. The errors are all m.e.

5. *Absolute dimensions of the components.*—The orbits and absolute dimensions of the components can be derived by combining the results of the spectroscopic and photometric observations, if the lines of both components are measurable for radial velocities. Besides the elements for the primary star, it is sufficient to know the semi-amplitude, K_2, of the secondary star. In the case of ζ Phe the lines of the secondary star were so weak and diffuse, and visible only near the nodal passages, that it was not thought advisable to try to determine very uncertain orbital elements. The value K_2 was found from differential measures of primary and secondary spectra on a number of plates obtained near the nodal passages. Distances between the lines were measured in microns, which, converted into velocities and combined with the results for the primary star, gave the velocities for the secondary star. The results are also shown in Table I. The Zeiss-Abbe comparator was of particular advantage for measuring the distances between the lines. The comparator has no screw, and so the plate carriage can be moved rapidly in both directions under the adjusting microscope. During this movement the eye can distinguish the very faint line of the secondary star more easily and gets a more definite impression of it. When the impression is sufficiently definite, the carriage is stopped with the index mark on the line, and the reading is made. From all available plates the value of K_2 was found to be 247 ± 10 km/sec. The combination of the spectroscopic results with the photometric figures of Hogg (3) gave the quantities shown in Table IV.

6. *Spectral class, absolute magnitude, parallax.*—From Mt Stromlo plates A. de Vaucouleurs has classified the primary star on the MK system as B6 V (6). Due to the poor quality of the lines, it was not possible to classify the secondary star and it was thus computed according to the method described by L. Plaut (7).

TABLE IV

Absolute values from spectroscopic orbit and photometric results

		Star 1	Star 2
Semi-major axis of the orbit km × 10^6		2·80	5·70
Mass	Solar Units	6·1	3·0
Radius	,, ,,	3·4	2·0
Mean density	,, ,,	·17	·37

Using Hogg's value of the ratio of the surface brightnesses, $J_1:J_2=1·8$, the computed spectral class of the secondary star becomes Ao V. The absolute magnitude as given by Morgan and Keenan (**8**), is $-1·1$ for the primary, and $+0·3$ for the secondary star. The spectroscopic parallax, using A. de Vaucouleurs' modulus $m_0-M=5·51$, is $0''·008$. The difference of $1^m·4$ between the two components is in good agreement with Hogg's value of $1^m·5$, from the ratio L_1/L_2.

Hogg lists a number of discrepancies between the values derived from photometric and spectroscopic observations. These difficulties are based on the assumption of the same spectral class for both components as B8 + B8, as given in the H.D. Catalogue, and on the values for the spectroscopic orbit of the secondary star by Colacevich. With regard to the spectral class of the secondary star of spectroscopic binaries, Plaut remarks generally: "The computed spectral type of the secondary component is to be preferred to the observed one". Already Hogg had come to the conclusion that the spectral type of the secondary is definitely later than B8. The orbital elements for the secondary star by Colacevich, however, must be considered as very uncertain. His radial velocity curve for the secondary star rests on five observations only, and these are not favourably placed for the only important element, K_2.

Assuming now the primary and secondary spectra to be of types B6 V and Ao V respectively, the present observations lead to results for masses, radii and densities which, as shown in Table V, agree well with the normal figures for stars of these types given by Allen (**9**).

TABLE V

Absolute values from spectroscopic and photometric observations compared with values from Allen's tables for stars of the same spectral type. (Units are solar units)

	Observed	Tabulated
Mass : primary star	6·1	5·1
secondary star	3·0	3·0
Mean radius : primary star	3·4	3·4
secondary star	2·0	2·2
Mean density : primary star	·16	·13
secondary star	·38	·28

7. *Conclusion.*—The system of ζ Phe seems to be a normal one under the assumption that the spectral type of the secondary star is Ao V. As the quality of the spectral lines is poor for the determination of radial velocities, it does not seem worthwhile to accumulate more spectroscopic observations. For the same reason, non-orbital effects in the observed radial velocities were not allowed for. Besides, the non-orbital effects influence the values of e and ω, which have a doubtful accuracy in nearly circular orbits, as that of ζ Phoenicis.

Acknowledgments.—It is a pleasure to thank Dr Hogg and Dr Przybylski for advice and criticism. I am indebted to Drs Buscombe, Gollnow, Heintz (Munich) and Przybylski for supplying the observations and to the Deutsche Forschungsgemeinschaft, Godesberg, for the loan of a Zeiss-Abbe comparator.

Mt Stromlo Observatory,
Canberra, A.C.T.,
Australia :
1958 *December* 17.

References

(1) R. E. Wilson, *L.O.B.*, **8**, 80, 1914.
(2) A. Colacevich, *P.A.S.P.*, **47**, 84, 1935.
(3) A. R. Hogg, *M.N.*, **111**, 315, 1951.
(4) F. Schlesinger, *Publ. All. Obs.*, **1**, 36, 1910.
(5) T. E. Sterne, *Proc. Ac. Sc., Washington*, **27**, 175, 1941. Harv. Repr. 222.
(6) A. de Vaucouleurs, *M.N.*, **117**, 449, 1957.
(7) L. Plaut, *Publ. Kapt. Astr. Lab.*, **55**, 25, 1953.
(8) *Astrophysics*, ed. by J. A. Hynek, New York 1951 (Chapter 1).
(9) C. W. Allen, *Astrophysical Quantities*, London 1955 (p. 185).

NOTES ON FIVE SOUTHERN GASEOUS NEBULAE

David S. Evans

(Communicated by H.M. Astronomer at the Cape)

(Received 1958 November 27)

Summary

The results of observations of the spectra, radial velocities, internal motions and form of five southern objects, NGC 3918, 6302, 6326, IC 4776, and Anon $16^h\ 13^m{\cdot}5$, $-51^\circ\ 52'$, made with the Radcliffe 74-inch reflector, are reported.

These notes aim at providing details of structure, radial velocity, internal motion and spectrum for these five nebulae, which have been observed in the course of a more general programme on planetary nebulae. The second of them, NGC 6302, does not, strictly, rank as a planetary nebula, although it has been so classified in the past, and, for the last-named, the velocity is not given.

Planetary nebulae show a very great range in form and surface brightness, and a considerable amount of experiment has had to be devoted to discovering the best methods of investigation. This is partly due to the fact that the best methods for obtaining different kinds of data are, to an extent, in conflict with each other.

For the determination of radial velocities and the description of the spectra, there are available four different dispersions at the Cassegrain spectrograph (known as a, b, c, and d) (**1**), together with the small spectrograph for use at the Newtonian focus (**2**). The c-dispersion of the former instrument (49 A/mm) has proved by far the most useful, and is now employed almost exclusively for Cassegrain work. This camera lens has the enormous advantage of producing a spectrum in excellent focus to beyond 5000 A, while as far as 6700 A the quality remains good, and perfectly adequate for line identification and the determination of line strengths.

For the reduction of these plates new tables were computed using two separate Hartmann formulae overlapping at 4500 A. The wave-lengths of the forbidden nebular lines were taken, as far as possible, from Ira S. Bowen (**3**), of permitted and other forbidden lines from Charlotte E. Moore (**4**), and other wave-lengths, e.g. of unidentified lines and of blends, from A. B. Wyse (**5**). In deriving velocities, the lines used were selected so as to exclude faint lines, blends, lines of uncertain wave-length, and all lines to the red of N_1. An iron arc comparison spectrum was used, with the exposure tripled as compared with the normal for stellar radial velocity work, in order to give a satisfactory number of comparison lines. The results from the Cassegrain spectra (Table I), show good agreement with those of Campbell and Moore (**6**). It now seems clear that an adequate coverage for determination of velocity and spectral

characteristics, for those objects observable with the Cassegrain instrument, can be secured with three plates of each: one fairly short exposure (e.g. 1–2 hours), on fast blue-sensitive plates (Kodak 103aO), and two long exposures, each pushed as far as is practicable, one blue (103aO), and one panchromatic (103aF). These long exposures are limited by the fact that, so far, it has not proved practicable to extend an exposure over more than one night, and, in consequence, the "depth" reached is usually not as great as that attained by Wyse (5). Only if an examination of the lines in the violet reveals structure is it worthwhile to attempt to secure spectra on higher dispersion for a study of internal motion.

TABLE I

Nebula	Maximum exposures (minutes) for various dispersions and emulsions (103a series)								
	a : O	c : O	c : B	c : F	d : B	N : O	V	$Vc+M$	Total plates
NGC 3918	90	135*	...	260	...	135	$-16{\cdot}1\pm0{\cdot}5$	$-16{\cdot}4$	9
6302	...	63	320	240	...	150	$-38{\cdot}0\pm0{\cdot}8$	-36	5
6326	...	270	120	...	180	155	$+\ 8{\cdot}8\pm0{\cdot}6$	$+11$	5
IC 4776	...	60	...	180	...	120	$+19{\cdot}1\pm0{\cdot}7$	$+18{\cdot}8$	7
Anon $16^h\ 13^m{\cdot}5$ $-51°\ 52'$	...	...	...	...	...	180	...	...	2

* Hg sensitized.

Direct photographs at the Newtonian focus have usually been available for the study of structure. At the same focus the small spectrograph giving a dispersion of 400 A/mm has been used to obtain "deep" spectra of bright objects, or to reach very faint ones. It might be hoped that, by duplicating observations of the same object at Cassegrain and Newtonian foci, sufficient information might be gained concerning the systematic and accidental errors of Newtonian radial velocities to open up the whole field of the velocities of very faint southern planetaries. Unfortunately, further work will be necessary before this hope can be realized. For objects with large velocity dispersion, such as extragalactic nebulae or globular clusters, a probable error of 20 km/sec from a single spectrum could be tolerated. For useful results on the planetaries, however, this figure must be reduced by a factor of at least four. Other things being equal, the reduced dispersion alone may be expected to put up the probable error of a Newtonian result by eight times as compared with the Cassegrain c-dispersion. The lines given by the Newtonian spectrograph are curved: for all extragalactic systems yet observed, the spectrum fills the whole dekker, the lines may be measured at mid-dekker, and a fairly well-established curvature correction applied. For the planetaries, the difficulties of offset guiding are such that the spectrum is not always centrally placed, and this introduces another uncertainty. Again, the best lines for extragalactics are H and K, where the prismatic dispersion is twice as great as near N_1 and N_2, usually the best lines for planetaries. Finally, the low dispersion of the Newtonian spectrograph leads to blending of lines, and the relative strengths of the components of a given blend usually vary from planetary nebula to planetary nebula.

However, even though satisfactory velocity determinations of the velocities of planetaries cannot yet be obtained with the Newtonian spectrograph, much information can be derived from these spectra. The instrument is extremely fast, and permits observations of objects completely out of reach of the Cassegrain spectrograph. For the brighter systems the continuum is usually well shown, and, although there is much absorption below 3900 A, this is still much less than in the Cassegrain spectrograph, so that a far better account of the violet and near ultra-violet spectrum is rendered.

After these preliminary remarks we may now return to a detailed discussion of the objects described in these notes. In Table II are listed the lines found in the various spectra, these being associated with numbers empirically indicating the relative line-strengths within each spectrum. No claim is made that these represent true line-strengths: it is only hoped that, in general, a larger number corresponds to a stronger line. The figures are based on eye-estimates (these have been found to be surprisingly consistent), adjusted for plate-sensitivity according to the manufacturer's specifications. For the extreme violet the intensities have been "built on", using the observed intensities in the Newtonian spectra.

TABLE II

λ	Ion	NGC 3918	Anon $16^h\ 13^m.5$ $-51°\ 52'$	NGC 6302	NGC 6326	IC 4776
3726·04	[O II]	12	ft.	1·5	18	11
3728·80	[O II]	8				3
3750·15	H I	1	...	...	0·2	...
3759·87	O III	2·5	...	ft.	...	...
3770·63	H I	1·5	?	ft.	0·4	...
3797·90	H I	3·5	...	ft.	0·6	0·9
3819·61	He I	...	...	ft.	...	...
3835·39	H I	3	...	ft.	1·1	0·7
3868·76	[Ne III]	26	...	12	23	16
3888·8	H I–He I	9	2	0·2	3·3	6
3967·47	[Ne III]	17	6	3	12	10
3970·07	H I	12		0·2	1·5	9
3994	...	...	?	...	...	...
4026·1	He I–He II	1·5	ft.	ft.	0·5	0·7
4068·60	[S II]	1·5	...	0·3	0·8	1·0
4076·35	[S II]	...	...	ft.	...	0·3
4097·31	N III	3	...	...	...	...
4101·74	H I(+N III)	20	15	2	11	21
4120·8	He I–O II	...	ft.	...	...	...
4177·21	[Fe II]	...	ft.	...	...	...
4199·9	He II–N III	1·5	...	ft.	...	...
4207·5	...	...	?	...	...	...
4244·00	[Fe II]	...	1	...	...	...
4267·2	C II	ft.	...	...	...	...
4287·40	[Fe II]	...	1	...	...	...
4340·47	H I	29	40	17	17	14
4363·19	[O III]	18	...	16	5	9
4387·93	He I	...	...	ft.	...	0·2
4415·6	O II–[Fe II]	...	1·5	...	...	...
4471·48	He I	7	2	0·1	23	9

TABLE II—(*continued*)

λ	Ion	NGC 3918	Anon $16^h\ 13^m{\cdot}5$ $-51°\ 52'$	NGC 6302	NGC 6326	IC 4776
4523·60	N III	...	?	...	...	...
4541·59	He II	6	...	ft.	0·8	...
4552·65	Si III ?	...	?	...	...	...
4628·8	...	...	...	ft.	...	...
4634·16	N III	7	...	ft.	...	...
4640·9	N III–O II	10	...	0·9	0·7	...
4649·1	C III–O II	ft.	...	...	...	...
4658·1	[Fe III]	...	17	...	...	0·5
4685·68	He II	51	...	71	18	...
4701·0	[Fe III]–O II	...	4	...	...	...
4711·9	[A IV]–He I	13	...	3	...	0·3
4724·7	...	2	...	...	...	...
4733·7	[Fe III]	...	ft.	...	...	...
4740·20	[A IV]	16	...	10	1·3	ft.
4769·3	[Fe III]	...	ft.	...	...	...
4861·33	H I	100	100	100	100	100
4871·58	O II	ft.	...	...	...	...
4921·93	He I	1·5	...	...	...	0·4
4958·93	[O III]	300	ft.	320	294	240
5006·86	[O III]	1000	8	1000	1040	640
5015·68	He I	...	...	...	...	1
5197·94	[N I]	...	...	v. ft.	...	...
5200·41	[N I]	...	...		...	...
5207·2	...	...	...	v. ft.	...	...
5754·57	[N II]	...	...	14	...	1
5875·6	He I	30	...	15	...	77
5978·4	? Si II	...	...	5	...	...
6242·5	...	...	...	...	...	ft.
6253	...	...	...	...	...	ft.
6300·31	[O I]	13	...	35	...	6
6312·06	[S III]	8	...	4	...	3·5
6363·82	[O I]	9	...	11	...	1
6403·7	...	...	...	6	...	...
6435·10	[A V]	6	...	8	...	...
6461	...	5	...	...	...	...
6493	...	ft.	...	...	...	...
6548·06	[N II]	55	...	470	...	37
6562·82	H I	324	...	1200	232	767
6583·37	[N II]	123	...	2100	...	156
6678·15	He I	11	...	...	...	41
6716·42	[S II]	9	...	30	...	5
6730·78	[S II]	13	...	170	...	15

NGC 3918, $11^h\ 47^m{\cdot}8$, $-56°\ 54'$ (1950), $l = 262°{\cdot}6$, $b = +4°{\cdot}4$.

This object has been discussed by Evans and Thackeray (7), who give a photograph (Fig. 9, Plate 9). It was then found to be a simple, round, very bright object, of diameter 13″, with no detectable central star. The spectra used in the present study show doubling of the lines on high dispersion. Ordinary measures of the separation on three a-dispersion plates gave a mean expansion velocity of 20·1 km/sec. On one plate the whole lengths of λλ 3686 and 3967

and, on another, of the former line were so well defined that it was possible to measure the shapes in detail. It was found that the shapes were consistent with the uniform expansion of a shell of diameter 18″·4 with a velocity of 19·9 km/sec. The diameter so inferred is rather greater than that observed, either on the Newtonian plates or in terms of the line-lengths of the Cassegrain spectra, and, indeed, the double lines fade away at their ends before forming a complete lens shape. On the Newtonian spectrum there is a continuum detectable down to approximately 3550 A; it shows a fine structure—too fine to be measurable—and a rapid decrement, interpreted as the head of the Balmer series. The numerous lines recorded on this spectrum, and the very small scale, make it impossible to be dogmatic, but there is nothing in the continuum which can definitely be identified as an absorption line originating in the spectrum of a central star. The " line-strengths " of Table II suggest an object of fairly high excitation.

Anon $16^h\ 13^m{\cdot}5$, $-51°\ 52'$, $l = 299°{\cdot}3$, $b = -2°{\cdot}1$.

This system is also included in Evans and Thackeray's list ((7), Fig. 15, Plate 11), but is far too faint to be within range of the Cassegrain spectrograph. Recently, two Newtonian spectra have been obtained. It will be seen from the line list of Table II, that this object has the N_2 line only just detectable, and N_1 less than one-tenth as strong as Hβ. Most of the lines in the spectrum seem to be attributable to forbidden Fe III, and the degree of excitation is phenomenally low. An example of the trouble given by blends may be instanced here. The [Fe III] line at λ 4658 is twice as strong as N_1, and it may be that the latter is badly blended with other lines of the same multiplet occurring close enough to it to form a blend at the very low dispersion which obtains. For any ordinary planetary, it would be fantastic to feel any such concern, but not in the case of this candidate for what has been called " The Chamber of Horrors " of planetary nebulae.

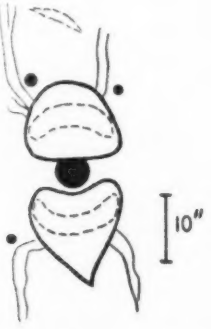

FIG. 1.—*Anon*, $16^h\ 13^m{\cdot}5$, $-51°\ 52'$. *Cf. Evans and Thackeray* ((7) *Fig.* 15, *Plate* 11).

As seen in the telescope this grisly creature seems to consist of no more than two arcs of nebulosity to north and south of the central star. A longer exposure such as that shown in Evans and Thackeray (7) plumps these out into two blobs of nebulosity, one of them being pointed. By an accident,

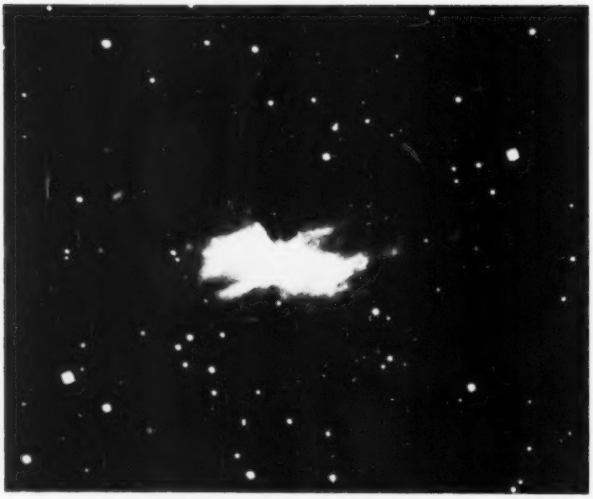

1956 *August* 5, 103*aO*, *no filter*, 30^m.
Scale: 3″·9/*mm.*

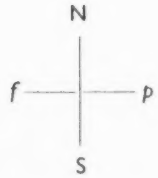

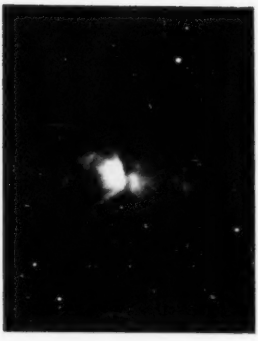

1950 *September* 13,
103*aO*, *no filter*, 7^m.
Scale: 3″·4/*mm.*

1956 *August* 8, 103*aE*+*Wratten filter* 1205, 45^m.
Scale: 3″·9/*mm.*

NGC 6302

this system has been included at the edge of two deeper plates taken on 1958 August 16 by Dr Thackeray and, particularly on the red plate of the pair (103aE plus GG 11 filter), it can be seen that the creature has legs which complete the ant-like form (Fig. 1). The dotted lines superposed on the blobs indicate the form as shown on short exposures. The dotted area to the north indicates a region of doubtful nebulosity.

NGC 6302, $17^h\ 10^m{\cdot}4$, $-37^\circ\ 03'$, $l = 317^\circ{\cdot}1$, $b = -0^\circ{\cdot}3$.

This is a very remarkable diffuse nebula, practically in the galactic plane, and only 10° from the galactic centre. The system is illustrated in the accompanying plates. The small sized reproduction shows a short exposure blue plate, from which it can be seen that the system comprises two lobes of luminous gas, shaped like the wings of a butterfly, separated by a relatively dark lane. There is no central star, but there are a number of stars involved in the system, suggesting that it is much larger and more distant than an ordinary planetary. The two other plates are of longer, matched exposures, and were taken under conditions of superb seeing. Reference to the list of line-strengths shows that, although Hα is very strong, λ 6583 is stronger still, and must really be responsible for the major part of the density on the red plate. This pair of plates repays closer study. The two halves of the system incorporate a series of opposed shells or fronts, and the regions of greatest luminosity lie within these fronts near the point where they are closest to each other. Behind these fronts lie a series of wisps of gas which, in the red plate, show fine filamentary structure, strongly reminiscent of that seen in solar prominences. Evidently the whole region contains a good deal of gas which, in the outer parts, is lighted up in a patchy way. For example, two filaments form the letters " ON " near one of the bright stars in the field, and there is another faint wisp Sf from this. The impression conveyed is that of dynamic interaction, as exemplified by the star immediately to the south of the centre of the system. On both plates this shows a patch of luminosity " banked up " on its preceding side. Another striking feature is the large number of extremely red stars which appear. The two prints are well-matched as far as the brighter stars are concerned, but half a dozen stars can be picked out by inspection which are bright on the red plate but almost invisible on the blue.

All the spectra have been taken by guiding on the brightest part of the nebula, with the slit east and west. The lines often resemble skittles showing the intensity drop at the centre. On the Newtonian spectrum, where there is no dekker for the nebular spectrum (only for the comparison), the extreme length of the lines corresponds to about 110″. The overall diameter on the prints is 3 to 4 minutes of arc. There is no distortion of the lines on the Cassegrain spectra due to differential radial velocity which could profitably be measured, and it is thought that deviations from the mean could not exceed at most 5 km/sec. The lines in the violet were only detected on the Newtonian spectrum, where the oxygen pair at λ 3726–28 is blended. On this film, continuous emission was detected, extending from about 3900 A to the limit of film sensitivity (103aO).

Since the form suggests dynamic interaction, but there is no marked radial velocity change along the lines, it may be inferred that the motions are predominantly transverse. A possible interpretation is that of a collision

with the production of shock fronts. It may be profitable to search for radio emission from this system, which, so far as the author is aware, has not previously been noted as a radio source.

NGC 6326, $17^h\ 16^m{\cdot}8$, $-51^\circ\ 42'$, $l = 305^\circ{\cdot}6$, $b = -9^\circ{\cdot}5$.

This object has been described by Evans and Thackeray ((**7**), Fig. 18, Plate 11). It may be a ring nebula with a bright spot on the ring, or a second star associated. Otherwise it is not particularly remarkable. The panchromatic plates have not shown up any lines in the red except Hα, and it does not seem as if there is a real paucity or weakness of lines in the red. The Newtonian spectrum shows a continuum starting well below λ 3727.

IC 4776, $18^h\ 42^m{\cdot}6$, $-33^\circ\ 24'$, $l = 329^\circ{\cdot}4$, $b = -14^\circ{\cdot}9$.

This object was described by W. H. Wright (**8**) as "a small bright irregularly elliptical nebula". Wright identified nine lines in its spectrum. The spectrum is very rich: the excitation is low. On the Newtonian spectrum the continuum due to the central star can be traced throughout the film sensitivity, (103aO), but no detail can be made out.

Acknowledgments.—The collection of the observational material has not been easy, and I am much indebted to the skilled assistance of Mr J. Churms and Dr P. A. Wayman in this task. My thanks are also due to Dr A. D. Thackeray for drawing my attention to his recent photographs of the anonymous system, and to Dr T. D. Kinman, who, both in personal discussion and by correspondence has kept me informed of his extremely careful and illuminating studies of the performance of the Newtonian spectrograph.

Note.—A referee has drawn my attention to the paper of L. H. Aller, I. S. Bowen and R. Minkowski on the spectrum of NGC 7027 (*Ap. J.*, **122**, 62, 1955). The nebular wave-lengths adopted there represent a further slight revision of those given by Bowen (**3**). Tests of the reduction of our spectra using these wave-lengths show a maximum change in the derived velocity of 0·6 km/sec and almost invariably a slight reduction in the probable error of the result. The changes are never significant in comparison with the probable error of the mean. So far as identifications go, there seems no need for change except to split the blend at 4712 A into 4711·34, [A IV] and 4713·17, He I, in fact assigning the tabulated lines to the former. It will probably be preferable to use the new wave-lengths in future work.

Royal Observatory,
Cape of Good Hope:
1958 *November.*

References

(**1**) M. W. Feast, A. D. Thackeray and A. Wesselink, *Mem. R.A.S.*, **67**, 51, 1954.
(**2**) David S. Evans, *M.N.*, **116**, 659, 1956.
(**3**) Ira S. Bowen, *Ap. J.*, **121**, 306, 1955.
(**4**) Charlotte E. Moore, *Princeton Univ. Cont.* 20, 1945.
(**5**) A. B. Wyse, *Ap. J.*, **95**, 356, 1942.
(**6**) W. W. Campbell and J. H. Moore, *Lick Obs. Pub.*, **13**, Part IV, 1918.
(**7**) David S. Evans and A. D. Thackeray, *M.N.*, **110**, 429, 1950.
(**8**) W. H. Wright, *Lick Obs. Pub.*, **13**, Part VI, 1918.

GLOBULAR CLUSTERS. I. THE RADIAL VELOCITIES OF SOUTHERN GLOBULAR CLUSTERS

T. D. Kinman

(Communicated by the Radcliffe Observer)

(Received 1959 February 6)

Summary

The radial velocities of 30 southern globular clusters are given and their errors are discussed. Spectra were obtained for 28 clusters using the Radcliffe Cassegrain spectroscope (86 A/mm) comprising spectra in integrated light for 15 clusters, spectra of individual stars for 10 clusters and spectra of both types for 3 clusters. No previous velocities were known for 16 of these clusters. Spectra were obtained with the Newtonian spectroscope (380 A/mm) in integrated light for 4 clusters, for 2 of which Cassegrain spectra were also available.

A comparison of the present velocities with those obtained by Mayall (5) and Joy (3) for the 12 clusters in common shows satisfactory agreement and a table of the velocities and distances of 70 globular clusters is given.

Introduction.—A study of the motions of the globular cluster system of the Galaxy is of particular interest because these clusters are prototypes of Baade's Population II and are believed to contain the oldest stars in the Galaxy. N. U. Mayall (5), in a remarkably fine investigation with the Crossley nebular spectroscope (430 A/mm at $H\gamma$), obtained velocities for fifty of these clusters, which is rather less than half of the known total. The distribution of the globular clusters in the sky is unfavourable to the northern observer; although Mayall managed to observe as far south as $\delta = -40°$, he noted that there were 23 clusters south of this limit, of which 17 might be observable spectroscopically. Many of these southern clusters are in the region of the antapex of the Sun's galactic motion and it is therefore important that their velocities should be observed in order to make a reliable determination of the solar motion with respect to the globular cluster system. An attempt has therefore been made to observe as many of these southern clusters as possible using the Cassegrain and Newtonian spectroscopes of the Radcliffe 74-inch reflector; in addition, twelve clusters for which either Mayall (5) or Joy (3) give velocities have been observed in order to obtain the velocities on a uniform system. The Cassegrain and Newtonian spectra are described and their reduction and errors are discussed in Sections 1 and 2 respectively of this paper. In Section 3, the radial velocities and distances are listed for 70 globular clusters. The spectral types obtained from the Radcliffe observations will be given and discussed in a second paper, while the analysis of the radial velocities of the 70 globular clusters is to be given in a third paper.

1. *Determination of velocities with the Cassegrain spectroscope*

1.1. *Observations.*—All spectra were taken using the shortest focal ratio camera of the Radcliffe 2-prism Cassegrain spectroscope (86 A/mm at $H\gamma$) (1)

with a slit width of 0·20 mm which projects to 27 μ on the plate. In general, if the core of a cluster is sufficiently bright and condensed to obtain a spectrum in integrated light then the individual stars are too faint for this spectroscope; conversely when the stars are bright enough to observe individually, the cluster is too extended to obtain integrated spectra. Only for four clusters were both types of spectra obtained and for one of these (47 Tuc) the stellar spectra were obtained by M. W. Feast and A. D. Thackeray and will be discussed by them elsewhere.

Sixty-nine spectra of 18 clusters were obtained in integrated light. The cluster cores were in general sufficiently unresolved for it to be unnecessary to put the image out of focus on the slit (cf. Mayall (**5**) and Morgan (**7**)); satisfactorily uniform spectra could be produced by trailing the image along the slit and by scanning in a perpendicular direction. Only for four clusters (NGC 104, 6397, 6752 and 7078) were the cores sufficiently resolved for it to be necessary to have the image out of focus. Projected slit heights of either 0·50 or 0·25 mm were used, depending upon the concentration and diameter of the cluster; exposures ranged from about one to six hours.

Sixty-four spectra of forty-one stars in 13 clusters were obtained; spectra of at least 3 stars per cluster were taken if the velocity of the cluster was previously unknown. Stars were selected from the cluster giants which under a power of about 300 often may be distinguished by their reddish colour. To increase the probability of finding a cluster member, stars close to the cluster centre were chosen, rejecting, however, any not well separated from fainter stars. Of the spectra taken, only 3 were rejected as being field stars: their velocities and spectra are quite different from those of other stars in the cluster concerned. The remaining stars, with one exception, are clearly cluster giants; the exception is a blue star in NGC 6752(*4) with almost the same velocity as the cluster. While its membership remains dubious, its inclusion has not affected the final velocity of this cluster. The projected slit height of the stellar spectra varies from 0·25 mm for the brightest stars observed ($m_{pg} \sim 12{\cdot}6$) to 0·10 mm for the untrailed spectra of the faintest ($m_{pg} \sim 14{\cdot}5$); the exposure times range from about one to six hours. Sixty-nine spectra of 48 standard stars of spectral types F0–K5 were taken concurrently with the cluster programme. Forty-one of these stars were of "a" quality in the Mount Wilson General Catalogue (**12**) and seven were stars for which the Cape kindly supplied well-determined velocities. All of these stars were observed within 25° of the zenith to reduce atmospheric dispersion errors, and neutral filters were used so that the exposure times were not less than 10 minutes.

An iron arc comparison spectrum was impressed on either side of all spectra at the beginning and end of each exposure and in the case of the cluster spectra at intervals during the exposure. All spectra were taken on Kodak 103aO emulsion and developed in a metolquinone developer for 5 minutes at 67 °F.

1.2. *Measurements.*—A slight curvature of the field of the F/2 camera lens of the spectroscope limits the spectrum range available for measurement to about 400 A in the photographic region. The range $\lambda\lambda$ 4400–4000 (centred on the wave-length of minimum deviation and the central ray of the photographic plate) does contain, however, almost all the features which are suitable for measurement in these cluster spectra. At the correct plate tilt, the departure from a flat field over this range does not exceed the accuracy of focusing

($\pm 15\ \mu$). All spectra were measured once (direct and reverse) on a standard Hilger photomeasuring micrometer. A few repeat measures gave almost identical results to the initial measures with similar residuals for given lines. This agrees with Mayall's conclusion (**5**) that the errors of measurement are smaller than inherent plate errors so that re-measurement is unnecessary.

TABLE I

Adopted wave-lengths for iron arc spectrum (86 *A/mm*)

3956·681	4030·755	4132·060	4282·406	4315·087	4383·547
3969·261	4045·815	4202·031	4294·128	4325·765	4404·752
4005·246	4071·740	4260·479	4307·906	4337·049	4415·125

TABLE II

Measured stellar wave-lengths (86 *A/mm; projected slit width* 27 μ)

λ (Go)	(F5)	(Ko)	λ (Go)	(F5)	(Ko)
4005·67 ± 0·08	0·00	0·00	4215·66 ± 0·08	+0·24	−0·36
4032·65 0·08	−0·07	+0·21	4226·52 0·08	−0·03	+0·07
4045·60 0·08	−0·04	+0·08	4254·93 0·14	0·00	0·00
4063·53 0·08	−0·07	+0·05	4260·39 0·11	−0·04	+0·06
4067·27 0·11	+0·03	+0·26	4272·31 0·11	−0·18	+0·24
4071·70 0·08	−0·01	+0·14	4290·02 0·14	−0·27	+0·27
4077·38 0·08	+0·14	+0·08	4325·30 0·14	+0·29	+0·01
4101·80 0·08	+0·08	−0·23	4339·89 0·12	+0·22	−0·33
4133·03 0·14	−0·04	+0·19	4352·10 0·12	+0·06	+0·09
4143·33 0·11	+0·06	+0·08	4375·06 0·12	+0·09	−0·07
4172·81 ± 0·11	−0·08	+0·18	4384·11 ± 0·15	+0·19	−0·19

Neither iron arc nor stellar wave-lengths are available for the present slit width and dispersion. In the first place, therefore, all visible features in the stellar spectra and apparently suitable unblended comparison lines were measured for a number of standard stars. Using I.A.U. iron arc wave-lengths as in (**1**), Hartmann dispersion curves were found for the iron lines in these spectra and those lines which consistently stood off the correction curves were rejected, leaving the 18 lines listed in Table I. Knowing the stellar velocities, mean provisional wave-lengths were then deduced for the features in the stellar spectra. The cluster spectra were then reduced following the method of J. S. Plaskett (**10**)*: standard micrometer readings being set up for both arc and stellar lines. The differences between the observed and standard readings for the stellar lines, when corrected from a curve derived from the arc line differences and multiplied by a factor found from the Hartmann formula, give the velocities directly. Similarly, velocities were found for the remaining spectra of standard stars observed concurrently with the clusters and from these a correction curve (in km/s) was plotted for twenty-two stellar lines as a function of spectral type. These corrections to individual lines were then applied to the cluster spectra. This procedure enabled almost all the features in the cluster spectra to be used, even though several features showed a strong wave-length dependence on spectral class; only the G-band components were invariably rejected from the features clearly visible in the range $\lambda\lambda$ 4400–4000. Col. 1 of Table II lists the final wave-lengths of the 22 features used for class Go together with an assessment of their internal consistency. Cols. 2 and 3 give

* The controlling temperature of the Radcliffe spectroscope is varied over a range of about 10 °C between summer and winter; the resultant change in the spectrum scale (~1·5 μ per mm) is small enough for only one standard Hartmann curve to be necessary.

the corrections to these wave-lengths for classes F5 to K0 and may be linearly interpolated.

The heliocentric cluster velocities are given in Col. 5 of Table III.

TABLE III

Radial velocities of globular clusters from Cassegrain spectra

Col. 1 NGC number of cluster; *I* = integrated spectrum, * = spectrum of individual star (spectra of the same star are bracketed) with identification number. The positions of these stars are shown on the finding charts.
2 Date.
3 Exposure time in minutes (t).
4 Number of lines measured (n).
5 Heliocentric radial velocity in km/s (V).
6 R.m.s. error of this velocity in km/s (derived from line residuals in the case of individual spectra and from plate residuals in the case of mean velocities) (σ).
7 Assigned weight on Mayall's system (W).

NGC		Date	t	n	V	σ	W
104	*I*	1957 7 21	87	18	− 22	± 5	4·4
	I	1957 8 5	113	11	− 21	5	4·4
	I	1957 9 18	60	11	− 24	8	4·4
	I	1957 10 6	97	16	− 27	3	4·4
	I	1957 10 16	90	16	− 28	3	4·4
				Mean	− 24	1	22
288	*1	1956 8 2	250	14	− 60	6	4·4
	*1	1957 9 19	268	8	− 49	9	4·4
	*2	1956 8 18	220	14	− 38	5	4·4
	*2	1957 8 15	265	15	− 48	5	4·4
	*3	1957 8 20	233	10	− 41	9	4·4
				Mean	− 47	4	22
362	*I*	1956 7 26	180	11	+221	6	4·4
	I	1956 7 29	210	14	+201	5	4·4
	I	1956 8 14	225	12	+218	6	4·4
	I	1956 8 21	305	5	+231	11	2·2
	I	1956 8 25	210	13	+238	9	4·4
	I	1957 9 7	144	15	+220	4	4·4
				Mean	+221	5	24
1261	*I*	1956 8 30	185	3	+ 63	25	2·2
	I	1956 9 24	170	4	+ 6	27	2·2
	I	1956 11 7	360	3	+ 50	16	2·2
				Mean	+ 40	18	7
1851	*I*	1956 11 12	57	14	+320	6	4·4
	I	1956 11 23	223	17	+319	5	4·4
	I	1956 12 22	215	14	+309	6	4·4
	I	1957 1 18	128	15	+320	9	4·4
				Mean	+317	3	18
1904	*I*	1956 12 30	300	5	+172	16	2·2
	I	1957 10 7	255	10	+168	9	4·4
	I	1957 10 17	230	4	+176	13	2·2
	I	1957 11 2	280	10	+200	12	4·4
				Mean	+181	8	13

TABLE III (*continued*)

NGC		Date	*t*	*n*	*V*	σ	*W*
2808	*I*	1956 4 8	180	12	+ 94	±10	4·4
	I	1956 5 17	210	15	+ 94	4	4·4
	I	1957 1 27	240	8	+119	11	4·4
	I	1957 2 12	217	8	+ 85	5	4·4
	I	1957 2 19	300	11	+113	8	4·4
	I	1957 4 5	183	16	+103	4	4·4
				Mean	+101	5	26
3201	*1	1956 4 17	265	11	+505	6	4·4
	*1	1956 4 29	270	16	+490	6	4·4
	*1	1956 5 2	270	14	+503	4	4·4
	*1	1956 5 27	180	13	+491	6	4·4
	*1	1956 6 1	180	14	+491	5	4·4
	*1	1957 3 6	130	18	+496	7	4·4
	*2	1957 4 19	180	17	+487	7	4·4
	*3	1957 4 25	180	12	+481	5	4·4
				Mean	+493	3	35
4372	*1	1957 5 10	185	13	+ 56	9	4·4
	*1	1957 6 20	317	12	+ 61	14	4·4
	*2	1957 5 22	242	5	+ 90	3	2·2
	*3	1957 6 17	303	5	+ 69	11	2·2
				Mean	+ 66	7	13
4833	*1	1956 5 27	180	6	+219	6	2·2
	*1	1957 6 14	335	11	+208	9	4·4
	*2	1956 6 19	265	5	+185	12	2·2
	*2	1957 6 23	81	5	+205	19	2·2
	*3	1956 6 25	205	5	+199	17	2·2
				Mean	+204	5	13
5139	*1	1956 4 20	123	11	+242	12	4·4
	*2	1956 6 1	180	11	+230	7	4·4
	*2	1957 5 21	135	12	+232	4	4·4
	*3	1957 4 5	120	20	+219	6	4·4
	*4	1957 4 25	160	10	+232	5	4·4
				Mean	+231	4	22
5286	*I*	1956 4 29	180	7	+ 45	7	4·4
	I	1956 5 2	210	10	+ 61	7	4·4
	I	1956 7 17	205	10	+ 38	16	4·4
	I	1957 4 14	230	18	+ 35	5	4·4
				Mean	+ 45	6	18
5904	*	1957 8 4	183	8	+ 42	10	4·0
6121†	*1	1956 7 29	223	17	+ 58	7	4·4
	*1	1957 8 19	200	14	+ 73	4	4·4
	*2	1957 3 26	195	18	+ 77	6	4·4
	*3	1957 4 26	170	14	+ 57	5	4·4
				Mean	+ 66	5	18

† In NGC 6121, stars 1, 2 and 3 correspond respectively to Greenstein's 113, 259 and 261 (*Ap. J.*, **90**, 401, 1939, in which a finding chart is given).

TABLE III (*continued*)

NGC		Date	*t*	*n*	*V*	*σ*	*W*
6139	*I*	1956 8 1	360	6	+ 19	±11	2·2
	I	1957 4 6	223	5	+ 66	12	2·2
	I	1957 8 14	310	6	+ 1	10	2·2
				Mean	+ 29	19	7
6266	*I*	1956 7 25	225	14	− 61	10	4
6362	*1	1956 6 19	205	10	− 23	7	4·4
	*1	1956 6 29	225	7	− 25	11	4·4
	*1	1957 6 7	300	13	− 11	5	4·4
	*2	1956 8 13	325	9	− 24	9	4·4
	*3	1956 8 20	324	17	− 9	6	4·4
	*4	1957 5 22	240	10	− 15	9	4·4
				Mean	− 18	3	26
6388	*I*	1956 4 9	167	14	+ 84	4	4·4
	I	1956 4 18	180	10	+ 84	14	4·4
	I	1956 4 21	180	13	+ 85	3	4·4
	I	1956 4 30	171	14	+ 76	3	4·4
	I	1957 4 20	186	17	+ 76	5	4·4
				Mean	+ 81	2	22
6397	*I*	1957 4 15	115	14	+ 22	7	4·4
	I	1957 5 14	140	11	+ 6	16	4·4
	*1	1956 5 28	195	11	+ 11	5	4·4
	*1	1956 6 2	180	13	+ 22	6	4·4
	*1	1958 3 26	60	9	+ 39	11	4·4
	*2	1956 8 24	133	11	− 8	4	4·4
	*2	1958 3 12	50	7	− 14	8	4·4
	*2	1958 3 26	50	7	+ 35	10	4·4
	*3	1957 6 23	180	18	+ 10	7	4·4
	*4	1957 6 20	175	17	− 11	6	4·4
				Mean	+ 11	6	44
6541	*I*	1956 7 17	191	9	−152	7	4·4
	I	1956 8 29	197	12	−156	8	4·4
	I	1957 5 11	165	6	−166	13	2·2
	I	1957 5 21	180	9	−115	11	4·4
	I	1957 6 14	165	6	−148	13	2·2
	I	1957 6 17	175	4	−171	14	2·2
				Mean	−148	8	20
6656	*1	1956 9 30	93	4	−134	12	2·2
	*1	1957 8 19	164	14	−146	6	4·4
	*2	1956 10 3	182	7	−149	8	4·4
	*3	1957 5 14	122	12	−135	9	4·4
				Mean	−142	5	15
6715	*I*	1956 9 29	164	14	+131	7	4·4
	I	1956 10 9	106	7	+124	8	4·4
	I	1957 6 24	200	15	+136	5	4·4
				Mean	+130	3	13

TABLE III (*continued*)

NGC		Date	*t*	*n*	*V*	σ	*W*
6752	*I*	1956 7 13	195	13	− 30	±8	4·4
	I	1956 10 24	240	11	− 32	9	4·4
	I	1957 5 22	155	13	− 48	6	4·4
	*1	1956 7 29	220	15	− 31	10	4·4
	*2	1956 9 23	185	16	− 45	6	4·4
	*2	1957 5 23	110	16	− 44	6	4·4
	*3	1957 4 26	120	15	− 29	4	4·4
	*4	1956 9 14	10	4	− 56	9	2·2
	*4	1956 9 20	92	6	− 26	12	2·2
	*4	1957 10 6	190	7	− 39	5	4·4
	*4	1957 10 16	60	9	− 51	6	4·4
				Mean	− 39	3	44
6809	*1	1956 8 17	220	8	+160	6	4·4
	*2	1956 8 24	256	14	+163	5	4·4
	*3	1956 9 9	232	16	+175	8	4·4
	*4	1956 9 28	180	16	+179	9	4·4
	*5	1956 10 7	190	15	+171	7	4·4
				Mean	+170	4	22
6864	*I*	1956 7 25	210	5	−158	6	2·2
	I	1956 6 20	185	14	−182	8	4·4
	I	1957 6 20	165	8	−203	6	4·4
	I	1957 9 18	210	13	−189	7	4·4
				Mean	−187	8	15
7078	*I*	1956 8 29	140	5	− 97	18	2·2
	I	1957 6 18	100	3	− 92	8	2·2
	I	1957 7 20	135	4	−103	9	2·2
	*1	1957 9 6	180	10	−100	12	4·4
				Mean	− 98	2	11
7089	*I*	1956 7 14	190	5	− 20	19	2·2
	I	1956 7 18	240	5	+ 9	5	2·2
	I	1957 6 21	180	6	− 24	13	2·2
				Mean	− 12	10	7
7099	*I*	1956 6 17	155	5	−196	17	2·2
	I	1957 6 8	145	2	−204	4	2·2
	I	1957 6 12	155	3	−169	28	2·2
	I	1957 6 15	165	2	−171	3	2·2
				Mean	−185	9	9

1.3. *Errors in these velocities.* (*a*) *Wave-length errors.*—The Royal Observatory, Cape, have kindly supplied wave-lengths determined by them for the same dispersion but with half the slit width. Of the 12 wave-lengths in common, 7 agree within the quoted Radcliffe errors. The difference for the other 5 lines is about twice the quoted Radcliffe error and may be due in part to the higher resolution of the Cape spectra. Synthetic wave-lengths were calculated for these 5 lines from Rowland revised wave-lengths (**11**) of the lines in the corresponding waveband to the measured line widths. The Rowland wave-lengths were weighted according to the equivalent widths derived from Mulders'

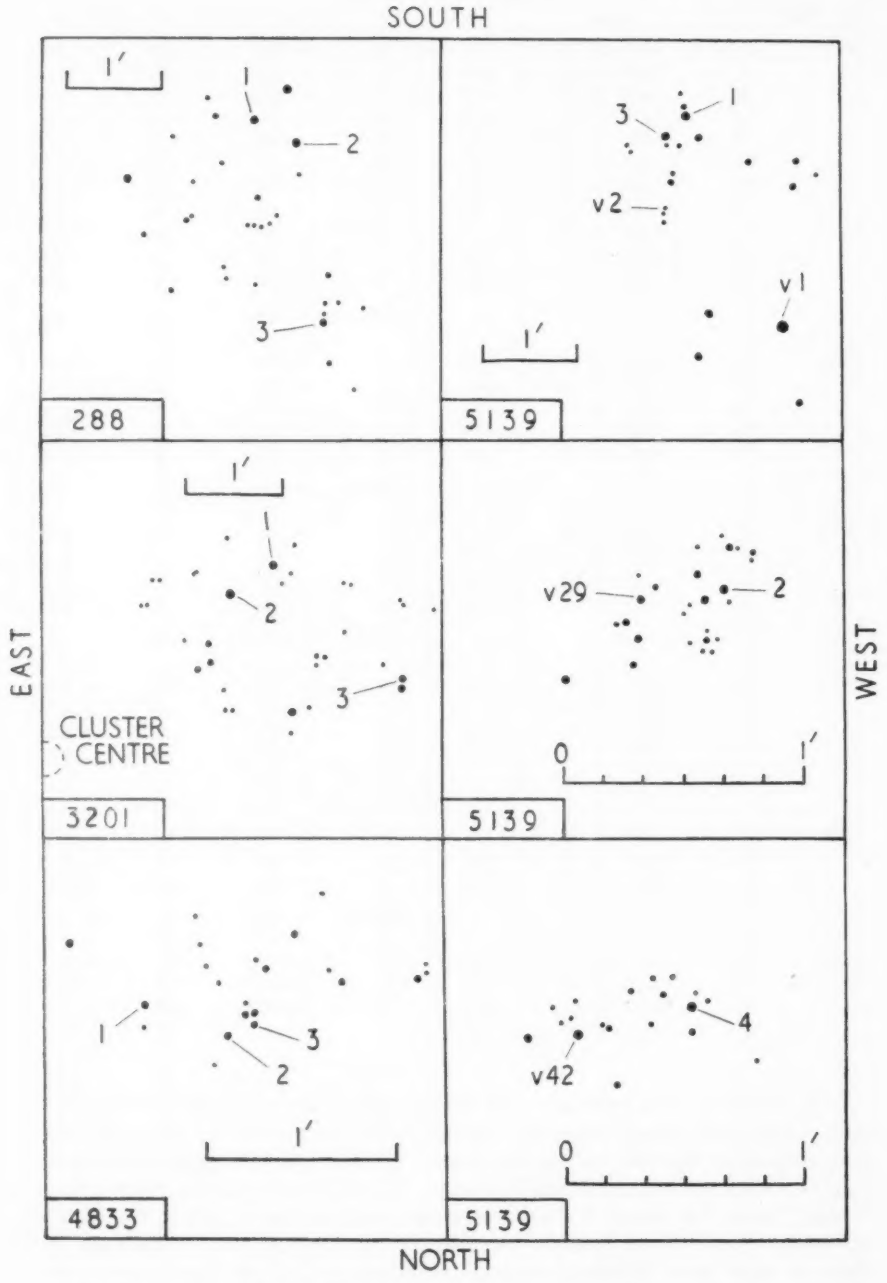

Finding Charts (1).—*The NGC number of each cluster is given at the bottom left hand corner of each chart. The star numbers are the same as those given in Table III, col. 1.*

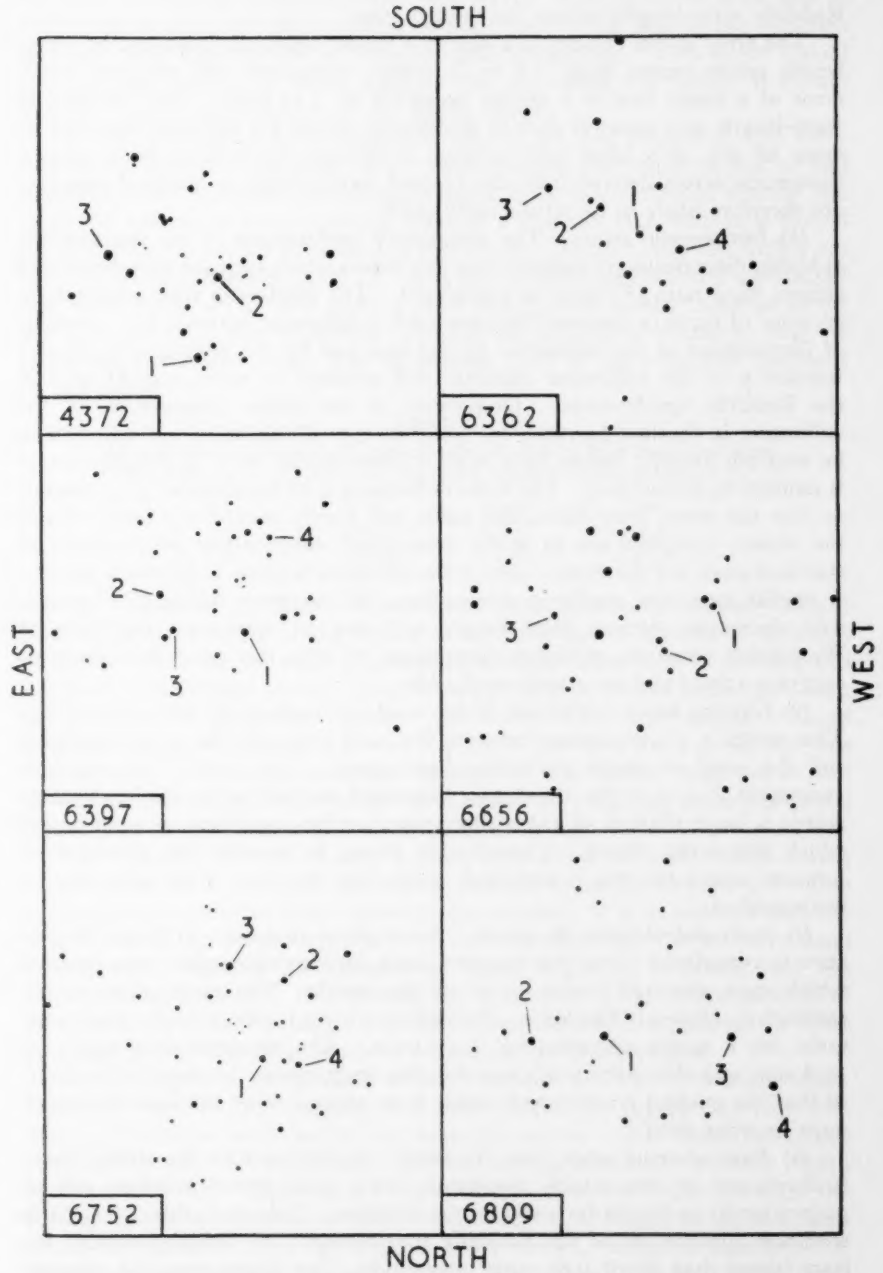

FINDING CHARTS (2).—*Scale for each of the above six charts: 5 × 5′ of arc.*

calibration (**8**). These synthetic wave-lengths show agreement with the Radcliffe wave-lengths within the quoted error.

The error in the velocity of a line in a cluster spectrum produced by wave-length errors ranges from ± 6 to ± 10 km/s compared with observed r.m.s. error of a single line in a cluster spectrum of ± 25 km/s. The variation of wave-length with spectral class is in different senses for different lines and an error of 0·3 of a class will produce a velocity error of about 2–3 km/s. Systematic errors derived from the adopted wave-lengths in the final velocities are therefore likely to be satisfactorily small.

(*b*) *Instrumental errors.*—The satisfactory performance of the spectroscope at higher dispersions (**1**) suggests that only errors which increase with decreasing camera focal ratio (F) need be considered. The Hartmann shift arising from an error of focus (ϵ microns) together with a difference between the centroids of illumination of the collimator by the star and by the comparison arc of a fraction p of the collimator diameter will produce an error $12\epsilon p/F^2$ km/s in the Radcliffe spectroscope. Uniformity of the stellar illumination of the collimator is checked periodically, while the arc illumination was adjusted to be uniform visually before each night's observations, so it is thought that p is unlikely to exceed 0·05. The error in focusing is of the order of ± 15 microns so that the error from Hartmann shifts can hardly exceed 2–3 km/s. Since the cluster velocities are in effect determined differentially with respect to standard stars, any systematic error from this cause is likely to be much smaller. A similar argument applies to errors from slit curvature which also increase with decreasing camera focal length. It may be shown on the basis of Wesselink's measures at higher dispersions (**1**) that this error is unlikely to exceed 0·1 km/s and so is quite negligible.

(*c*) *Guiding errors.*—The slit width used corresponds to 162 km/s at Hγ. This width is a compromise between the need to match the plate resolution and the need to obtain maximum light grasp. The present slit width is equivalent to 1″·2 at the Cassegrain focus and so enables the spectroscope to accept a large fraction of the stellar image under conditions of good seeing which frequently obtain. Considerable errors in velocity can clearly arise however unless the star is accurately guided on the slit. Two cases may be distinguished:

(i) *Stars observed near the zenith.* A sample of 16 spectra of G and K type stars is considered (from the standard stars used to determine wave-lengths) which were observed within $\pm 10^\circ$ of the zenith. The mean value of the residuals: General Catalogue − Radcliffe $= -0{\cdot}5 \pm 1{\cdot}1$ km/s with an r.m.s. error for a single spectrum of $\pm 4{\cdot}5$ km/s. The corresponding figure at 49 A/mm and slit width 0·075 mm for this spectroscope is about $\pm 2{\cdot}0$ km/s, so that the guiding errors which result from using a wide slit near the zenith must be quite small.

(ii) *Stars observed away from the zenith.* For these stars the stellar image is drawn out by atmospheric dispersion into a small spectrum which will be perpendicular to the slit for a star on the meridian. Colours in this atmospheric spectrum (on the slit of the Radcliffe spectroscope) are indistinguishable for stars fainter than about 10th visual magnitude. For fainter stars the observer may therefore be expected to guide with the visual wave-lengths of the image centred on the slit and with the photographic image systematically displaced

from the slit so that a guiding error will result. The spectrum lines will be shifted to the blue for objects south of the zenith in the case of the Radcliffe telescope and spectroscope in their normal orientation. The effect should increase with increasing zenith distance and increasing slit width; it should decrease with increasing size of the seeing image.

Velocities obtained from integrated spectra are not subject to this error because an extended source is used. Consequently one might expect to find a difference (Δ) between the velocities found from the integrated spectra and from the spectra of the individual stars of a cluster; this difference should increase with the zenith distance ζ of the cluster. Mean values of ζ and Δ are given for three clusters in Table IV. It is seen that the differences Δ are smaller than their r.m.s. errors and show a slight change with zenith distance in the opposite sense to that expected. It may be concluded therefore that no significant systematic errors due to guiding exist in the velocities discussed in this paper.

TABLE IV

The difference (Δ) *between the cluster velocity obtained from individual stars and from the integrated cluster light as a function of zenith distance* (ζ)

NGC	6397	6752	104
ζ	28° S	35° S	47° S
Δ	-4 ± 16	-1 ± 7	$+4\pm6$

1.4. *Comparison of cluster velocities with those from other sources.*—Mayall (*loc. cit.*) gave weights to the velocities found from the spectra of different observers which are inversely proportional to their dispersion. Following this procedure, the present spectra are given weight 4·4 on Mayall's scale on which each of his low dispersion spectra (430 A/mm) have unit weight. Those Radcliffe spectra which contain only 6 lines or less have been given half this weight (2·2). The mean velocities obtained by this simple weighting in fact differ little from those which would be obtained by weighting according to the square root of the number of lines in each spectrum.

The weights used show only a weak correlation with the r.m.s. errors derived from plate residuals (σ), which perhaps is hardly surprising because of the small number of plates available per cluster. If it is assumed that the weight should be proportional to σ^{-2}, then the Radcliffe spectra have been slightly underweighted with respect to Mayall's spectra by taking only the dispersion into account; this presumably is because of the larger number of lines in the Radcliffe spectra. Since, however, this effect is difficult to allow for satisfactorily, Mayall's system of weighting has been retained.

Table V gives a comparison of the velocities for twelve clusters which have been observed in common with either Mayall or Joy (3) together with their r.m.s. errors and weight on Mayall's system. The mean difference (Radcliffe–Mayall) is $+4\pm8$ km/s and the average difference without regard to sign is 20 km/s. This may be regarded as satisfactory since, although the differences for some clusters (NGC 1904 and NGC 6864) are greater than would be expected from the internal r.m.s. errors, similar comparisons by Mayall suggest that his adopted velocities may be in error by several times their internal error (i.e. from ±15 to ±20 km/s). If we discount Joy's single spectrum of a variable star in NGC 5139 (ω Cen) the mean difference

(Radcliffe–Joy) equals $+3 \pm 7$ km/s and the average difference without regard to sign is 11 km/s, which is also satisfactorily small. The final column of Table V gives the mean adopted velocities with r.m.s. errors based upon the weighted velocities of the different observers.

TABLE V

A comparison of globular cluster velocities (in km/s)

NGC	Radcliffe (R)	Mayall (M)	Joy (J)	R–M	R–J	Adopted velocity
1851	+317± 3 (18)	+291± 8 (8)	...	+26	...	+309± 12 (26)
1904	+181 8 (13)	+228 10 (6)	...	−47	...	+196 22 (19)
5139	+231 4 (22)	...	+176 (½)	...	+55	+230 8 (22)
5904	+ 42 10 (4)	+ 45 11 (13)	+ 52± 1 (25)	− 3	−10	+ 49 3 (42)
6121	+ 66 5 (18)	...	+ 62± 9 (8)	...	+ 4	+ 65 2 (26)
6266	− 61 10 (4)	− 81 17 (9)	...	+20	...	− 75 9 (13)
6656	−142 5 (15)	−148 8 (8)	−143± 9 (11)	+ 6	+ 1	−144± 4 (34)
6715	+130 3 (13)	+107 9 (7)	...	+23	...	+122 2 (20)
6864	−187 9 (15)	−222 8 (7)	...	+35	...	−198 17 (22)
7078	− 98 2 (11)	−108 7 (15)	−138±16 (3)	+10	+30	−107± 8 (29)
7089	− 12 10 (7)	− 3 7 (17)	− 4± 4 (18)	− 9	− 8	− 5± 2 (42)
7099	−185 9 (9)	−163 10 (9)	...	−22	...	−174± 9 (18)

2. *Determination of velocities with the Newtonian spectroscope*

2.1. *Observations.*—A single prism spectroscope has been used at the Newtonian focus of the Radcliffe reflector to obtain low dispersion (380 A/mm at Hγ) spectra of 2 clusters (NGC 1261 and NGC 6139), for which only a few low weight Cassegrain spectra were available, and also 11 spectra for 2 clusters (NGC 5927 and NGC 6584) which are too faint for the Cassegrain spectroscope. The few remaining clusters which are important for a solar motion study proved to be beyond the range of this instrument but the programme would in any case have been limited by the time available. In this spectroscope the light is collimated by an aluminized parabolic mirror of diameter 55 mm. The collimated beam is then intercepted by a perforated flat placed just behind the slit—an arrangement originally due to Pfund (**9**). Dispersion is produced by a single 60° dense flint prism and the camera consists of a detachable Schmidt system with uviol correcting plate and focal length 45 mm nominally working at $F/1$. The effective focal ratio must be larger however because of substantial vignetting in the system. All optical components of this spectroscope except the dense flint prism were made by Messrs. Cox, Hargreaves and Thomson.

The H and K lines must be clearly recorded in order to obtain useful velocities at this dispersion. At this wave-length the transmission of the spectroscope after the slit can hardly exceed 15–20 per cent with the principal light loss occurring in the prism: the difficulty of obtaining spectra of faint reddened objects will therefore be appreciated. Nevertheless the mean exposure times for six clusters showed that this spectroscope is $4{\cdot}1 \pm 0{\cdot}9$ times faster than the Cassegrain spectroscope at its lowest dispersion (86 A/mm).

A cluster was maintained on the slit by off-set guiding on a nearby star. Since the cluster could not be viewed on the slit, a suitably integrated spectrum covering most of the dekker width was obtained by placing the slit 8 mm

outside the Newtonian focus. A comparison arc was provided from an He discharge tube which together with a diffusing screen could be swung in front of the slit. A straight slit of width 0·15 mm (projected width 28 μ) was used and because of the short focal length camera the spectrum lines are therefore noticeably curved (radius ~5 cm). Spectra were obtained on disks of 103aO film, 0·85 cm in diameter, which were cut out by a special stamp. The film was processed in a perforated test tube and was then permanently mounted between two microscope slides.

2·2. *Measurement and reduction.*—The mounted spectra were measured direct and reverse on a Hilger photomeasuring micrometer. The reduction was performed using a standard Hartmann curve as for the Cassegrain spectra; M.I.T. wave-lengths (**6**) were used for the He arc and the Lick extra-galactic nebulae wave-lengths (**2**) for the cluster absorption features. Twenty spectra of nine clusters with known velocities were used to derive corrections (in km/s) which were applied to individual lines to obtain the correct velocity. Since the calcium H line is blended with Hϵ, two corrections were found for this line: one for type F (NGC 1261, 6139 and 6584) and one for type G (NGC 5927); no correction for spectral type was needed for other lines. This correction to individual lines takes into account line curvature and other systematic errors such as may be caused by slit irregularities or differential Hartmann shifts between arc and cluster spectra due to non-uniform illumination of the collimator. As with the Cassegrain spectra, the velocities are essentially measured differentially with respect to those known velocities of objects of similar spectra. The accuracy obtainable from different lines shows considerable variation so weights were given which were proportional to the inverse square of their r.m.s. errors in the standard spectra. These weights are listed in Table VI; the difference between Lick and Radcliffe weights for the K line may be due to underexposure of the Radcliffe spectra at this wave-length. Final heliocentric velocities are given in Table VII.

TABLE VI

Newtonian spectroscope wave-lengths

	Radcliffe			Lick			Mt Wilson
Line		λ	W_R		λ	W_L	λ
K		3933·86 ± 0·34	0·376		3933·28	384	3933·7
H	(G)	3968·37 ± 0·24	1·000	H	3968·38	301	3968·5
	(F)	3968·72		H(2) + Hϵ(1)*	3968·54	10	...
				H(1) + Hϵ(2)	3969·01	37	...
				H + Hϵ(=)	3969·23	34	...
Hδ		4102·06 ± 0·38	0·376		4101·25	120	4101·7
G		4302·76 ± 1·06	0·085		4303·52	140	4304·4
Hγ		4339·17 ± 0·90	0·141		4340·61	36	4340·5

W_R and W_L are the relative weights adopted by Radcliffe and Lick respectively.
* Numbers in brackets give hypothetical intensities of the unresolved components.

TABLE VII

Radial velocities of globular clusters from Newtonian spectra

Col. 1 NGC number of cluster.
2 Date.
3 Exposure time in minutes (t).
4 Heliocentric radial velocity in km/s (V).
5 R.m.s. error of this velocity in km/s (derived from line residuals in the case of individual spectra and from plate residuals in case of mean velocities) (σ).
6 Assigned weight on Mayall's system (W).

NGC	Date	t	V	σ	W
1261	1957 10 25	280	+ 32	±58	0·81
	1957 11 25	240	+ 96	31	1·00
	Mean (Newtonian)		+ 67	32	1·8
	Mean (Cassegrain)		+ 40	18	6·6
	Mean		+ 46	14	8·4
5927	1957 5 1	185	−204	90	0·74
	1958 3 18	185	−118	53	0·81
	1958 5 19	190	−118	37	0·74
	1958 6 19	230	+ 3	63	0·74
	1958 7 13	360	− 71	18	0·74
	1958 7 17	360	− 68	34	0·74
	Mean		− 96	28	4·5
6139	1958 8 14	150	− 10	67	0·93
	1958 8 14	145	− 12	17	0·93
	Mean (Newtonian)		− 11	1	1·9
	Mean (Cassegrain)		+ 29	19	6·6
	Mean		+ 20	15	8·5
6584	1957 8 26	70	+114	...	0·51
	1958 5 20	230	+210	43	0·93
	1958 5 22	215	+245	57	0·70
	1958 6 17	243	+184	61	0·93
	1958 6 20	240	+ 42	73	0·89
	Mean		+160	37	4·0

2.3. *Errors in these velocities.*—It is hoped to publish a fuller description of the spectroscope and its performance later; consequently only the results of tests of various sources of error are summarized below.

(*a*) *Flexure and thermal stability.*—A null result with a r.m.s. error of ±5 km/s was found for flexure alone. The mean shift of the λ 4046 Hg line registered on long exposures with respect to the laboratory value was −9 ± 25 km/s.

(*b*) *Emulsion shifts.*—For differential shifts occurring over short ranges (~1 mm), no difference was found between 103aO Cassegrain plate and Newtonian film. The r.m.s. error corresponds to ±25 km/s.

(*c*) *Consistency of measurement.*—The r.m.s. consistency of measuring a single spectrum is ±37 km/s.

The r.m.s. error of a single Radcliffe spectrum derived from plate to plate variation is ±58 km/s, which is little larger than that derived from the

agreement between the lines within a spectrum (Table VII, col. 5). For the 20 denser standard spectra the error is ±50 km/s. Corresponding errors for other low dispersion spectra are: Lick (globular clusters (**5**)) ±33 km/s; Mt Wilson (extragalactic nebulae (**2**)) best quality ±39 km/s, poorer quality ±52 km/s; Lick (extragalactic nebulae (**2**)) ±81 km/s.

The errors in the present spectra may be considered to be largely random and the spectra may therefore be weighted according to line weights: spectra on which all listed lines were used are given unit weight on Mayall's system. The adopted weights are given in the final column of Table VII.

3. *Velocities and distances for seventy globular clusters*

It has been suggested that in the present case weights should be assigned according to the dispersion rather than by using the r.m.s. errors. Apart from invalidation by systematic errors (which should be small for the Radcliffe velocities), r.m.s. errors afford a poor indication of the accuracy if the number of spectra is small. Application of the χ^2 test shows that if the r.m.s. error derived from a sample of four spectra be σ, then there is a 20 per cent chance that the true value of this error in the parent population exceeds 2σ and a 7 per cent chance that it exceeds 3σ. The r.m.s. errors of Mayall's velocities of weight four (four spectra) range from ±5 to ±53 km/s; weighting by the standard method according to σ^{-2} is thus inadmissible.

The probable errors have *in general* been assigned according to the weight on the following scale:

Weights		P.E.
	4– 6 (low dispersion only)	±20 km/s
	8–10	15
	10–20	10
	20–30	7
	above 30	5

These values have however served only as a general guide: each cluster has been considered individually taking into account the agreement between different observers.

TABLE VIII

Velocities and distances for seventy globular clusters

NGC	*V*	*W*	P.E.		*R* (kpc)	
104	− 24	(22)	± 3	4·8	5·8	6·9
288	− 47	(22)	7	9·6	12·6	16·6
362	+221	(24)	7	9·1	12·6	17·4
1261	+ 46	(8)	15	19	29	44
1851	+309	(26)	8	11·0	16·6	25
1904	+196	(19)	15	9·6	13·2	18·2
2298	+ 64	(5)	20	20	30	46
2419	+ 14	(5)	20	55	69	87
2808	+101	(26)	7	5·5	7·9	11·5
3201	+493	(35)	5	3·3	4·6	6·3
4147	+191	(4)	20	24	26	29
4372	+ 66	(13)	10	4·0	6·0	9·1
4590	−116	(4)	20	8·3	11·5	15·8
4833	+204	(13)	10	3·8	5·2	7·2
5024	−112	(10)	15	15·8	20	25

TABLE VIII (*continued*)

NGC	*V*	*W*	P.E.	*R* (kpc)		
5139	+230	(22)	±7	3·6	5·0	6·9
5272	−153	(54)	3	12·6	13·8	15·1
5286	+ 45	(18)	10	7·6	11·5	17·4
5634	− 63	(4)	18	18·2	23	29
5694	−187	(4)	18	32	42	55
5824	− 58	(4)	20	32	46	66
5904	+ 49	(42)	3	7·6	8·3	9·1
5927	− 96	(4)	20	1·5	3·2	6·6
5986	+ 2	(4)	30	9·6	13·8	20
6093	+ 18	(10)	10	8·7	11·0	13·8
6121	+ 65	(26)	5	1·8	2·3	2·9
6139	+ 20	(8)	15	7·9	12·6	20
6171	−147	(4)	20	2·4	3·0	3·8
6205	−241	(43)	8	6·3	6·9	7·6
6218	− 16	(12)	25	4·6	5·8	7·2
6229	−150	(9)	10	20	25	32
6254	+ 71	(18)	7	4·2	5·0	6·0
6266	− 75	(13)	10	5·5	6·9	8·7
6273	+102	(9)	18	5·2	6·9	9·1
6284	+ 22	(4)	20	12·6	16·6	21·9
6293	− 73	(4)	18	11·0	14·4	19·0
6304	− 98	(5)	20	4·0	5·8	8·3
6333	+224	(6)	15	6·3	7·9	10·0
6341	−118	(14)	5	9·6	11·0	12·6
6356	+ 31	(4)	20	7·9	10·5	13·8
6362	− 18	(26)	7	4·6	6·9	10·5
6388	+ 81	(22)	5	7·2	12·6	22
6397	+ 11	(44)	8	1·6	2·3	3·3
6402	−129	(9)	10	5·8	7·2	9·1
6440	−133	(6)	20	2·8	4·4	6·9
6441	− 70	(4)	18	6·0	8·7	12·6
6541	−148	(20)	10	3·0	4·2	5·8
6544	− 12	(4)	18	2·5	5·0	10·0
6584	+160	(4)	25	8·3	12·6	19·0
6624	+ 69	(4)	18	8·7	12·6	18·2
6626	+ 1	(8)	12	3·6	4·6	5·8
6637	+ 95	(5)	20	5·0	7·2	10·5
6638	− 14	(5)	20	10·5	13·8	18·2
6652	−124	(4)	18	11·0	15·8	23
6656	−144	(34)	5	2·4	3·0	3·8
6681	+198	(4)	20	13·8	20	29
6712	−131	(4)	20	4·8	6·0	7·6
6715	+122	(20)	7	12·0	15·1	19·0
6723	− 3	(4)	20	7·9	10·0	12·6
6752	− 39	(44)	5	4·4	6·3	9·1
6779	−145	(21)	8	11·0	13·8	17·4
6809	+170	(22)	8	4·4	5·8	7·6
6838	− 80	(4)	20	3·5	5·5	8·7
6864	−198	(22)	11	18·2	24	32
6934	−360	(6)	15	13·2	16·6	21
6981	−255	(5)	25	14·4	18·2	23
7006	−348	(6)	18	46	60	79
7078	−107	(29)	7	13·8	15·1	16·6
7089	− 5	(42)	3	13·2	15·8	19·0
7099	−174	(18)	10	10·0	12·6	15·8

Table VIII gives the radial velocity in km/s (V), weight (W) and probable error (P.E.) for seventy clusters. The heliocentric distances of these clusters in kiloparsecs (R) found in a previous discussion (**4**) are also given; the second figure in this column is the estimated distance, and the first and third are the limits corresponding to the probable error of the moduli.

Acknowledgments.—I should like to express my sincere thanks to the Radcliffe Observer (Dr A. D. Thackeray) for the generous help and encouragement which he has given to me at all times. I am also grateful to the Radcliffe Trustees for a Radcliffe Travelling Fellowship which enabled this work to be undertaken at Pretoria.

Radcliffe Observatory,
Pretoria:
1958 *December.*

References

(1) M. W. Feast, A. D. Thackeray and A. J. Wesselink, *Mem. R.A.S.*, **67**, Part II, 52, 1955.
(2) M. L. Humason, N. U. Mayall and A. R. Sandage, *A.J.*, **61**, 97, 1956.
(3) A. H. Joy, *Ap. J.*, **110**, 105, 1949.
(4) T. D. Kinman, *M.N.A.S.S.A.*, **17**, No. 3, 1958 (Radcliffe Observatory Reprint No. 9).
(5) N. U. Mayall, *Ap. J.*, **104**, 290, 1946.
(6) M.I.T. Wavelength Tables, John Wiley, 1939.
(7) W. W. Morgan, *P.A.S.P.*, **68**, 509, 1956.
(8) G. F. W. Mulders, *Zs. f. Ap.*, **8**, 62, 1934.
(9) A. H. Pfund, *J.O.S.A.*, **14**, 337, 1927.
(10) J. S. Plaskett, Report of Chief Astronomer, Ottawa, p. 95, 1907.
(11) Rowland Revision, Carnegie Inst. Washington, 1928.
(12) R. E. Wilson, *General Catalogue of Stellar Radial Velocities*, Carnegie Inst. Washington, 1953.

THE BRIGHTNESS DISTRIBUTION WITHIN THE RADIO SOURCES CYGNUS A (19N4A) AND CASSIOPEIA A (23N5A)

R. C. Jennison and V. Latham

(Received 1958 December 8)

Summary

Measurements are described of the amplitude and phase of the Fourier transform of the distribution of brightness at 127 Mc/s within the intense radio sources Cygnus A (19N4A) and Cassiopeia A (23N5A) along an axis in the East–West direction. The brightness distribution is computed from the observed readings and in the case of Cygnus A is shown to confirm the existence of two major emitting regions of almost equal intensity. The α component, leading in right ascension, is slightly brighter than the β component. Measurements are also described of the determination of the position of the major axis of the source. It is evident that the diameter of the Cygnus source in a position angle close to 187° must be relatively very small. The measurements on Cassiopeia indicate the presence of a faint spur near position angle 90° together with probably slight limb brightening of the main body of the source.

---

1. *Introduction.*—The existence of asymmetry in the radio source Cygnus A (19N4A) was shown in the initial measurements of Hanbury Brown, Jennison and Das Gupta (**1**). These measurements indicated that, to a first order, the shape of the source was elliptical, approximately two minutes ten seconds of arc in diameter in position angle 113° and thirty-five seconds of arc in position angle 177°. The major axis appeared to lie between position angle 90° and position angle 120°. These dimensions were not compatible with those of the photographic object observed by Baade and Minkowski (**2**) within the position rectangle given by Smith (**3**). The photographic object, interpreted by Baade and Minkowski as a collision between two late-type spiral nebulae, is elliptical in form, measuring 18″ × 30″ with the major axis in position angle 150°. The nuclei of the two galaxies are separated by 2″ in position angle 115°. The distance of this object, obtained from the red shift of a neighbouring galaxy, is approximately 100 M parsecs*. This distance has been confirmed in the radio frequency spectrum by the hydrogen line absorption measurements of Lilley and McClain (**4**).

A more detailed study of the structure of the object at radio frequencies was performed by Jennison and Das Gupta (**5, 6**) who showed that the source consisted of two major components, each approximately 50″ × 30″, separated along the direction of their major axis by 1′ 25″ between their centres. On the assumption that the position and identification of the source were correct, this model straddled the photographic object and required the generation of the radio frequency radiation to take place at a considerable distance from the main mass of the nebula. The interferometer system used by Jennison and

* Using a value for the Hubble constant of 180 km/sec/Mpsc.

Das Gupta was not suitable for the measurement of the phase of the Fourier components and the model given was not unique, though other solutions in general increased the overall size of the radio object. It was evident that a more refined technique was required for work on this problem.

The intense radio source Cassiopeia A (23N5A) has been identified (**2**) as an unusual emission nebulosity within the Galaxy. The structure of the Cassiopeia source which appears on photographic plates taken at the 200-inch telescope, consists of a number of small filamentary structures and condensations distributed over an area five minutes of arc in angular diameter. To the north of the area there is a brighter arch of nebulosity of bluer colour. The diffuse filaments exhibit large internal random motions and are extremely transient; their structure has been observed to change over a period of a few years. The filaments also exhibit signs of an ordered expansion which indicates an origin 280 years ago if the expansion velocity is still constant (**8**).

The angular diameter of the Cassiopeia A source was first determined at radio frequencies by Smith (**9**) in position angle 90°, and by Hanbury Brown, Jennison and Das Gupta (**1**) in three position angles inclined to each other at 120°. These measurements showed that the object was approximately radially symmetrical and had a diameter of the order of five minutes of arc.

Further measurements by Jennison and Das Gupta in position angle 113° extended the resolution to baselines of over 3 000 wave-lengths (**6**). It was found that the correlation function of the radiation from the Cassiopeia source fell off rapidly up to a spacing of 900 wave-lengths, thereafter apparently exhibiting a tail which approached zero in the neighbourhood of 1 500 wave-lengths. No subsidiary maxima were observed but, as the correlation function measured by the equipment corresponded to the square of the Fourier transform obtained by conventional interferometer systems, the equipment was not sensitive to small readings and it was fundamentally incapable of determining the phase associated with such maxima. In order to obtain a more detailed picture of the radio frequency distribution of brightness of these objects, a high resolution, phase-sensitive interferometer was constructed and used in a series of measurements on the source at a frequency of 127 Mc/s during the period 1955–1956.

2. *The equipment and method.*—A three-station interferometer system was developed in which most of the errors usually associated with the equipment and aerial siting were nullified, and both the amplitude and phase of the Fourier components could be measured concurrently over large spacings of the aerial systems. The equipment and the method of measurement have been more fully discussed in a previous paper (**7**).

The measurements were made by spacing three aerial systems *A*, *B* and *C* and their associated relay transmitters in a line along which the readings were required. The signals received from the three stations were then combined in pairs by means of three switched interferometer systems in which the arguments of the fringes could be controlled by electrically-driven phase-rotating condensers. By spacing the aerials at equal distances the measurement of amplitude could be made absolute whilst relative measurements could be obtained at other spacings. The measurement of phase was relative to a datum obtained from measurements at short spacings and involved a cumulative error which increased with aerial separation.

Under the illumination of a complex source, the phase angle given by subtracting the sum of the arguments of the fringes formed between A and B and between B and C from the arguments of the fringes formed between A and C is given by the expression

$$\phi = \xi_{AC} - (\xi_{AB} + \xi_{BC})$$

where ξ_{AB}, ξ_{BC} and ξ_{AC} represent the phase of the Fourier transform at spacings AB, BC and AC respectively.

This result is independent of the phase errors and the angular velocity of the phase rotation. It enables an estimate to be made of the relative phase contributions due to the source structure only, and is applicable when the aerials are spaced by arbitrary distances. In the general case, when the transform is complex but the aerial spacings are unequal, the phase change over any extension of the baseline may be determined and normalized against those points where the phase is absolutely known or where the phase change is constant. By this means the whole phase function may be mapped.

The measurement of the amplitude of the Fourier transform of the intensity distribution across the source may be made concurrently with the measurement of phase. We may form the function

$$\eta = \frac{|AB| \times |AC|}{|BC| \times |A|^2}$$

where $|AB|$, $|BC|$ and $|AC|$ are the moduli of the fringe systems between channels A and B, B and C, and A and C respectively, and $|A|^2$ is the total power due to the source recorded in channel A. It has been shown (**7**) that the function η may also be written as

$$\eta = \frac{Kf(ab) \times f(ac)}{f(bc)}$$

where $f(ab)$, $f(bc)$ and $f(ac)$ are the amplitudes of the transform for the baselines AB, BC and AC, and K is a constant of the equipment which may be checked regularly.

3. *Measurements on Cygnus* (19*N*4*A*)

(*a*) *The East–West distribution.*—A series of measurements was undertaken in position angle 90° in which the phase and amplitude of the Fourier components were determined at a number of spacings extending to the region of the second maximum of the transform. Topographical features prevented the taking of readings in the immediate vicinity of the first minimum, though these readings would have been of considerable value in the analysis. At each spacing of the aerial systems the angular velocity of the rotating phase shifters was set to a suitable value for measurements to be made of the fringe pattern on the recording meters. The relative values of the natural fringe frequency and the phase shifter frequency were noted, since the sign of this parameter determined the interpretation of the measured phase shifts as leading or lagging and hence the interpretation of the relative position of the asymmetrical component of the source.

The measured values of the amplitudes and phases of the complex visibility function corresponding to the Fourier transform of the brightness distribution are listed in Table I.

TABLE I

Aerial spacing (wave-lengths)	Amplitude	Phase
224	$0{\cdot}98 \pm 0{\cdot}02$	$-4° \pm 5°$
534	$0{\cdot}67 \pm 0{\cdot}05$	$+1° \pm 5°$
828	$0{\cdot}51 \pm 0{\cdot}07$	$-5° \pm 8°$
1060	$0{\cdot}32 \pm 0{\cdot}05$	$+22° \pm 11°$
1540	$0{\cdot}24 \pm 0{\cdot}03$	$+166° \pm 13°$
2160	$0{\cdot}46 \pm 0{\cdot}04$	$+190° \pm 23°$

Each of the readings tabulated was the mean of the observations obtained on several successive days, usually about ten in number. In addition each daily record yielded a number of separate measurements of the phase function from the individual fringe displacements, whilst the amplitude was also deduced independently from several points on the envelope of each fringe pattern.

It will be seen that the amplitude of the second maximum of the transform of the source is comparable to, but slightly less than, the value previously obtained by Jennison and Das Gupta (**6**). The phase function undergoes a

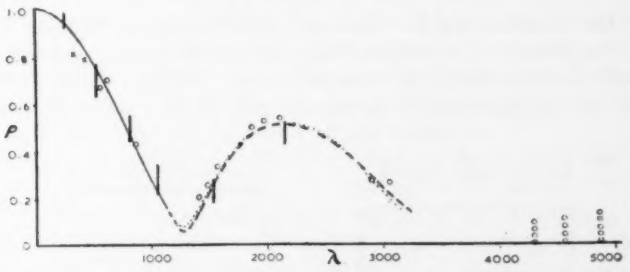

FIG. 1.—*Cygnus A* (19*N*5*A*), *amplitude of visibility function at* 127 *Mc/s in position angle* 90°. *The vertical lines represent readings taken with the phase sensitive interferometer. The crosses are readings by Smith and the circles are readings by Jennison and Das Gupta; the readings between* 4 000 *and* 5 000 *wave-lengths were zero in the latter measurements of the function* ρ^2, *on conversion to* ρ *the errors are as shown. The two curves refer to the alternative brightness distributions in Fig.* 3.

sudden change in the region of the first minimum, in agreement with the assumptions made by the above workers in interpreting their results, but there is a detectable sinusoidal component contributing a small degree of asymmetry to the source.

(*b*) *Analysis of East–West distribution.*—The readings given in Table I may be transformed to give the brightness distribution of the source smoothed by the convolution with the Fourier transform of the maximum aperture of 2 160 wave-lengths; only the major components of the source are therefore resolved but the solution within these limits, and within the errors, is unique. The readings obtained for the amplitudes are plotted in Fig. 1, together with the readings obtained by Jennison and Das Gupta and by Smith. The phases are plotted in Fig. 2. Superimposed on the amplitude and phase plots are

the curves corresponding to the transforms of the distributions shown in Fig. 3. It will be observed that both these distributions transform within the error of the readings and it is not possible to distinguish between them without

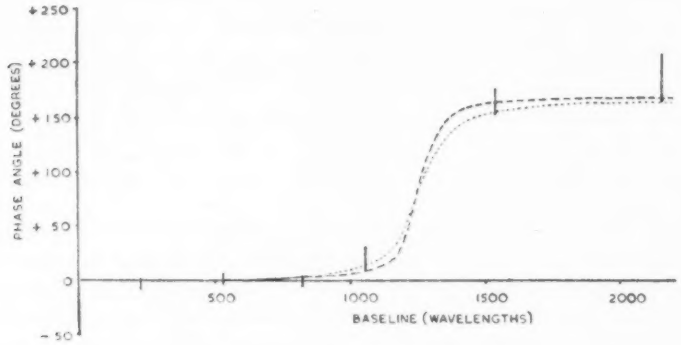

FIG. 2.—*Phase of the visibility function at 127 Mc/s, in position angle 90° across the radio source Cygnus A (19N4A). The vertical lines refer to the observed readings whilst the two curves correspond to the two distributions in Fig. 3.*

exceeding the baselines used. The two distributions are similar in that the integrated brightness of corresponding components is the same, but in one distribution the diameters of the components are the same whilst the brightness of one of the components is increased, and in the other distribution the

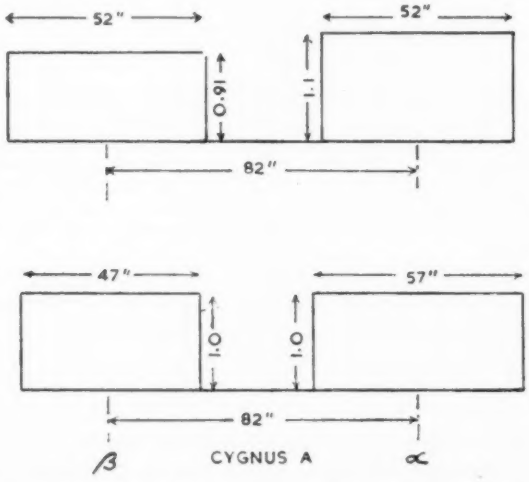

FIG. 3.—*Alternative primary brightness distributions at 127 Mc/s in position angle 90° across the radio source Cygnus A (19N4A).*

brightness of the two components are the same but the asymmetry is obtained by controlling their diameters. The separation between the centres of

radiation, 82 seconds of arc, is accurate to a few seconds of arc. The ratio of the intensities of the two components has an associated error of the order of 10 per cent. The major component, which we shall designate Cygnus Aα, leads in right ascension. Though the distributions in Fig. 3 indicate only the primary regions of emission and cannot show the finer details, the contribution at 127 Mc/s from the central reading of the system is evidently very small and cannot exceed a few per cent of the brightness of the α and β components. The errors in the readings combined with the smoothing imposed by the restriction of aperture do not enable the exact extent of this radiation, if it exists, to be determined from the present measurements.

(*c*) *The determination of the position angle of the major axis.*—The measurements of Hanbury Brown, Jennison and Das Gupta showed that the major axis of the Cygnus source had a position angle between 90° and 120°. Measurements of this position angle by varying the azimuth of the baseline of a high resolution interferometer are liable to the large errors usually associated with changes of baseline in a two element system. In order to establish the position angle with greater accuracy three stations were used in the following ways.

The intensity distribution measured by an interferometer system is that projected on to the tangent of a great circle on the celestial sphere which has the baseline as its diameter and which also passes through the source. As the source moves across the sky, the observed distribution will change. If the source is not radially symmetrical the observed fringe amplitude will be a maximum when the major axis is orthogonal to the plane containing the baseline and the source. The method used is therefore to observe the time at which the fringe amplitude reaches a maximum; the position angle of the major axis may then be found from the geometry of the situation.

The main aerial system was phased to look in the approximate direction at which the maximum amplitude was expected and a second aerial system consisting of a simple dipole and reflector was sited at a distance of 4 km and an azimuth of 177°. A third aerial system, also consisting of a dipole and reflector, was sited 50 m from the first station at an azimuth of approximately 315°. The phases of the signals from both outstations were artificially rotated to give suitable fringes on recorders multiplying their outputs with that of the home station. The small aerial sited close to the home station served as a monitor to remove the effect of the polar diagram of the large aerial system. The envelope of the fringes formed by mixing this channel with the signals from the home station depended only upon the polar diagram of the large aerial, whilst the envelope of the fringes formed by the large aerial and the other outstation depended primarily on both the polar diagram of the large aerial and the brightness distribution of the source. Suitable delays were included in the equipment to compensate for the distance of the furthermost outstation.

The results of the observations are plotted in Fig. 4, in which the ordinate scale is the observed fringe amplitude after correction for aerial gain. Each point represents the mean of five observations. The measured amplitude corresponds to a position angle of the major axis of 97°, though this is subject to a slight systematic error arising from uncertainty in the correct setting of the delay lines. The diameter of the source in position angle 187° will be less than that observed by Jennison and Das Gupta in position angle 177°. Further

measurements at baselines in excess of 3 000 wave-lengths in position 187° would be of considerable value.

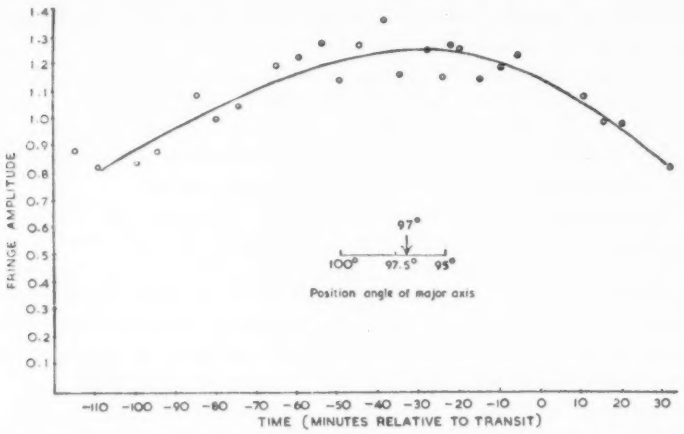

FIG. 4.—*Cygnus A* (19*N*4*A*), 127 *Mc/s. Variation of fringe visibility with position of source for the determination of the position angle of the major axis. Azimuth of the baseline of the interferometer is* 177°. *The scale in the centre of the diagram gives the position angle corresponding to the maximum fringe visibility.*

4. *Measurement on Cassiopeia* (23*N*5*A*).—The measurements made with the equipment were confined to the distribution across the source along an axis in the East–West direction. The measurements were made concurrently with measurements on the Cygnus A source and with the time and manpower available it was not possible to take a fully representative set of readings. Considerable care was taken to establish the position of the first minimum, at which the fringe visibility was reduced below the noise level of the equipment. This minimum was found to occur at 840 wave-lengths; topographical difficulties prevented the measurement of visibility in the region of 900 wave-lengths though a reading at this aerial separation was desirable to establish the position of the minimum with greater accuracy.

The measurement of the phase function clearly showed the existence of the second and third maxima of the transform of the brightness distribution of the source. These maxima could not have been detected from the amplitude measurements alone unless many more readings had been taken. Both the amplitude and phase functions showed a depression at short aerial spacings. This depression indicated an asymmetrical extension of the object seen as a projection into position angle 90°.

The values obtained for the amplitude and phase of the complex visibility function corresponding to the Fourier transform of the brightness distribution of the Cassiopeia source are listed in Table II. The magnitude of the errors in the phase function at large aerial spacings is due to the cumulative effect of the deviations from zero at short spacings (7). The readings for both amplitude and phase at 224 wave-lengths were the mean of a number of observations on slightly different baselines. In general each of the readings tabulated was the mean of the observations obtained on several successive

days, usually about ten in number. In addition, each daily record yielded a number of separate measurements of the phase function from the individual fringe displacements, whilst the amplitude was also deduced independently from several points on the envelope of the fringe pattern.

TABLE II

Aerial spacing (wave-lengths)	Amplitude	Phase
224	0·78 ±0·05	2° ± 5°
534	0·36 ±0·05	2° ± 11°
811	0·045 ±0·03	47° ± 16°
828	0·0 ±0·01	—
1060	0·19 ±0·02	236° ± 22°
1540	0·028 ±0·01	280° ± 32°
2160	0·05 ±0·01	135° ± 43°

The observed amplitude of the visibility function is plotted in Fig. 5, in which the vertical lines represent the errors associated with each point. The broken curves drawn on this plot correspond to simple rectangular slit and disk models. They do not pass through the two points at large aerial spacings, but these are satisfied by slightly tapering the slit distribution or limb brightening the disk.

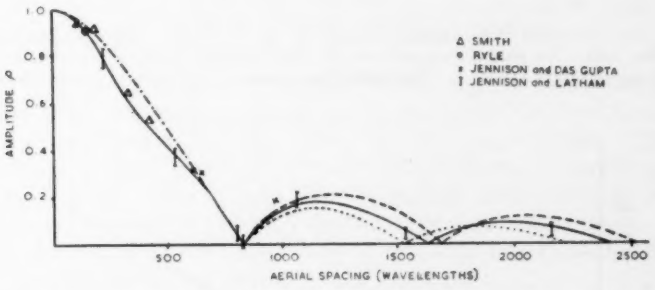

FIG. 5.—*The amplitude of the visibility function of the Cassiopeia A (23N5A) source along the East–West axis. The dotted curve on the diagram represents the transformation of a simple disk source; the dashed curve represents a simple slit whilst the full curve is the transformation of the mean of the two distributions in Fig.* 8.

The phase of the visibility function is plotted in Fig. 6. From this function it is clearly seen that the points at 1 540 and 2 150 wave-lengths lie in the second and third maxima of the visibility function. The shaded portion in Fig. 6 encloses the range of brightness distributions lying between the two illustrated in Fig. 8.

Fig. 7 shows the residual to the phase function after subtraction of the symmetrical component. The asymmetry apparent in the neighbourhood of 500 wave-lengths will be seen to coincide with a depression in the amplitude function (Fig. 5) in this region. The general slant of the residual phase function is due to the shift of the centre of radiation to the main body of the nebula as the spur in position angle 90° is resolved with extension of the baseline.

The brightness distribution within the radio source in position angle 90° is shown in Fig. 8. The two diagrams in this figure embrace the limits of

brightness distribution permitted by the experimental results. The most noticeable feature of the distributions is the faint spur on the left of the diagrams. This is seen as a projection into position angle 90° and the true position angle

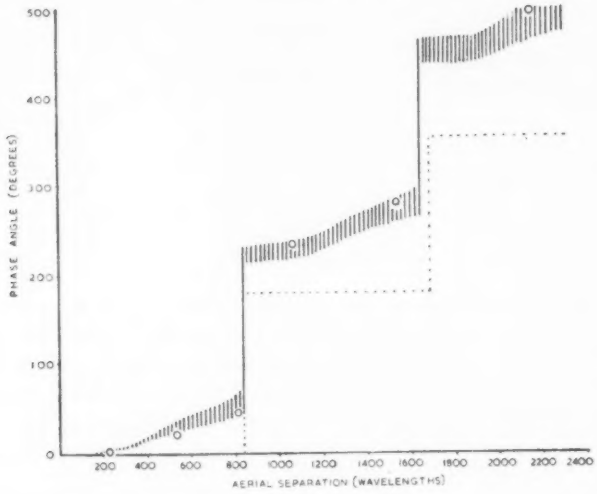

FIG. 6.—*The phase of the visibility function of the Cassiopeia A (23N5A) source along the East–West axis. The shaded area embraces the region contained between the transformations of the two models shown in Fig. 8. The dotted line represents the phase of a symmetrical source.*

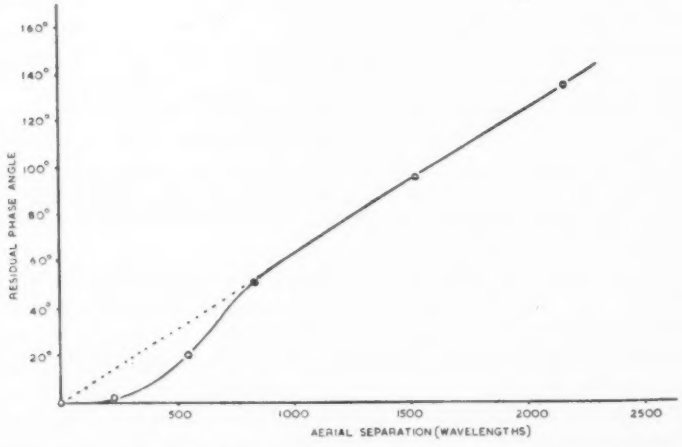

FIG. 7.—*The residual to the phase function after subtraction of the symmetrical component.*

cannot be determined without further measurements taken with a baseline of different orientation. A few unpublished measurements, made on short baselines at Jodrell Bank in the course of testing the phase sensitive interferometer, failed to show a significant contribution in the North–South direction,

and it is probable that the spur actually lies close to the position angle 90°. If this is not so, an allowance must be made for the projected length of the spur into this position angle; the true length will be somewhat greater than that indicated by the present measurements.

The main body of the nebula appears to be reasonably symmetrical within the error of the present readings, but the readings imply that there may be slight limb brightening over the distribution otherwise given by that of a

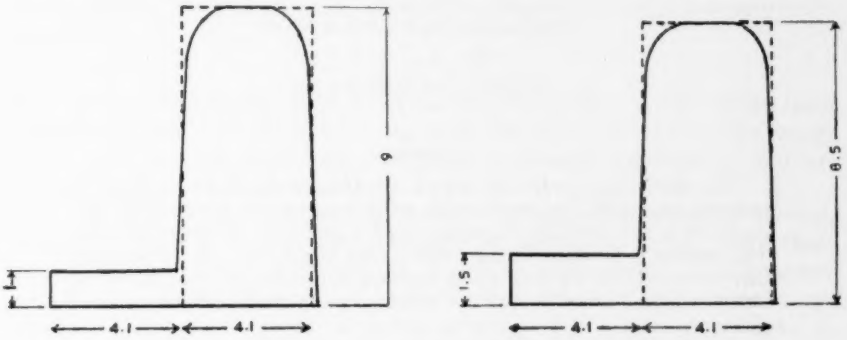

FIG. 8.—*Limiting brightness distribution for the Cassiopeia A (23N5A) source along the East–West axis at a frequency of 127 Mc/s.*

uniformly illuminated disk. The presence of the asymmetrical spur does not appreciably affect the position quoted by Smith (3) for the right ascension of the object as measured at baselines of less than 200 wave-lengths. The phase function shown in Fig. 6 may be used to correct the position at larger apertures.

Acknowledgments.—The authors wish to express their thanks to Professor A. C. B. Lovell and to Mr Hanbury Brown for their encouragement. One of us (V. L.) is indebted to the Department of Scientific and Industrial Research for a studentship during the period of the experiment.

Jodrell Bank Experimental Station
(University of Manchester),
Lower Withington, Cheshire :
1958 *December* 5.

References

(1) Hanbury Brown, R., Jennison, R. C. and Das Gupta, M. K., *Nature*, **170**, 1061, 1952.
(2) Baade, W. and Minkowski, R. L., *Ap. J.*, **119**, 206, 1954.
(3) Smith, F. G., *Nature*, **168**, 555, 1951.
(4) Lilley, A. E. and McClain, E. F., *Ap. J.*, **172**, 123, 1956.
(5) Jennison, R. C. and Das Gupta, M. K., *Nature*, **172**, 996, 1953.
(6) Jennison, R. C. and Das Gupta, M. K., *Phil. Mag.*, **1**, 65, 1956.
(7) Jennison, R. C., *M.N.*, **118**, 276, 1958.
(8) Minkowsky, R. L., " Radio Astronomy " by H. C. Van de Hulst, C.U.P., 1957, p. 118.
(9) Smith, F. G., *Nature*, **170**, 1065, 1952.

THE RELATION OF COSMIC RADIO EMISSION TO THE ELECTRONIC COMPONENT OF COSMIC RAYS

Harriet Tunmer

(Communicated by F. Graham Smith)

(Received 1958 December 22)

Summary

The similarity between the spectra of cosmic rays and of the relativistic electrons responsible for cosmic radio waves suggests that the electrons may derive from the collisions of primary cosmic rays with the interstellar gas. The relation to be expected from this process is examined, and it is shown that the form of the electron energy spectrum is determined primarily by the different losses which prevail for different parts of the electron energy spectrum.

It is found that the observed spectra of various different types of radio source agree with the theoretical spectra, and that it is possible to obtain information on various physical conditions in the radio sources.

Introduction.—It is generally agreed that non-thermal cosmic radio noise is emitted by high energy electrons accelerated in weak magnetic fields. This is the familiar synchrotron mechanism. From the observed variation of radio emission with frequency, in which the power in unit frequency interval is proportional to $\nu^{-s/2}$, one may deduce directly that the number of electrons in unit energy interval, which we shall call $\pi(E)$, is proportional to $E^{-(1+s)}$. The similarity of this spectral variation to that of cosmic rays, the number of which in unit energy interval is proportional to $E^{-(1+p)}$, suggests that the electron flux is related in some way to that of cosmic rays. Since electrons lose energy much faster than protons, no original electrons (that is, those injected with the protons) would be left in a steady system. They will be continually injected, though, as the decay products from the collisions of cosmic rays with the interstellar gas; it is the energy spectrum to be expected from this process which will be examined in this paper.

We cannot expect the indices p and s to be identical, chiefly because the electrons' rate of loss of energy varies very much with energy. It is found that the effective spectral index s increases slowly with energy since the spectral index of the observed radio spectrum increases slowly with frequency. The radio spectra of several sources are now well known and it appears that they accord well with the assumption that the electrons are produced by primary cosmic rays. Small deviations may be due to the effects of acceleration processes but, provided that these are unimportant, the radio spectra may be used to explore physical conditions in the various kinds of radio source.

Characteristics of synchrotron radiation.—Let

$$\pi(E)\,dE = KE^{-(1+s)}\,dE$$

be the number of electrons of energy E to $E+dE$. The radio emission is then J_ν where

$$J_\nu = \frac{K}{2}\cdot\frac{\sqrt{3}e^3}{mc^2}\left(\frac{3e}{4\pi m^3c^5}\right)^{s/2}\cdot H^{1+s/2}\cdot\nu^{-s/2}\,I \text{ ergs sec}^{-1}\,(\text{c/s})^{-1}.$$

H is the magnetic field in gauss. I is an integral of the order of 2 which varies slightly with s. An electron emits most of its radiation near its critical frequency ν_c, where

$$\nu_c = 6{\cdot}3\times10^{18}\,HE^2 \text{ c/s}.$$

E is the electron's energy in ergs. To account accurately for any given radio emission, therefore, we must know the field, because it affects both the energy of the electrons responsible for a particular frequency (through ν_c) and the number required (through J_ν).

Energy losses.—The determining factor in the general form of the electron energy spectrum is rate of loss of energy by various processes, since these processes show marked, and different, variations with energy. Consequently we shall first examine these losses and then their effect on an electron energy spectrum where the source of electrons at energy E is simply proportional to the proton number density, $E^{-(1+p)}$.

Electrons may lose energy by (i) ionizing the surrounding medium; (ii) bremsstrahlung; and (iii) synchrotron radiation in weak magnetic fields.

The first is predominant at very low energies, decreases quickly as the energy increases, and at energies greater than 10^6 eV is nearly constant. The very slow increase in the rate of loss is proportional to $\log E$ only. The energy is lost by small steps in many encounters with the surrounding medium, so that the rate of the energy loss may be treated mathematically as continuous. Bremsstrahlung is more important at energies greater than the so-called critical energy ($3{\cdot}82\times10^8$ eV in hydrogen) but, unlike ionization losses, it occurs in large discrete events.

In any accurate treatment one must use only the probability that an electron will lose a certain amount of energy in a particular length of path. The theoretical expression I shall use is valid in neutral hydrogen at energies much greater than the critical ($3{\cdot}8\times10^8$ eV). The effect of using such an expression in the energy region just above $3{\cdot}8\times10^8$ eV is to overestimate the loss by no more than a factor of two. Synchrotron radiation loss is, mathematically speaking, continuous, and is proportional to the square of the energy. In the usual weak interstellar magnetic fields, it is smaller than bremsstrahlung except at very high energies. The conditions under which it supersedes bremsstrahlung will be discussed in detail in another section.

Positive and negative electrons may annihilate each other; this process has a negligible cross-section at the energies under consideration*.

The effect of energy losses on the electron energy spectrum. Qualitative discussion.—In Figs. 1 and 2, the various rates of loss of energy (in ergs per radiation length) have been plotted as functions of energy. Even though bremsstrahlung losses are, strictly speaking, not continuous (i.e. "rate of loss"

* Heitler, *The Quantum Theory of Radiation*, O.U.P., 1944, p. 230.

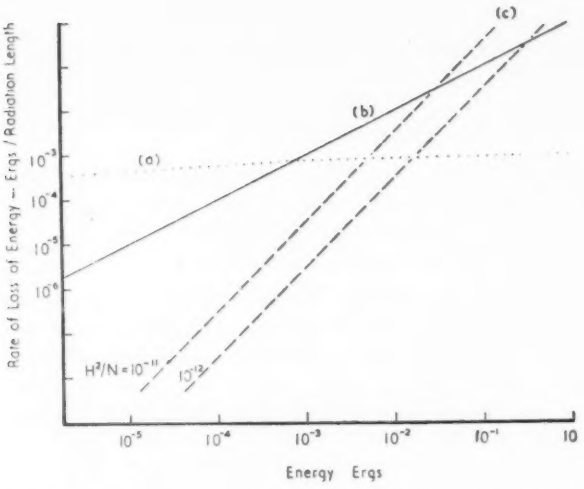

FIG. 1.—*Rate of energy loss (ergs per radiation length) plotted as a function of energy (ergs). (a) is the loss due to ionization. (b) is the loss due to bremsstrahlung. (c) is the loss due to synchrotron radiation for the different values of* H^2/N.

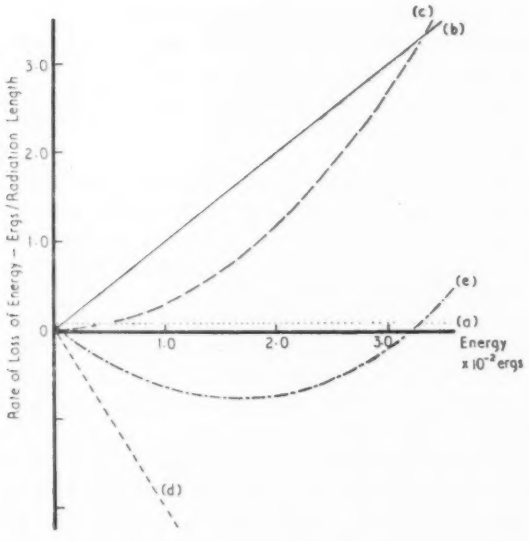

FIG. 2.—*The rates of loss are plotted directly instead of logarithmically. The same notation is used as in Fig. 1 and an acceleration (negative loss) (d) has been added, assuming that* $\alpha = 2$ *and* $H^2/N = 10^{-11}$. *The sum of all these is (e) which shows that there is a net gain of energy (negative loss) for energies* $10^{-3} < E < 3{\cdot}2 \times 10^{-2}$ *ergs.*

is a meaningless term), yet, on the average, an electron loses its own energy in one radiation length. This is a length of path which depends on the medium and its density. In neutral hydrogen, it is 69 gm cm^{-2}. The curve R represents the average loss by bremsstrahlung. I is the continuous loss by ionizing collisions, H is continuous loss by synchrotron radiation for various values of H^2/N, where N is the number density in cm^{-3}. The total loss curve, therefore, is fairly flat in the energy region (*a*), linear in (*b*) and parabolic in (*c*).

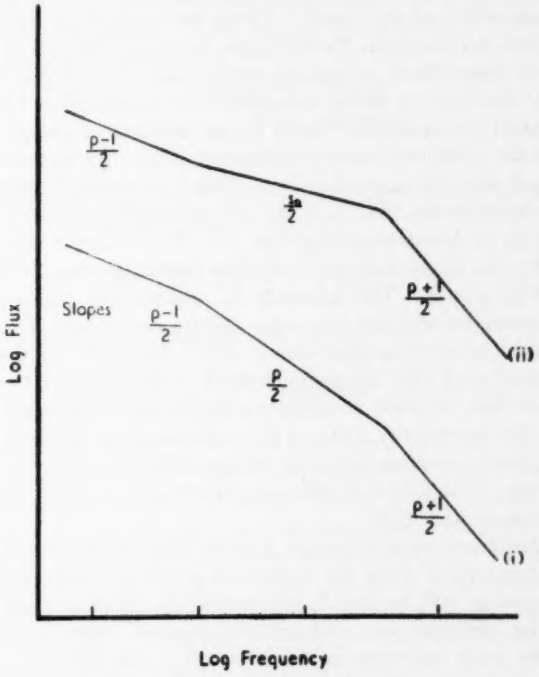

FIG. 3.—*Hypothetical spectral indices: (i) acceleration never predominant; (ii) acceleration predominant for energies within a range varying by a factor of nearly* 10 *to* 1.

Suppose now that there is a source of electrons akin to the cosmic rays in spectrum, say of index p. Let the source be $Q_0E^{-(1+p)}$. In a steady state, the number of electrons leaving a particular energy interval is the same as the number gained. Therefore

$$\frac{\partial}{\partial E}\pi(E)\{\text{rate of energy loss by one electron}\}+Q_0E^{-(1+p)}=0.$$

The rate of energy loss is the sum of a constant, a linear and a quadratic term, call it $a+bE+cE^2$. Then

$$(E)=\frac{Q_0E^{-(1+p)}}{p}\left(\frac{a}{E}+b+cE\right)^{-1}.$$

Compare this with the electron energy distribution which has been set proportional to

$$E^{-(1+s)},$$

The effective index s of the flux of electrons whose energy is in region (a), where the constant term of the loss curve predominates, is $p-1$; the index is p, the same as in the source for electrons whose energy is in region (b), where the linear term of the loss curve predominates; the index at the highest energies, region (c), is $p+1$. Then the curve of log radio power against log frequency for a radio source due to such electrons would look like Fig. 3 (i).

The effect of acceleration.—Electrons will be accelerated in exactly the same way as other charged cosmic-ray particles, but the effect may be negligible compared to the effect of the losses. There are many theories on accelerating mechanisms (see, for example, Parker 1958, for a resumé), all of which predict the same linear dependence of rate of energy gain on energy. It is sufficient for the present therefore to define a coefficient of acceleration α such that αE is the energy gained per radiation length by an electron of energy E. So far as we know from the observed index of primary cosmic rays and assumed collision cross-sections, α does not exceed unity. This it must do if electrons are to be accelerated independently, that is, if the rate of acceleration αE is to exceed the approximate rate of bremsstrahlung loss, E. For a purely hypothetical case, where $\alpha=2$, the loss curve and the equivalent radio spectrum have been plotted (Fig. 2 and Fig. 3 (iii)). The accuracy of present flux measurements is not sufficient to determine whether any radio spectra are curves of this sort or not.

The production of electrons from cosmic rays.—In detail, the discussion above has not concerned itself with the precise nature of the source of electrons. It has merely assumed that they are secondary particles of the primary flux of heavy cosmic rays. We know very little of the cross-sections for meson production and especially their variation with the energy of the incoming particle and the outgoing electron. The following attempt to devise a source function is therefore at best only an approximation.

We know that an electron of energy E is the result of the collision of a proton of some higher energy E' with the nucleus of an atom of interstellar hydrogen. The available energy will be distributed among the residual nuclei, mesons and neutrinos. The electrons are, incidentally, positive since no π^- mesons are produced in the $p+p$ collisions in the interstellar medium.

We shall assume first that E is proportional to E' at energies too low for multiple mesons and strange particles, i.e.

$$E'=aE.$$

At very much higher energies, one may use Fermi's statistical theory (1950). Electrons of energy E are produced with a multiplicity s from a collision of energy E'.

$$E=cE'^{3/4}, \qquad c=0{\cdot}049\left(\frac{Mc^2}{2}\right)^{1/4}$$

where

$$s=bE'^{1/4}, \qquad b=1{\cdot}8\left(\frac{Mc^2}{2}\right)^{-1/4}.$$

Secondly we assume that the number of collisions is proportional to the number of cosmic-ray protons, i.e.

$$P(E')=P_0E'^{-(1+p)}.$$

Thirdly, that at the lower energies, where $E' = aE$, the proportion of meson-producing nuclear collisions increases with energy. As an approximation to the curve reported by Riddiford (1957), let us say that

$$K\sigma\left\{1-\left(\frac{E'}{E_0}\right)^{-\tau}\right\}$$

is the probability that a proton of energy E' produces a meson in one radiation length, where σ is the total cross-section gm cm^{-2}, K is (69 gm cm^{-2})$^{-1}$, τ is a constant of the order of $\frac{1}{2}$. This expression is zero, if $E' < E_0 = 300$ MeV, the threshold for meson production.

If $E' > 10^{12}$ eV the source function used will be

$$K\sigma P_0 \frac{4}{3}\cdot\frac{b}{c}\cdot\left(\frac{E}{c}\right)^{-2(3(1+2p)} . \tag{1}$$

There are energies between 10^{12} and 10^{11} eV about which little can be said.

If $E' < 10^{11}$ eV the source function will be

$$K\sigma P_0 a\left\{1-\left(\frac{aE}{E_0}\right)^{-\tau}\right\}(aE)^{-(1+p)} . \tag{2}$$

The equation governing the electron flux is therefore

$$\frac{\partial\pi(E)}{\partial t} = Q - \int_0^1\left\{\pi(E) - \frac{1}{1-v}\pi\left(\frac{E}{1-v}\right)\right\}\psi(v)\,dv + \frac{\partial}{\partial E}\pi(E)\{\epsilon_0 - \alpha E + \beta E^2\} \tag{3}$$

where Q is the source, either (1) or (2), t is the distance along the electron's path measured in radiation lengths, $\psi(v)$ is the probability that a fraction v of the electron's energy will be lost by bremsstrahlung in one radiation length. By definition, its average value is unity. ϵ_0 is the energy lost by ionization per radiation length. It will be assumed that it will be constant and of the order of the critical energy. αE represents the possible energy gained by acceleration per radiation length. βE^2 is the energy lost by synchrotron radiation per radiation length. If E is in ergs, the magnetic field H is in gauss, and the number density of the gas is N cm^{-3}, then the coefficient β is $3 \times 10^{12} H^2/N$.

Solutions of the equation.—To simplify the problem first of all, only stationary solutions have been looked for; that is, $\partial\pi/\partial t$ has been set equal to zero. Secondly the equation has been solved in different energy regions where the appropriate approximations may be made.

$E > 10^{11} eV$.

Synchrotron radiation predominates as the loss mechanism at these electron energies even in fairly weak fields. The energy E' of the parent nuclei is sufficiently large for Fermi's statistical theory to be applicable (1)

$$\pi(E) = \frac{\kappa\sigma P_0}{\beta}\cdot\frac{6}{p-\frac{1}{4}}\cdot\left(\frac{E}{c}\right)^{-\frac{1}{4}(4p+5)}\cdot\frac{1}{1-\dfrac{\alpha}{\beta E}} . \tag{4}$$

$10^{11} eV > E > 5 \times 10^8 eV$.

The continuous losses by ionization and by synchrotron radiation have been neglected, and the lower energy electron source has been used (2).

$$\pi(E)=\frac{\kappa\sigma P_0}{E}\left\{\left(\frac{aE}{E_0}\right)^{-s_0}\cdot\frac{E_0{}^{-p}}{\alpha-A'(s_0)}\cdot\frac{\tau}{(p-s_0)(p+\tau-s_0)}+\frac{(aE)^{-p}}{A(p)-\alpha p}\left(1-\left(\frac{aE}{E_0}\right)^{-\tau}\frac{A(p)-\alpha p}{A(p+\tau)-\alpha(p+\tau)}\right)\right\} \quad (5)$$

where

$$A(s)=\int_0^1(1-v^s)\psi(v)\,dv$$

and $A'(s)$ is its derivative with respect to s. $A(s)$ is tabulated by Rossi (1952), p. 296. s_0 is the root of $A(s)-\alpha s=0$.

If α, the acceleration coefficient, is small, s_0 is large and the first term of (5) varies too rapidly with energy to be important. The electron spectrum is governed entirely by the second term, that is, by the proton flux. Physically this means that the electrons are kept up by their source in the decayed mesons from cosmic-ray collisions against energy losses predominantly by bremsstrahlung.

If, on the other hand, α is of the order of unity, the root s_0 is less than p. Now it is the first term of the solution (5) which is important. Physically, this means that acceleration is overcoming radiation losses and the electron flux can grow independently of its source.

$3\times10^8/a<E<5\times10^8$.

Ionization losses are now predominant. The spectrum is flatter and joins up with the second term of the previous solution when $E=\epsilon_0$

$$\pi(E)=\frac{K\sigma P_0}{\epsilon_0}(aE)^{-p}\left\{\frac{1}{p}-\left(\frac{aE}{E_0}\right)^{-\tau}\frac{1}{p+\tau}\right\}.$$

If α is large, ionization losses do not overtake acceleration until lower energies are reached, i.e. $\alpha E=\epsilon_0$.

$E<3\times10^8/a$ *eV*.

The source is negligible at these energies and $\pi(E)\times$(ionization loss) is constant.

Non-relativistic energies are of little interest so far as radio emission is concerned, for the intensity drops off very quickly with decreasing energy. In addition, the simple formulae relating spectral index to the index of the electrons no longer hold.

Applications

1. *The Galaxy.*—We may now examine the relation between the spectral indices of cosmic rays and galactic radio waves using the following information.

(i) At the Earth cosmic rays are observed having an energy density of the order of 1 eV/cm^3 and an index p which varies slightly with energy.

E	p	
10^9 eV	1·2	(Popov 1957)
10^{11}	1·5	
10^{15}	2·0	

(ii) The background radio emission from the Galaxy is due to an electron flux of index $s=1{\cdot}0\pm0{\cdot}2$ (Adgie and Smith 1956).

(iii) The emissivities at 80 Mc/s of the halo and disk are $1{\cdot}8\times10^8$ and $3{\cdot}2\times10^9$ w.s.$^{-1}$(c/s)$^{-1}$ respectively (Baldwin 1955).

(iv) The estimated magnetic field in the spiral arm is 6×10^{-6} gauss (Fermi and Chandrasekhar 1953).

(v) On the average the number density N of the interstellar gas is roughly unity; hence H^2/N is roughly 2×10^{-11}.

From (ii) and (iv) we may calculate that it is the electrons of energy 10^9 eV that are chiefly responsible for 80 Mc/s emission, and that their energy density must be roughly 0·035 eV/cm^3 in the disk and arms. The same energy density can account for the halo, if the field there is 10^{-6} gauss. Provided of course that the Galaxy is in a steady state, the electrons of energy 10^9 eV in the galactic field should obey equation (5), since their energy losses are mostly by bremsstrahlung. The field is not large enough for the synchrotron losses to be predominant.

If we neglect acceleration and hence the first term of equation (5) we have

$$\pi(E) = \frac{ak\sigma P_0 (aE)^{-(1+p)}}{A(p)-\alpha p} \cdot \left\{ 1 - \frac{A(p)-\alpha p}{A(p+\tau)-\alpha(p+\tau)} \left(\frac{aE}{E_0} \right)^{-\tau} \right\}$$

as the solution for the electron flux. The second term in the brackets is small and the bracket is ~ 1.

Now the constant a was introduced quite arbitrarily to represent the efficiency of energy transfer from the colliding proton (E') to its daughter electron of energy E. Because the electron is the result of three distinct decay processes its share of the original energy E' may be quite small, 10 per cent or less,

$$\begin{aligned} p + p &\rightarrow p + n + \pi^+ \\ &\rightarrow p + p + \pi^0 \\ \pi^+ &\rightarrow \mu^+ + \nu \\ \mu^+ &\rightarrow \beta^+ + \nu. \end{aligned}$$

If then $E' = aE$, a is large; the index p is that appropriate to protons of energy ten to a hundred times the electrons' (E), i.e.

$$1{\cdot}2 < p \leqslant 1{\cdot}5.$$

The observed index is $1{\cdot}0 \pm 0{\cdot}2$, which is not far from the expected value. The difference, if significant, may mean that acceleration should not have been ignored.

2. *Cassiopeia A.*—The radio emission from Cassiopeia A has been shown to come from a galactic nebulosity identified by Minkowski (1958) as a supernova 256 years old. It is therefore not possible to assume that a stationary solution for $\pi(E)$ applies. Nevertheless, the slope of its radio spectrum, $-0{\cdot}8 \pm 0{\cdot}05$, suggests that the index s of the electrons is $1{\cdot}6 \pm 0{\cdot}1$, a value not significantly different from the value of p for galactic cosmic rays.

3. *Cygnus A.*—The radiation is from two colliding galaxies whose radio spectrum exhibits a sharp break at about 350 Mc/s. Above this frequency, the spectrum has a slope of $-1{\cdot}02 \pm 0{\cdot}1$ (corresponding to $s = 2{\cdot}04 \pm 0{\cdot}2$) and below, the slope is $-0{\cdot}66 \pm 0{\cdot}6$ (corresponding to $s = 1{\cdot}32 \pm 0{\cdot}12$). Any observed steepening of the radio spectrum at the high frequencies must indicate a real change in the index s of the electrons for the only confusion which might arise is thermal emission which of course varies in the opposite way with frequency. On the other hand the flattening at the low frequency and around 10 Mc/s may be due to absorption in H II regions through which the

radiation has passed, and not due to a real flattening of the electrons' spectrum, which is expected as ionization losses take over at the low energies corresponding to 10 Mc/s.

The break in the spectrum at the high frequency end is interesting. It should occur roughly at the critical frequency of those electrons whose synchrotron losses are just overtaking the bremsstrahlung losses. If their energy is E, the former is $3 \times 10^{12}(H^2/N)E^2$ ergs per radiation length, and the latter is E in the same units. Their critical frequency ν_c is given by

$$\nu_c = 6{\cdot}29 \times 10^{18} HE^2 \text{ c/s}, \tag{6}$$

$$E = 3 \times 10^{12} \frac{H^2}{N} E^2 \text{ ergs}. \tag{7}$$

If E is eliminated between (6) and (7) we obtain

$$H = 8{\cdot}9 \times 10^{-3} N^{2/3} \nu_c^{-1/3}.$$

N is the number density of the hydrogen gas in the source and may be of the order of unity. Putting $\nu_c = 350$ Mc/s, we find $H = 1{\cdot}3 \times 10^{-5}$ gauss.

It is possible to derive an estimate for the magnetic field quite independently by using the following data.

(i) $s = 2$.

(ii) The power at 80 Mc/s is $P_{80} = 1{\cdot}87 \times 10^{27}$ watts c/s^{-1} ster^{-1}.

(iii) Distance 93·5 Mpc.

(iv) Volume 3×10^{68} cm^3.

If it is assumed that the electron density and magnetic fields are the most important components of the total stored energy in the galaxies and that this total energy has its minimum value consistent with the power emitted, then the magnetic field is $H = 5 \times 10^{-5}$ gauss. The two estimates are reasonably close.

4. *Other sources.*—The spectral indices of "point" radio sources taken as a whole vary between rather narrow limits: $-0{\cdot}5$ to $-2{\cdot}0$. The corresponding electron index s lies between 1 and 4, and therefore limits on p may be set immediately: $p < 5$. On closer inspection, however, it appears probable that the real limits are much stricter. I have shown that all radio spectra may be expected to be steeper at high frequencies. Whitfield has observed that the mean index of galactic sources is less than that of the identified extra-galactic sources and that both are less than the mean index of unidentified sources*. Following this observation, Ryle has suggested (in the Bakerian Lecture to the Royal Society, 1958) that most radio sources are extremely distant and that the steeper spectra expected at high frequencies are brought into view by the red shift. His suggestion is supported by Dewhirst's identification of a number of sources whose distances are so great, and consequently whose radio powers are so enormous, that the origin of their energy is difficult to understand if the better part is wasted in bremsstrahlung and ionization losses. Synchrotron losses therefore, must predominate, and hence it is the steep part of the spectrum where $s = p + 1$ which is observed. If so, stricter limits may be set on p, i.e. $p \leqslant 3$.

* The spectral index $-0{\cdot}28$ of Taurus A or the Crab Nebula is exceptionally low. The corresponding electron flux index is $s = 0{\cdot}56$. But in this source, a remnant of a supernova explosion 900 years ago, no steady state obtains. A radiation length is equivalent to $5 \times 10^6/N$ years. The number density cannot be greater than 10^2; therefore, one radiation length is 5×10^4 years, a value very much greater than the age of the nebula.

It is interesting that the index of the local flux of cosmic rays also lies within these limits, but it is surprising that they may be generalized to such widely differing regions of space such as most radio sources. This conclusion is based of course on the assumption of a stationary flux of cosmic rays which may be unjustifiable.

Acknowledgments.—The author would like to thank Mr M. Ryle, Dr F. G. Smith and Dr L. Mestel for their advice and encouragement. The work was carried out during the tenure of an Isaac Newton Studentship and a Tucker-Price Studentship from Girton College, Cambridge.

Mullard Radio Astronomy Observatory,
Cavendish Laboratory,
Cambridge:
1958 *December* 17.

References

Adgie, R. and Smith, F. G., *The Observatory*, **76**, 181, 1956.
Baldwin, J. E., *M.N.*, **115**, 690, 1955.
Burbidge, G. M., *Ap. J.*, **127**, 48, 1958.
Fermi, E., *Phys. Rev.*, **75**, 1169, 1949.
Fermi, E., *Prog. Theor. Phys.*, **5**, 570, 1950.
Fermi, E. and Chandrasekhar, S., *Ap. J.*, **118**, 116, 1953.
Minkowski, R., Paris Symposium on Radio Astronomy, 1958.
Oort, J. H. and Walraven, Th., *B.A.N.*, **12**, 1956.
Parker, E., *Phys. Rev.*, **109**, 1328, 1958.
Pikelner, S. B., *Astron. Journal Moscow*, **33**, 785, 1956.
Popov, Iu. A., *Sov. Phys.* (JETP in translation), **4**, 85, 1957.
Riddiford, L., reporting at the Rochester High Energy Conference, 1957.
Rossi, B., *High Energy Particles*, 1952.
Ryle, M., *Proc. Roy. Soc.* A, **248**, 289, 1958.
Whitfield, G. R., *M.N.*, **117**, 680, 1957.

РЕЗЮМЕ ДОКЛАДОВ, В ПЕРЕВОДЕ НА РУССКИЙ ЯЗЫК

НУТАЦИЯ: СРАВНЕНИЕ ТЕОРИИ С НАБЛЮДЕНИЯМИ

Х. Джеффрис

Даются теоретические значения для основного, полугодового и полумесячного членов нутации, основанные на моделях Земли: модели Роша и точечной. Они сравнивались со значениями, полученными Федеровым из наблюдений. Согласие получилось лучше, чем во всех предыдущих случаях. Полумесячные члены имеют почти одинаковые значения для обеих моделей и согласуются с наблюдением. Величины обоих компонентов полугодовой составляющей лучше всего согласуются со схемой точечной модели. Наблюденное 19-летнее изменение в наклонении лучше всего согласуется с точечной моделью, а изменение в долготе—с моделью Роша; некоторое разногласие с наблюдениями должно оставаться и для любой другой модели.

РЕКОМБИНАЦИЯ ИЗЛУЧЕНИЕМ ВОДОРОДНЫХ ИОНОВ

М. Ситон

Учитывая первые три члена асимптотического разложения множителя Крамерса-Гаунта проведено вычисление скорости рекомбинации и средней кинетической энергии рекомбинирующихся электронов.

РЕШЕНИЕ УРАВНЕНИЙ КАСКАДНОГО ЗАХВАТА ДЛЯ ВОДОРОДА

М. Ситон

Вычисления проведены для $T = 2{,}5 \times 10^3$, 5×10^3, 1×10^4 и 2×10^4 °К, учитывая бесконечное число уровней, однако принимая $b_{nl} = [(2l+1)/n^2]b_n$. Показано, что результаты, полученные Бейкером и Мензелом, ошибочны приблизительно на 5% для Случая А и на 20% для Случая В.

Улучшенный метод вычислений получается, если ввести каскадную матрицу, элементы которой $C_{n'n}$ дают полную вероятность перехода $n' \to n$ с учетом всех возможных каскадных путей.

НАБЛЮДЕНИЯ СОЛНЕЧНОЙ ГРАНУЛЯЦИИ С АЭРОСТАТА С ЭКИПАЖЕМ

Д. Блекуэлл, Д. Дьюхерст и А. Дольфюс

По-видимому существует практический предел разрешению, достижимому при фотографировании Солнца с Земли. Пытаясь получить значительно лучшее разрешение, авторы производили фотографирование при помощи 29-см рефрактора, монтированного под корзиной аэростата, на высоте ~ 5500 м. Было осуществлено два полета; во время второго полета, 1 апреля 1957 г., было снято 480 кадров. Хотя условия видимости на Земле во время полета были очень плохими, фотографии, полученные с аэростатным телескопом во время второго полета, превосходят по качеству лучшие снимки, из всех полученных на земных станциях.

Сложная структура фотосферы иллюстрируется фотографиями. Даны автокорреляционные кривые для двух фотометрических разрезов наилучших снимков. Точные функции пропускания для телескопа в целом (объектив, окуляр, фотографическая эмульсия) были измерены при помощи синусоидальных решеток, а полученные результаты были использованы для исправления микрофотометрических измерений контраста. Среднее исправленное значение контраста между гранулами и межгранульными областями составляет 40% для λ 5300.

ЗВЕЗДЫ ГЛАВНОЙ ПОСЛЕДОВАТЕЛЬНОТСИ

С. Хейзелгров и Ф. Хойл

Интегрирование проведено для однородных звезд типов I и II. По-видимому ширина полосы, разделяющей типы звездного населения, соответствующая нулевому возрасту в пределах главной последовательности, не превышает 0,1 звездной величины, если только используется правильная шкала эффективных температур.

ВОЗРАСТЫ СУБГИГАНТОВ ТИПОВ I И II

Ф. Хойл

Эволюционные последовательности, очень близкие к нижним частям
а) последовательностей шаровых скоплений,
в) последовательности M 67, были построены при помощи вычислительной машины IBM 704. Эти нижние части последовательностей определяют возрасты звезд типов I и II.

Используя полученные из наблюдений звездные величины для близлежащих звезд типа I с большими тригонометрическими параллаксами и налагая условие, что звезды типа II должны быть старше звезд типа I, автор приходит к следующим выводам:

1. Переменные типа скоплений не могут быть ярче $M_V = +0{,}6$.
2. Возраст Галактики должен быть больше 10^{10} лет.

Приведено также соображение в пользу того, что первоначальное содержание гелия в звездах типа II было низким.

ЗАМЕТКА О ПЕРЕМЕННЫХ ТИПА RR ЛИРЫ

Т. Кинман

Пульсационный критерий $P\sqrt{\rho} = Q$ использован для получения абсолютных величин переменных типа RR Lyr как функции их цвета и периода; исправлена ошибка, допущенная Сандиджем в аналогичном выводе. Согласно этой модели наблюденное различие в средних периодах переменных в M 3 и ω Cen объясняется различием в $0^m{,}3$ абсолютной визуальной величины между звездами этих двух скоплений. Получено грубо приближенное согласие между предвычисленными абсолютными величинами и величинами, полученными по тригонометрическим параллаксам для четырех переменных звездного поля с $P < 0^d{,}2$.

Пульсационная модель предсказывает различие в $0^m{,}7$ между цефеидами типа *ab* с аномально коротким периодом, обнаруженными Гапошкиным в направлении галактического центра, и нормальными цефеидами типов *ab* и *c* в той же области неба. Так как этого не наблюдается, то или пульсационная модель, или величины периодов аномальных переменных неверны.

В списке приводится 16 звезд типа *ab* с периодом $P < 0^d{,}36$ в общем поле. Показано, что эти звезды лежат ближе к галактической плоскости, чем лежала бы случайная выборочная группа нормальных переменных типа *c* такого же периода, в согласии с обнаруженным Детре относительно меньшим солнечным движением для этих звезд. Необходимы дальнейшие наблюдения для подобных звезд, расположенных как в направлении галактического центра, так и в общем поле.

СИСТЕМА ζ ФЕНИКСА

Г. Хейгман

Лучевые скорости измерены по 71 новой спектрограмме ζ Phe, полученной на обсерватории Маунт Стромло. Вычислена спектроскопическая орбита главной звезды и из дифференциальных измерений определена полуамплитуда K_2 спутника. Абсолютные размеры обоих компонентов установлены из сопоставления спектроскопических орбит и фотометрических наблюдений Хогга. Определен спектральный класс спутника. Некоторые трудности теории системы по-видимому удалось разрешить.

ЗАМЕЧАНИЯ О ПЯТИ ЮЖНЫХ ГАЗОВЫХ ТУМАННОСТЯХ

Д. С. Эванс

Сообщаются результаты наблюдений спектров, лучевых скоростей, внутренних движений и формы для пяти южных объектов IGC 3918, 6302, 6326, IC 4776 и Anon $\alpha = 16^h\ 13^m{,}5$ $\delta = -51^\circ\ 52'$, проведенных с Радклиффским 74″ рефлектором.

ШАРОВЫЕ СКОПЛЕНИЯ. I. ЛУЧЕВЫЕ СКОРОСТИ ЮЖНЫХ ШАРОВЫХ СКОПЛЕНИЙ

Т. Кинман

Приводятся лучевые скорости 30 южных шаровых скоплений и обсуждаются их ошибки. При помощи Радклиффского Кассегреновского спектроскопа (дисперсия 86 А/мм) получены спектрограммы 28 скоплений, в том числе для 15 скоплений в интегральном свете, спектрограммы отдельных звезд для 10 скоплений и спектрограммы обоих типов для трех скоплений. Для 16 из этих скоплений ранее вовсе не было известно скоростей. При помощи Ньютоновского спектроскопа с дисперсией 380 А/мм были получены спектрограммы четырех скоплений, для двух из которых имелись спектрограммы, полученные с Кассегреновским спектроскопом. Сравнение наших лучевых скоростей с данными Мейалла и Д-коя показали удовлетворительное согласие. Приводится таблица лучевых скоростей и расстояний 70 шаровых скоплений.

РАСПРЕДЕЛЕНИЕ ЯРКОСТИ В ПРЕДЕЛАХ ИСТОЧНИКОВ РАДИОИЗЛУЧЕНИЯ ЛЕБЕДЬ А (19N4A) И КАССИОПЕЯ А (23N5A)

Р. Дженнисон и В. Латам

Описываются измерения амплитуды и фазы преобразования Фурье распределения яркости на частоте 127 Мгц в пределах интенсивных источников радиоизлучения Лебедь А (19 ^h4A) и Кассиопея А (23 ^h5A) вдоль оси в направлении восток-запад. Распределение яркости было вычислено по наблюдаемым отсчетам. Показано, что в случае источника Лебедь А оно согласуется с существованием двух больших излучающих областей почти равной интенсивности. α-компонент, опережающий по прямому восхождению, несколько ярче β-компонента. Описываются также измерения, связанные с определением положения больших осей источников. Очевидно диаметр источника Лебедь в позиционном угле, близком к 187°, должен быть относительно очень небольшим. Измерения для Кассиопеи указывают на наличие какого-то слабого выступа вблизи позиционного угла 90°, а также, вероятно, на наличие небольшого увеличения яркости к краю основного источника.

СВЯЗЬ КОСМИЧЕСКОГО РАДИОИЗЛУЧЕНИЯ С ЭЛЕКТРОННЫМ КОМПОНЕНТОМ КОСМИЧЕСКИХ ЛУЧЕЙ

Х. Таммер

Сходство между спектрами космических лучей и релятивистских электронов, обусловливающих космическое радиоизлучение, наводит на мысль, что электроны могут появляться при столкновениях частиц первичного компонента космических лучей с межзвездным газом. Рассмотрена связь, которую можно ожидать при этом процессе, и показано, что характер энергетического спектра электронов определяется прежде всего различными потерями, которые преобладают в различных частях энергетического спектра электронов.

Найдено, что наблюдаемые спектры источников радиоизлучения различных типов согласуются с теоретически вычисленными спектрами и что имеется возможность получать сведения о различных физических условиях в этих источниках радиоизлучения.

NOTICE TO AUTHORS

1. *Communications.*—Papers must be communicated to the Society by a Fellow. They should be accompanied by a summary at the *beginning* of the paper conveying briefly the content of the paper, and drawing attention to important new information and to the main conclusions. The summary should be intelligible in itself, without reference to the paper, to a reader with some knowledge of the subject; it should not normally exceed 200 words in length. **Authors are requested to submit MSS. in duplicate. These should be typed using double spacing and leaving a margin of not less than one inch on the left-hand side. Corrections to the MSS. should be made in the text and not in the margin.** Unless a paper reaches the Secretaries more than seven days before a Council meeting it will not normally be considered at that meeting. By Council decision, MSS. of accepted papers are retained by the Society for one year after publication; unless their return is requested by the author, they are destroyed.

2. *Presentation.*—Authors are allowed considerable latitude, but they are requested to follow the general style and arrangement of *Monthly Notices.* References to literature should be given either in the traditional form of serial numbers in the text related to a numbered list at the end of the paper, or in the form recommended in *Notes on the preparation of scientific papers to be communicated to the Royal Society.*

3. *Notation.*—For technical astronomical terms, authors should conform closely to the recommendations of Commission 3 of the International Astronomical Union (*Trans. I.A.U.*, Vol. VI, p. 345, 1938). Council has decided to adopt the I.A.U. 3-letter abbreviations for constellations where contraction is desirable (Vol. IV, p. 221, 1932). In general matters, authors should follow the recommendations in *Symbols, Signs and Abbreviations* (London: Royal Society, 1951) except where these conflict with I.A.U. practice.

4. *Diagrams.*—**These should be designed to appear upright on the page, drawn about twice the size required in print and prepared for direct photographic reproduction except in the lettering, which should be inserted in pencil. Legends should be given in the manuscript indicating where in the text the figure should appear.** Blocks are retained by the Society for 10 years; unless the author requires them before the end of this period they are then destroyed.

5. *Tables.*—**These should be arranged so that they can be printed upright on the page.**

6. *Proofs.*—Costs of alteration exceeding 5 per cent of composition must be borne by the author. Fellows are warned that such costs have risen sharply in recent years, and it is in their own and the Society's interests to seek the maximum conciseness and simplification of symbols and equations consistent with clarity.

7. *Revised Manuscripts.*—When papers are submitted in revised form it is especially requested that they be accompanied by the original MSS.

Reading of Papers at Meetings

8. When submitting papers authors are requested to indicate whether they will be willing and able to read the paper at the next or some subsequent meeting, and approximately how long they would like to be allotted for speaking.

9. Postcards giving the programme of each meeting are issued some days before the meeting concerned. Fellows wishing to receive such cards whether for Ordinary Meetings or for the Geophysical Discussions or both should notify the Assistant Secretary.

ЗАМЕЧАНИЯ О ПЯТИ ЮЖНЫХ ГАЗОВЫХ ТУМАННОСТЯХ

Д. С. Эванс

Сообщаются результаты наблюдений спектров, лучевых скоростей, внутренних движений и формы для пяти южных объектов IGC 3918, 6302, 6326, IC 4776 и Anon $\alpha = 16^h\ 13^m{,}5$ $\delta = -51^\circ\ 52'$, проведенных с Радклиффским 74″ рефлектором.

ШАРОВЫЕ СКОПЛЕНИЯ. I. ЛУЧЕВЫЕ СКОРОСТИ ЮЖНЫХ ШАРОВЫХ СКОПЛЕНИЙ

Т. Кинман

Приводятся лучевые скорости 30 южных шаровых скоплений и обсуждаются их ошибки. При помощи Радклиффского Кассегреновского спектроскопа (дисперсия 86 А мм) получены спектрограммы 28 скоплений, в том числе для 15 скоплений в интегральном свете, спектрограммы отдельных звезд для 10 скоплений и спектрограммы обоих типов для трех скоплений. Для 16 из этих скоплений ранее вовсе не было известно скоростей. При помощи Ньютоновского спектроскопа с дисперсией 380 А мм были получены спектрограммы четырех скоплений, для двух из которых имелись спектрограммы, полученные с Кассегреновским спектроскопом. Сравнение наших лучевых скоростей с данными Мейалла и Дюон показали удовлетворительное согласие. Приводится таблица лучевых скоростей и расстояний 70 шаровых скоплений.

РАСПРЕДЕЛЕНИЕ ЯРКОСТИ В ПРЕДЕЛАХ ИСТОЧНИКОВ РАДИОИЗЛУЧЕНИЯ ЛЕБЕДЬ А (19N4A) И КАССИОПЕЯ А (23N5A)

Р. Дженнисон и В. Латам

Описываются измерения амплитуды и фазы преобразования Фурье распределения яркости на частоте 127 Мгц в пределах интенсивных источников радиоизлучения Лебедь А (19 N4A) и Кассиопея А (23 N5A) вдоль оси в направлении восток-запад. Распределение яркости было вычислено по наблюдаемым отсчетам. Показано, что в случае источника Лебедь А оно согласуется с существованием двух больших излучающих областей почти равной интенсивности. α-компонент, опережающий по прямому восхождению, несколько ярче β-компонента. Описываются также измерения, связанные с определением положения больших осей источников. Очевидно диаметр источника Лебедь в позиционном угле, близком к 187°, должен быть относительно очень небольшим. Измерения для Кассиопеи указывают на наличие какого-то слабого выступа вблизи позиционного угла 90°, а также, вероятно, на наличие небольшого увеличения яркости к краю основного источника.

СВЯЗЬ КОСМИЧЕСКОГО РАДИОИЗЛУЧЕНИЯ С ЭЛЕКТРОННЫМ КОМПОНЕНТОМ КОСМИЧЕСКИХ ЛУЧЕЙ

Х. Таммер

Сходство между спектрами космических лучей и релятивистских электронов, обусловливающих космическое радиоизлучение, наводит на мысль, что электроны могут появляться при столкновениях частиц первичного компонента космических лучей с межзвездным газом. Рассмотрена связь, которую можно ожидать при этом процессе, и показано, что характер энергетического спектра электронов определяется прежде всего различными потерями, которые преобладают в различных частях энергетического спектра электронов.

Найдено, что наблюдаемые спектры источников радиоизлучения различных типов согласуются с теоретически вычисленными спектрами и что имеется возможность получать сведения о различных физических условиях в этих источниках радиоизлучения.

NOTICE TO AUTHORS

1. *Communications.*—Papers must be communicated to the Society by a Fellow. They should be accompanied by a summary at the *beginning* of the paper conveying briefly the content of the paper, and drawing attention to important new information and to the main conclusions. The summary should be intelligible in itself, without reference to the paper, to a reader with some knowledge of the subject; it should not normally exceed 200 words in length. **Authors are requested to submit MSS. in duplicate. These should be typed using double spacing and leaving a margin of not less than one inch on the left-hand side. Corrections to the MSS. should be made in the text and not in the margin.** Unless a paper reaches the Secretaries more than seven days before a Council meeting it will not normally be considered at that meeting. By Council decision, MSS. of accepted papers are retained by the Society for one year after publication; unless their return is requested by the author, they are destroyed.

2. *Presentation.*—Authors are allowed considerable latitude, but they are requested to follow the general style and arrangement of *Monthly Notices.* References to literature should be given either in the traditional form of serial numbers in the text related to a numbered list at the end of the paper, or in the form recommended in *Notes on the preparation of scientific papers to be communicated to the Royal Society.*

3. *Notation.*—For technical astronomical terms, authors should conform closely to the recommendations of Commission 3 of the International Astronomical Union (*Trans. I.A.U.*, Vol. VI, p. 345, 1938). Council has decided to adopt the I.A.U. 3-letter abbreviations for constellations where contraction is desirable (Vol. IV, p. 221, 1932). In general matters, authors should follow the recommendations in *Symbols, Signs and Abbreviations* (London: Royal Society, 1951) except where these conflict with I.A.U. practice.

4. *Diagrams.*—**These should be designed to appear upright on the page, drawn about twice the size required in print and prepared for direct photographic reproduction except in the lettering, which should be inserted in pencil. Legends should be given in the manuscript indicating where in the text the figure should appear.** Blocks are retained by the Society for 10 years; unless the author requires them before the end of this period they are then destroyed.

5. *Tables.*—**These should be arranged so that they can be printed upright on the page.**

6. *Proofs.*—Costs of alteration exceeding 5 per cent of composition must be borne by the author. Fellows are warned that such costs have risen sharply in recent years, and it is in their own and the Society's interests to seek the maximum conciseness and simplification of symbols and equations consistent with clarity.

7. *Revised Manuscripts.*—When papers are submitted in revised form it is especially requested that they be accompanied by the original MSS.

Reading of Papers at Meetings

8. When submitting papers authors are requested to indicate whether they will be willing and able to read the paper at the next or some subsequent meeting, and approximately how long they would like to be allotted for speaking.

9. Postcards giving the programme of each meeting are issued some days before the meeting concerned. Fellows wishing to receive such cards whether for Ordinary Meetings or for the Geophysical Discussions or both should notify the Assistant Secretary.

CONTENTS

PAGE

Harold Jeffreys, Nutation: comparison of theory and observations 75

M. J. Seaton, Radiative recombination of hydrogenic ions 81

M. J. Seaton, The solution of capture–cascade equations for hydrogen 90

D. E. Blackwell, D. W. Dewhirst and A. Dollfus, The observation of solar granulation from a manned balloon. I. Observational data and measurement of contrast 98

C. B. Haselgrove and F. Hoyle, Main-sequence stars 112

F. Hoyle, The ages of Type I and Type II subgiants 124

T. D. Kinman, A note on the RR Lyrae variables 134

G. Hagemann, The system of ζ Phoenicis 143

David S. Evans, Notes on five southern gaseous nebulae 150

T. D. Kinman, Globular clusters. I. The radial velocities of southern globular clusters 157

R. C. Jennison and V. Latham, The brightness distribution within the radio sources Cygnus A (19N4A) and Cassiopeia A (23N5A) 174

Harriet Tunmer, The relation of cosmic radio emission to the electronic component of cosmic rays 184

Russian translations of summaries of original papers 194

РЕЗЮМЕ ДОКЛАДОВ, В ПЕРЕВОДЕ НА РУССКИЙ ЯЗЫК 194

Printed in London by Taylor & Francis, Ltd., 1959 *June*